The Dissertation Committee for Beatriz Garcia-Fresca certifies that this is the approved version of the following dissertation:

Outcrop-Constrained Flow and Transport Models of Reflux Dolomitization

Committee:

_____
F. Jerry Lucia, Co-Supervisor

_____
John M. Sharp Jr., Co-Supervisor

_____
Charles Kerans

_____
Gareth D. Jones

_____
Jay L. Banner

Outcrop-Constrained Flow and Transport Models of Reflux Dolomitization

by

Beatriz Garcia-Fresca, B.S.; M.S.

Dissertation

Presented to the Faculty of the Graduate School of

The University of Texas at Austin

in Partial Fulfillment

of the Requirements

for the Degree of

Doctor of Philosophy

The University of Texas at Austin

December 2009

"Essentially, all models are wrong, but some are useful"

George Box, 1979

Dedication

Lehenik eta behin etxekoei, bihotzez.

To Bob Goldhammer for bringing out the carbonater in me.

To Mike for his love and support during the good times.

To all who were there during the bad times (y'all know who you are).

Y especialmente a Irene, por su paciencia y cariño en estas ultimas semanas.

Acknowledgements

Thousand thanks to spread around the following:

Jack Sharp for making a scientist of me by encouraging me to question, ponder and discover. Jerry Lucia for instigating this research project (that probably doesn't look anything like he envisioned a few years ago), for educating me through discussion, and keeping me on track. Charlie Kerans for taking me out to the Algerita for the first time and teaching me the intricacies of sequence stratigraphy, boots on and loupe in hand. Gareth Jones for reminding me to keep my mind open and challenging me to push this project beyond its original reach. My devoted field assistants, Meghan (Ward) Playton, Rob Forkner, Ted Playton, Ryan Phelps, Nabiel Eldam, Alexandra Ponnette, and Keith Nelson. The beloved mentors I've picked up along the road, Luiggi Folk, Xris Kendall, Mitch Harris, and others. Philip Guerrero for helping me manage every expired deadline and paperwork crisis. Dennis Trombatore for being the best geological literature research engine.

The Reservoir Characterization Research Laboratory and its Industrial Associates for funding this project The following grants and scholarship

programs for additional funding: Jackson School of Geosciences and Geology Foundation; American Chemical Society Petroleum Research Fund; Chevron Scholarship; BHP Billiton Petroleum Geoscience Scholarship; American Association of Petroleum Geologists Grants in Aid Program; Geological Society of America Graduate Research Grant; American Association of Petroleum Geologists Southwest Section Graduate Student Scholarship; and American Association of Petroleum Geologists Student Chapter. Finally, the carbonate groups at Shell IEP and Chevron ETC for two productive and fun internship opportunities.

Outcrop-Constrained Flow and Transport Models of Reflux Dolomitization

Beatriz Garcia-Fresca, Ph.D.

The University of Texas at Austin, 2009

Supervisors: F. Jerry Lucia and John M. Sharp Jr.

Two hydrogeologic models explore reflux dolomitization using two outcrop datasets at different scales to constrain transient boundary conditions and heterogeneous petrophysical properties. A platform-scale petrophysical model of the Permian San Andres Formation was built from outcrop and subsurface data following a reservoir modeling approach that preserves outcrop heterogeneity and incorporates a sequence stratigraphic framework. This model was used as input for hydrogeological simulations of hypersaline fluid flow and solute transport during the accumulation and compaction of the platform. Boundary conditions change over time, as relative sealevel fluctuations drive sedimentation, depositional environment migration, topographic gradients, and location, size and

salinity of the brine source. The potential volume and distribution of dolomite formed is inferred by a magnesium mass-balance. The composite result of reflux events at various orders of stratigraphic hierarchy is a complex dolomite pattern that resembles that observed on San Andres outcrops. Dolostone bodies across the platform may be generated by different combinations of favorable conditions, including proximity to the brine source, zones of higher permeability, permeability contrasts, and latent reflux.

A meter-scale reactive transport model of the Albian Upper Glen Rose Formation simulates deposition of three high-frequency cycles punctuated by three brine reflux events. The simulator determines flow, solute and reactive transport along the flow paths, revealing the spatial and temporal distribution of calcite dissolution, and precipitation of dolomite and sulfate. The model recreates fully and partially dolomitized cycles within the time and lithological constrains on Glen Rose outcrops. Our results show that the distribution of dolomite within a high-frequency cycle may be the net result of intercycle processes, whereby dolomitizing fluids sourced from younger cycles flow across stratigraphically significant boundaries. We also show that variations in dolomite abundance and the unfulfilled

dolomitization potential control the contemporaneous propagation of multiple dolomite fronts and the coalescence of discrete dolomite bodies.

Results show that reflux is an effective and efficient mechanism to dolomitize carbonate formations that progresses simultaneously with sediment accumulation. Dolomitization is the cumulative result of many short-lived reflux events, sourced in different locations and times, and amalgamation of successive dolostone bodies. This model contrasts with previous studies that approached dolomitization of a carbonate platform as a discrete reflux event and current interpretations that relate dolomite bodies to their most immediate stratigraphic surfaces.

Table of Contents

List of Tables

List of Figures

List of Plates

Introduction

OUTCROP-CONSTRAINED FLOW AND TRANSPORT MODELS OF REFLUX DOLOMITIZATION

This dissertation addresses early dolomitization of carbonate sediments by brine reflux. The approach followed consists of using outcrop observations and a robust sequence stratigraphic framework to constrain computer models of synsedimentary brine circulation and explore its role on dolomitization.

Background and previous works

Dolomitization is the object of vigorous research as revealed by the large amount of work produced in the last few decades (e.g. Pray and Murray, 1965; Zenger et al., 1980; Zenger and Mazzullo, 1982; Machel and Mountjoy, 1986; Hardie, 1987; Shukla and Baker, 1988; Morrow, 1990a, b; Purser et al., 1994; Warren, 2000; Braithwaite et al., 2004; Machel, 2004). Dolomitization is a common diagenetic process in carbonate rocks and can occur early or late after deposition, in shallow settings or at different stages of burial and, thus, under a broad range of pressures and temperatures. It can also result from a broad range of diagenetic fluid

sources, compositions, and flow regimes, as long as sufficient magnesium can be transported to replace calcium in the crystal lattice. However, dolomite is sparse on modern carbonate environments (Zenger and Dunham, 1980) and experimental failure to precipitate the mineral at low pressures and temperatures (Land, 1998) has led to a poor understanding of the thermodynamics and kinetics of the reactions at the earth surface. It is broadly accepted that dolomitization requires a large source of magnesium and an active hydrogeologic system (Land, 1985). Based on these premises, different dolomitization models have been proposed (Land, 1985; Machel and Mountjoy, 1986; Morrow, 1990b; Warren, 2000; Machel, 2004). The different models imply that different geologic settings and flow regimes result in different extents and geometries of the resulting dolomite bodies (e.g. Wilson et al., 1990; Whitaker and Smart, 1993; Machel, 2004).

This dissertation focuses on the process of reflux dolomitization. “Reflux” was defined by King (1947) as the circulation mechanism of seawater in a lagoon, driven by the density contrasts between seawater flowing into the lagoon and increasingly more saline water landward. Subsequently, Adams and Rhodes (1960) proposed that the seepage of such refluxing brine could result in dolomitization of the underlying sediments.

Throughout this dissertation I use a broader definition for reflux, according to the more current usage of the term (e.g. Jones et al., 2002; Whitaker et al., 2004). It encompasses a variety of styles and scales of synsedimentary dolomitization near the surface by the downward circulation of marine-derived brines. It implies that when restricted seawater evaporates and concentrates, its density increases in comparison to underlying pore fluids. Such a density gradient generates convective circulation of brine, resulting in dolomitization of underlying strata. Described conditions are found in a variety or restricted peritidal environments (e.g. tidal flats, sabkhat, brine pans, coastal salinas, and hypersaline lagoons).

Since the time when Adams and Rhodes (1960) proposed that this mechanism was responsible for the dolomitization of Permian carbonates in west Texas, two questions have arisen: (1) is this mechanism indeed capable of generating the large dolomitized successions described in the rock record? And (2) is it possible to document reflux in modern environments? Reflux is a broadly accepted model for dolomitization of carbonate strata, supported by stratigraphic and petrographic observations (e.g. Lucia, 1972; Montañez and Read, 1992), geochemical analyses (e.g. Leary and Vogt, 1990) and flow modeling (e.g. Whitaker et

al., 2004). Many examples from the rock record demonstrate that reflux can indeed dolomitize large carbonate successions (e.g. Ordovician Red River Fm, Clement, 1985; Ordovician upper Knox Group, Montañez and Read, 1992; Permian Capitan Fm, Melim and Scholle, 2002; Mississippian Madison Fm, Smith et al., 2004, Katz et al., 2007; Upper Jurassic Arab Fm, Swart et al., 2005; Cretaceous Cupido Fm, Altobi, 2007; Cretaceous Upper Glen Rose Fm, Fullmer, 2005, Phelps and Kerans, 2009).

Deffeyes et al. (1965) described dolomitization by refluxing brine on Plio-Pleistocene outcrops in the island of Bonaire, and inferred reflux was currently happening under the hypersaline lake Peekelmeer. That led to active research in pursuit of documenting reflux dolomitization in modern sedimentary environments of the Caribbean (Bahamas, Shinn et al., 1965; Bonaire, Lucia, 1968; West Caicos, Perkins et al., 1994; Floriday Bay, Juster et al., 1997), Persian Gulf (Patterson, 1972; Mckenzie Hsu and Schneider, 1980; Wood et al., 2002), and the Texas coast (Amdurer and Land, 1982; Fenstemaker et al., 2001, Stevens et al., in press). There have been two different approaches to this problem. The sedimentologists' approach has focused on finding settings with modern dolomite, carrying out exhaustive descriptions of the sediments, their mineralogy, stratigraphy, petrography, and geochemistry. Flow regimes were inferred

to explain field observations of water table depths, pore fluid salinity, and dolomite occurrence. Different authors proposed differing flow regimes and dolomitization models for the same setting, and whether or not reflux was taking place was questioned. However, actual flow rates, hydraulic heads and fluid fluxes were not measured or were not measured properly. For example, in order to compute the hydraulic head of fluids of varying salinity, a correction must be applied to account for density effects. Most of the mentioned studies were not completely incorrect, but provided a skewed or incomplete view of the system. Parallel efforts by hydrogeologists succeeded at documenting reflux in modern environments (Amdurer and Land, 1982; Juster et al., 1997; Fenstemaker et al., 2001; Stevens, 2007; Stevens et al., in press). Their results show the transient nature of fluid circulation in modern coastal environments, in general, and the ephemeral nature of reflux, in particular. Fluid flux and direction changes rapidly over time, in response to changing hydrologic regime and climatic factors. When it occurs, density-driven flow is capable of transporting solutes (i.e. magnesium) more efficiently than advective flow alone (Simmons et al., 2001).

However, there appears to be a disconnect between the volumes of dolomite observed in the rock record and the paucity of dolomite

precipitation in modern sedimentary environments (Zenger and Dunham, 1980). Studies of modern environments provide direct observations of ongoing sedimentary and diagenetic processes. However, they represent a mere snapshot in time and do not provide a picture of the finalized product. Outcrop studies, in the other hand, record long-term processes and display the final product, but rely heavily on interpretation for identifying diagenetic processes and their paragenesis. If one assumes modern processes are the key to the past, the missing link must be time. The challenge resides in linking the field observations in modern environments and the rock record. This can be accomplished by understanding the reflux process as a whole, the hydrodynamics and geochemistry of brines, the sedimentology, stratigraphy and geochemistry of sediments, within a prolonged and temporal context. A robust sequence stratigraphic framework provides boundary conditions for modeling synsedimentary diagenesis over time and space.

Certain depositional environments with restricted marine circulation, such as tidal flats, are the source of concentrated fluids capable of dolomitizing carbonate sediments (Lucia, 1968; Patterson, 1972). The position of such environments is constrained by the position of the shoreline and variations in relative sealevel. Lucia (1972) and Lucia and Major (1994) propose that

the migration of such environments in response to relative sealevel fluctuations, allows for these fluids to migrate across the platform and dolomitize the underlying strata. Studies of the rock record also show that specific stratigraphic settings are more favorable to dolomitization than others. Dolomite is more abundant in restricted platform environments and falling sealevel stages, compared to environments with open ocean circulation and rising relative sealevel (e.g. Montañez and Read, 1992). Hypersalinity and concomitant dolomitization may also develop during sealevel rises associated with the formation of restrictive barriers to marine circulation (e.g. Sonnenfeld, 1996; Smith et al., 2004). Thus, fluid circulation through a carbonate platform is controlled by sequence stratigraphic parameters: the duration of favorable conditions for the flow regime to be active depend on the rate of relative sealevel rise and fall; hydraulic gradients depend on relative sealevel position, the topography of the platform top and density gradients resulting from the presence of brines in restricted depositional environments; and porosity and permeability can be related to mud content and, thus, linked to the distribution of specific depositional environments. This study proposes to integrate these premises by means of hydrogeological computer models.

Significant progress has been made in studying the hydrodynamics of refluxing brines using mathematical models. Simms' (1984) carried out the first hydrodynamic analysis of reflux circulation in a carbonate platform and demonstrated its suitability and effectiveness to deliver reactants. He also concluded that mesohaline brine circulation was also capable of delivering enough magnesium to cause pervasive dolomitization in successions with no record of evaporites. Shields and Brady (1995) combined an analytical flow model based on Darcy's Law and a magnesium mass balance to determine dolomitization potential in the Western Canada Sedimentary Basin. Their simplistic hydrogeologic model provides broad constraints on the physical and temporal limits of reflux and concluded that such a flow mechanism has the physical capacity to account for the necessary volumetric flux of brine using geologically reasonable hydraulic conductivities or permeabilities. They recognized the potential relevance of permeability anisotropy and that reflux circulation could be interrupted periodically, for example due to marine transgression or platform exposure.

Kaufman's (1994) simple numerical models simulated a variety of hydrogeological regimes conductive to dolomitization, including reflux circulation. He demonstrated the usefulness of computer simulations

applied to modeling carbonate diagenesis and placed broad spatial and temporal constraints on different mechanisms. Simmons and Narayan (1997) built a numerical model of haline free-convection below a brine-disposal basin. They showed that the brine front movement is related to both the ability of the dense saline fluids to mix convectively with underlying groundwaters and the strength of the regional advective velocity. They concluded that dense brines can reflux and mix with groundwater and travel over distances several orders of magnitude greater than by diffusion alone. Jones et al. (2000) modeled free convection in Enewatak Atoll and studied the opposing effects of geothermal and brine reflux circulation. They showed that reflux can overwhelm geothermal circulation, with flow velocities 1.5 orders of magnitude larger, and used a magnesium mass balance to conclude that both mechanisms contribute to dolomitization of the atoll at a temporal scale of a million years. A model of the Devonian Western Canada Sedimentary Basin (Jones and Rostron, 2000) highlighted the importance of using appropriate boundary conditions and realistic parameters in the model. They also studied the effect of permeability anisotropy on brine circulation. Jones et al. (2002) showed that brines could remain in the subsurface, after the source of reflux has disappeared, and have residence times that are orders of magnitude longer than the duration of

reflux. They called this phenomenon latent reflux and implied that dolomite precipitation and recrystallization may continue at depth in the absence of a coeval reflux source. The Upper Devonian Grosmont platform model of Jones et al. (2003) presents a more realistic platform geometry and boundary conditions than previous studies, including a salinity gradient on platform top, simulating four stages of platform accumulation and heterogeneous permeability values. They used relatively high permeability values and a magnesium/calcium exchange efficiency of 100%, however, simulated flow rates were not sufficient to pervasively dolomitize the platform. Jones et al. (2004) carried out simulations of geothermal and reflux circulation in a generic platform model to identify critical parameters that control reflux dolomitization. This study placed general constraints in the following parameters: salinity, temperature, permeability, permeability anisotropy, and latent reflux. Whitaker et al. (2004) assess the dolomitization potential of different circulation systems. They propose that fluid flow is the product of simultaneous drivers and that the balance between them changes over time. Thus, they conclude that dolomite geometry cannot be predicted based on a steady state set of boundary conditions.

The above hydrodynamic studies rely on a simplistic magnesium mass balance to address dolomitization. A magnesium/calcium replacement efficiency coefficient is used to account for a variety of geochemical and biochemical aspects of dolomite precipitation. This approach does not adequately represent the geochemical complexity of diagenetic processes. Fluid-rock interaction results in the precipitation and dissolution of minerals along flow paths and the concomitant feedbacks on brine composition and petrophysical properties which, again, influence fluid flow. Such complex relationships can be explored using reactive transport models, a technique increasingly being applied in geosciences to address a variety of geological problems including CO_2 sequestration, characterization of groundwater contamination and remediation, geothermal systems, metamorphic alteration (e.g., Lichtner et al., 1996; Steefel et al., 2005) and dolomitization (Wilson et al., 2001; Jones and Xiao, 2006; Xiao and Jones, 2006). Jones and Xiao (2005) built a two-dimensional model of reflux to study the spatial and temporal distribution of replacement dolomite, dolomite cement, anhydrite cement and porosity. They identified and placed broad constraints on the principal controls: fluid concentration, temperature, flow rate, reactive surface area, permeability heterogeneity heterogeneity, and porosity/permeability feedbacks. Xiao and Jones' (2007) simple model of reflux reveals the complexity of reflux

circulation and dolomite/anhydrite patterns in three dimensions, for a homogeneous permeability distribution.

It is important to note that some of these models the petrophysical properties controlling fluid flow are homogeneous and isotropic, which does not reflect natural variability observed in rocks. Some of them have questionable boundary conditions. In some of them, reflux is approached as a single fluid circulation event affecting a carbonate platform at a particular time, ignoring the transient nature of boundary conditions due to sediment accumulation, sealevel fluctuations, and the concomitant migration of depositional environments. As a result, some of these models demand large temporal scales and/or high permeability values.

The hydrogeological simulations presented here are based on petrophysical models that reflect heterogeneity at the scale of interest. Heterogeneity and anisotropy in the permeability field has major effects on flow and transport in porous media (e.g. Schincariol and Schwartz, 1990; Kerans et al., 1994; Simmons et al., 2001; Jennings, 2000; Jones and Xiao, 2005). These parameters cause flow paths to deflect with respect to hydraulic gradients, generate complex circulation patterns, and disperse the transport of solutes. A major cause of heterogeneity in a carbonate

strata is stems from the various fabrics of sedimentary facies (Lucia, 1995). Kerans et al., (1994) showed that inverting the direction of flow in a reservoir model with a heterogeneous permeability field results in different flow patterns. Simmons et al., (2001) and Shi (2005) showed that the onset, growth, and decay of saline fingers are closely related to the structure of the heterogeneity of the permeability field. A critical cause of anisotropy is the stratigraphic layering of fabrics, which imposes strong permeability contrasts to vertical flow. In the case of density-driven flow, layered heterogeneity may cause saline plumes to pond at permeability contrasts and force them to flow downdip along the contact, whereas lenticular heterogeneity may disperse saline plumes (Schincariol and Schwartz, 1990).

Heterogeneity in the permeability field occurs at all scales of observation. Sudicky (1986) proposed that heterogeneity at the scale of tens to hundreds of meters is important in controlling advective flow, whereas heterogeneity at the centimeter-to-meter scale controls dispersion. Thus, values should be estimated at scales appropriate to the particular problem. Estimating new values for a property at increasing scales is known as “upscaling”. Sudicky (1986) highlighted the relevance of incorporating geological data in characterizing heterogeneity and flow in

aquifers. This was sufficiently proven by studies that combine outcrop observations of permeability distributions (facies variations and bedding) into reservoir performance simulations (e.g. Hinrichs et al., 1986; Lucia et al., 1992a; Eisenberg et al., 1992; Kerans et al., 1994; Wang et al., 1994; Grant et al., 1994; Eisenberg et al., 1994; Jennings et al., 1998; and Jennings, 2000). These studies present statistical analyses of high-resolution outcrop permeability measurements that show several scales of heterogeneity of permeability in two dimensions, and conclude that rock fabric bodies are the representative elementary volume (Bear, 1972) at the reservoir scale. Lucia (2007) postulated that a sound geologic model for reservoir performance simulations should incorporate a chronostratigraphic framework and information on the processes that form and modify petrophysical properties. He proposed the following steps in constructing such petrophysical model: 1) relating rock fabrics to petrophysical parameters (Lucia, 1995), 2) identifying the geological processes that generated those fabrics, 3) describing a sequence stratigraphic framework based on high-frequency cycles, and 4) distributing petrophysically significant rock-fabric bodies within the stratigraphic framework.

Petrographic and geochemical studies are commonly used to study dolomitized rocks. However, the present character of a dolomite does not reflect that of the precursor carbonate and/or dolomitizing fluid (Land, 1980) but the cumulative diagenetic effects that operated throughout the history of the rock. Most ancient dolomites have undergone early stabilization and multiple episodes of recrystallization and, thus, their trace element and isotopic signatures are changed in this process. It depends on the chemistry of the precursor carbonate, the chemistry of the interacting fluids, and the extent of fluid-rock interaction (Banner, 1995). Regional and covariant trends in the composition of trace elements, isotopes of oxygen, carbon and strontium, and fluid inclusions, together with detailed petrographic studies, help recognize different types of dolomite within a formation, the evolution between end-member minerals and fluids, locate fluid sources and delineate pathways, and study fluid-rock interaction processes (Kupecz et al., 1983; Banner, 1995; Warren, 2000; Banner, 2004). Some general trends are observed (Kupecz et al., 1983; Warren, 2000): as recrystallization of dolomite progresses crystal size tends to increase; the number of crystal faces decreases; the stoichiometry and atomic ordering increases; the mineral gets depleted in $\delta^{18}O$, strontium and sodium, and enriched in iron and manganese; and the strontium isotopic composition may be inconsistent with the age of the

rock. Differences in cathodoluminescece may also help identify growth stages or dolomite types (e.g. Banner et al., 1988). Spatial variations in stoichiometry may also provide a tool to explore the history of recrystallization.

Stratigraphic, sedimentologic, petrographic and geochemical studies indicate that the bulk of San Andres dolomite was formed soon after deposition by refluxing brines and was probably recrystallized by younger fluids. Figure 0.1 shows photomicrographs, in transmitted parallel light and cathodoluminescence, of San Andres Formation dolostone from Pot Hole Tank section (Figure 2.2) in the Algerita Escarpment. The principal dolomite phase is matrix replacive and has a range of crystal sizes and habits. Crystal sizes range from <10 to 100 microns. Mudstones and wackestones (Figure 0.1a, c and d) have finer crystal sizes relative to packstones and grainstones (Figure 0.1b). Crystals are cloudy because of fluid inclusions, non-planar to planar-S in habit (sensu Sibley and Gregg, 1987) and are fabric destructive. Crystals become less planar as crystal size increases. Under cathodoluminescence the crystals show no zoning and are dully-luminescent dark red color (Figure 0.1a, b), which is indicative of a high content of quenching trace elements such as iron. Pore types include intercrystalline and moldic pores of dissolved skeletal

allochems, which are sometimes filled with blocky dolomite. These dolomite crystals are limipid, planar-S to planar-E habit, and range in size from 100 to 200 microns. Their luminescence is the same as the cloudy dolomite and no zoning is observed other than, perhaps, a very thin more luminescent rind (the poor quality of the polishing made it impossible to discriminate whether it was indeed an overgrowth or the relief of the crystal). These limpid crystals are much less abundant than the cloudy crystals and could have formed later. Similar petrographic characteristics are common for San Andres dolomites in outcrop (Kerans et al., 1994) and subsurface (e.g. Ruppel and Cander, 1988a; Fogg and Lucia, 1990; Lucia et al., 1992b).

Given and Lohmann (1985) derived the isotopic composition of Permian marine cements (Figure 0.2), which should approximate those of Permian seawater. Stable oxygen isotope of seawater-derived dolomites tend to be enriched in comparison to contemporaneous calcites (Land, 1980). $\delta^{18}O$ and $\delta^{13}C$ for San Andres and adjacent formations is compiled in Figure 0.2. San Andres dolomites are enriched in $\delta^{18}O$ and $\delta^{13}C$ values compared to seawater, which is consistent with dolomites generated from fluids derived from evaporated seawater (Warren, 2000). According to Ruppel and Cander (1988a, b) and Leary and Vogt (1990) diagenetic events that

can be recognized in the Central Basin Platform include an early dolomitization event immediately after deposition, either replacing primary carbonates or by stabilization of non-stoichiometric penecontemporaneous dolomite; a second more pervasive dolomitization event attributed to the seepage of brines at gypsum saturation, soon after deposition but possibly before compaction and burial diagenesis; formation of replacive and pore-filling anhydrite postdating dolomitization; and meteoric diagenesis related to Tertiary uplift. Melim and Scholle (2002) proposed that mesohaline brines derived from the backreef lagoon dolomitized the reef and forereef facies of the overlying Guadalupian Capitan Formation. In this overlying succession, older units are more dolomitized, indicating they underwent more episodes of reflux than the less dolomitized younger part of the section. Their petrographic and stable isotopic data shows a continuum of fabrics and compositions between the fabric preserving (main phase) and fabric destructive (less abundant) dolomite, suggesting progressive recrystallization of the former over time. The authors also concluded that dolomitization by fluids from overlying evaporitic Ochoan units was probable, but volumetrically of less relevance. A number of studies of the evaporitic successions of the San Andres Fm of the Palo Duro Basin in north Texas were carried out by Bein and Land (1982), Hovorka (1987), Bein et al. (1990), Gao et al. (1990). They conclude that the dolomitizing

fluid was probably derived from evaporation of seawater. A similar paragenesis is proposed by Colgan (1990) for the Algerita Escarpment (Figure 0.3) as follows: 1) micritization; 2) early cementation; 3) compaction; 4) dolomitization; 5) evaporite precipitation; 6) allochem dissolution; 7) silicification; 8) evaporite dissolution; 9) calcite precipitation; 10) dedolomitization and collapse brecciation; and 11) kaolinite precipitation.

Contributions of this study

In this dissertation, I address reflux dolomitization using computer models constrained by outcrop data and containing petrophysical heterogeneity. I address the stratigraphic controls on brine circulation and the transient boundary conditions responding to relative sealevel fluctuations over the deposition of carbonate formation. The principal contributions of this work include:

1. It is the first study to use a reservoir modeling approach to convert outcrop and subsurface data into a digital petrophysical model.
2. I use a sophisticated heterogeneous petrophysical model as input for hydrogeologic simulations.

3. Although other workers have explored reflux circulation using numerical models, this study is the first to address reflux as a synsedimentary process. I accomplished this by using a sequence stratigraphic framework to constrain the evolving boundary conditions for hydrogeologic simulations.

4. I demonstrate that stratigraphic surfaces and dolomite geobodies may not be concordant in time nor in space, as suggested by current paradigm.

5. I link platform-scale and high-frequency cycle-scale models of reflux.

Hypotheses

The hypotheses considered through this dissertation are the following:

1. Reflux is an effective mechanism to dolomitize large carbonate successions; concentrated seawater can efficiently circulate through sediments driven by both topographic and density gradients and deliver reactants for dolomitization.

2. Dolomite patterns can be explained by integrating sequence stratigraphy, sedimentology, petrophysics, hydrogeology, and geochemistry.

3. The source of dolomitizing brines has a transient behavior, it may turn on and off, shrink and grow, and have variable residence times depending on the migration of depositional environments in response to relative sealevel fluctuations. Thus, brine reflux pulses can be interpreted according to sequence stratigraphic principles.

4. Reflux is a process that operates simultaneously with the accumulation of a carbonate platform, rather than one discrete event.

5. Reflux events may occur in nested scales, mimicking stratigraphic hierarchy.

6. Several fluid pulses can coalesce and continue to dolomitize at depth, cutting through stratigraphic surfaces and facies boundaries.

Approach

The general approach of this study consists on integrating sequence stratigraphy, sedimentology, petrophysics, geochemistry, and hydrology to explore the dynamics of reflux. Outcrop-based geologic models are used to construct petrophysical models to be used in hydrogeologic simulations of synsedimentary brine reflux. I use observations from modern settings to supplement those from the rock record. Current rock fabrics are correlated to facies and environments in which they were deposited and, thus, one can assign them values of petrophysical properties of modern carbonate

sediments. The geologic model provides boundary conditions for the hydrogeologic modeling: stratal geometry; relative sealevel position; location, extent, and concentration of fluid sources; and spatial distribution of facies and petrophysical properties. These parameters change over time and can be constrained by sequence stratigraphic principles. We used outcrops of two formations to constrain our computer models: the Permian San Andres Formation in west Texas and New Mexico, and the Albian Upper Glen Rose Formation of central Texas.

San Andres Formation model summary

I used measured sections of San Andres Formation outcrops to construct a platform-scale model for hydrogeologic simulations. Petrophysical properties based on facies descriptions at the sub-meter scale required significant upscaling, which was accomplished using Lucia's (2007) reservoir modeling approach. Facies were grouped according to vertical successions of similar permeability. Such packages were correlated laterally between measured sections to generate modeling layers and petrophysical properties were averaged within each layer. Averages were grouped into six categories and the average porosity and permeability of each group was used to define six rock types. This approach resulted in a petrophysical model that respects the chronostratigraphic framework of

Kerans and Kempter (2002) and preserves a degree of heterogeneity of petrophysical properties that is appropriate for hydrogeologic simulations at the platform scale.

I used this model to simulate fluid circulation and solute transport through the San Andres platform using the code Basin2 (Bethke et al., 2002). The model simulates the accumulation of the platform over time and, thus, it has transient boundary conditions: the thickness of the platform varies as sediment accumulates and compacts, hydraulic gradients vary as the geometry and topography of the platform evolves, the size and extent of the brine source changes in response to shoreline migration, and the heterogeneously distributed petrophysical properties change as a consequence of compaction. Then, the potential amount of dolomite that could be generated was calculated by means of a magnesium mass balance, on the basis of simulated time, salinities, and flow rates.

Upper Glen Rose Formation model summary

The Upper Glen Rose Formation was used to build a meter-scale model of reflux using Fullmer's (2005) outcrop descriptions and petrophysical reconstruction of an idealized high-frequency cycle. Because of its relative simplicity, no upscaling was required for the petrophysical properties. The

reactive transport simulator TOUGHREACT (Xu et al., 2005) was used to recreate several cycles of sedimentation and reflux circulation along one flow path. Dolomitization is calculated based on density-driven brine flow, solute transport and mineral dissolution and precipitation reactions.

Dissertation structure

This dissertation is organized in four parts, contained in chapters 1 through 4. Chapter 1 is a study of San Andres Formation lithologies in the subsurface, using well logs, that allowed us to reconstruct the San Andres Formation eroded from outcrop, which is also the interpreted source of dolomitizing fluids. Chapter 2 describes the process of building a platform-scale geological and petrophysical model of the Permian San Andres Formation based on outcrop data and using a reservoir modeling approach. Chapter 3 reports the hydrogeologic simulations of brine circulation and solute transport during the accumulation of the San Andres platform and its implications for the synsedimentary dolomitization of the formation. Chapter 4 recounts the reactive transport simulations based on the Albian Upper Glen Rose Formation outcrops at the high-frequency cycle scale. The final section summarizes the conclusions of the previous chapters and puts this research into a broader prospective.

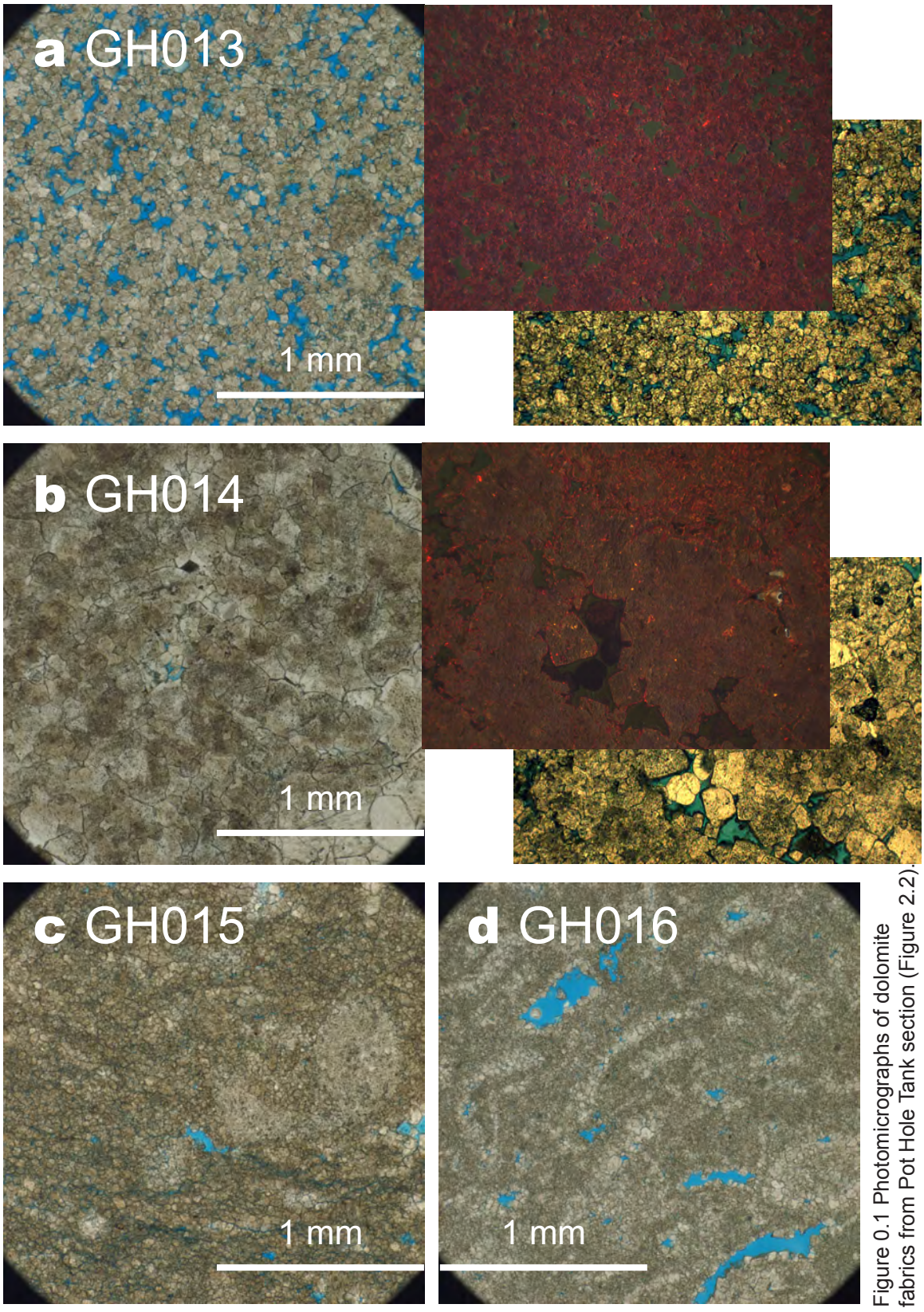

Figure 0.1 Photomicrographs of dolomite fabrics from Pot Hole Tank section (Figure 2.2).

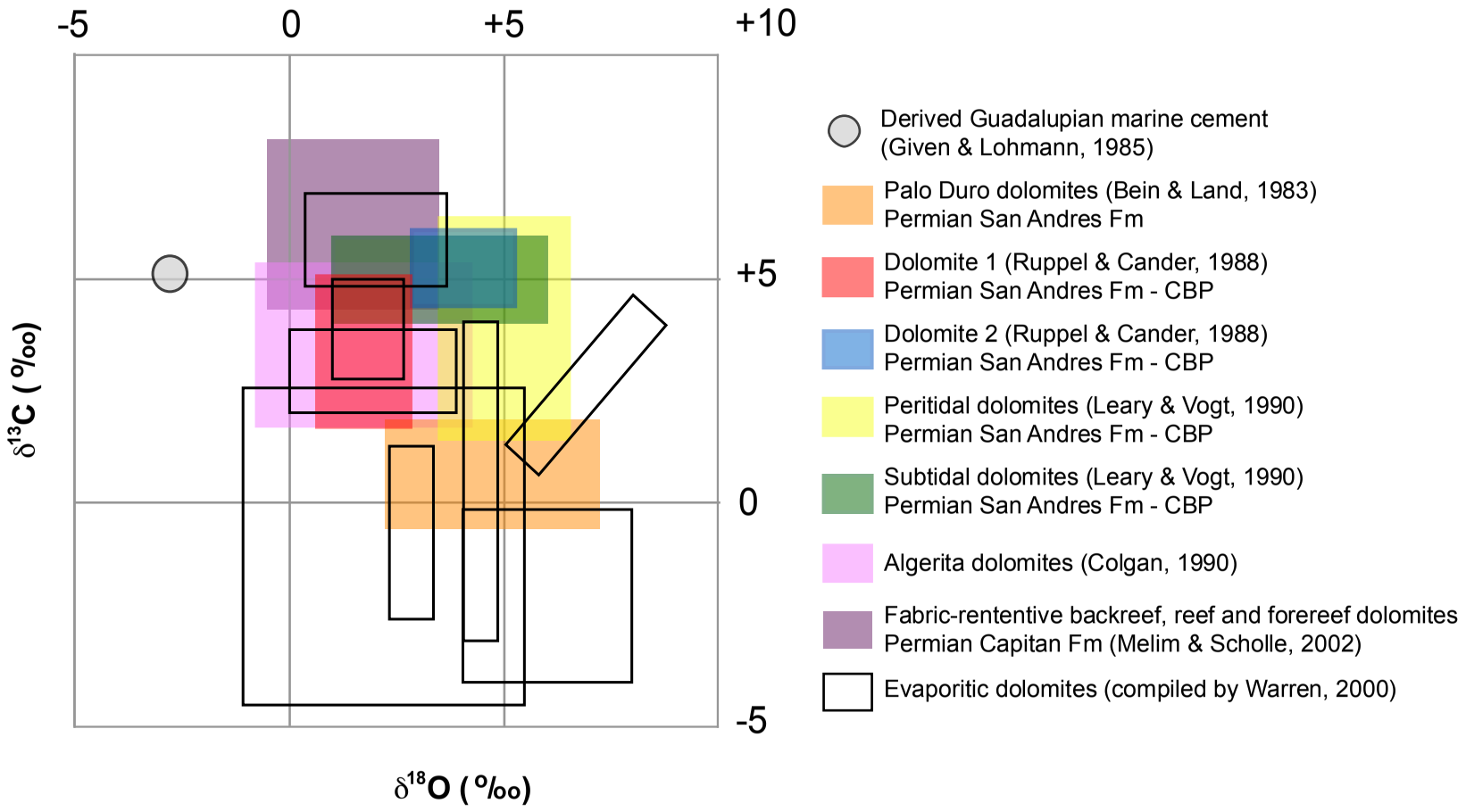

Figure 0.2: Oxygen and carbon isotope values for San Andres dolomites in the Palo Duro evaporitic basin, the Central Basin Platform, and the Algerita Escarpment, compared to values for evaporitic dolomites compiled by Warren (2000)

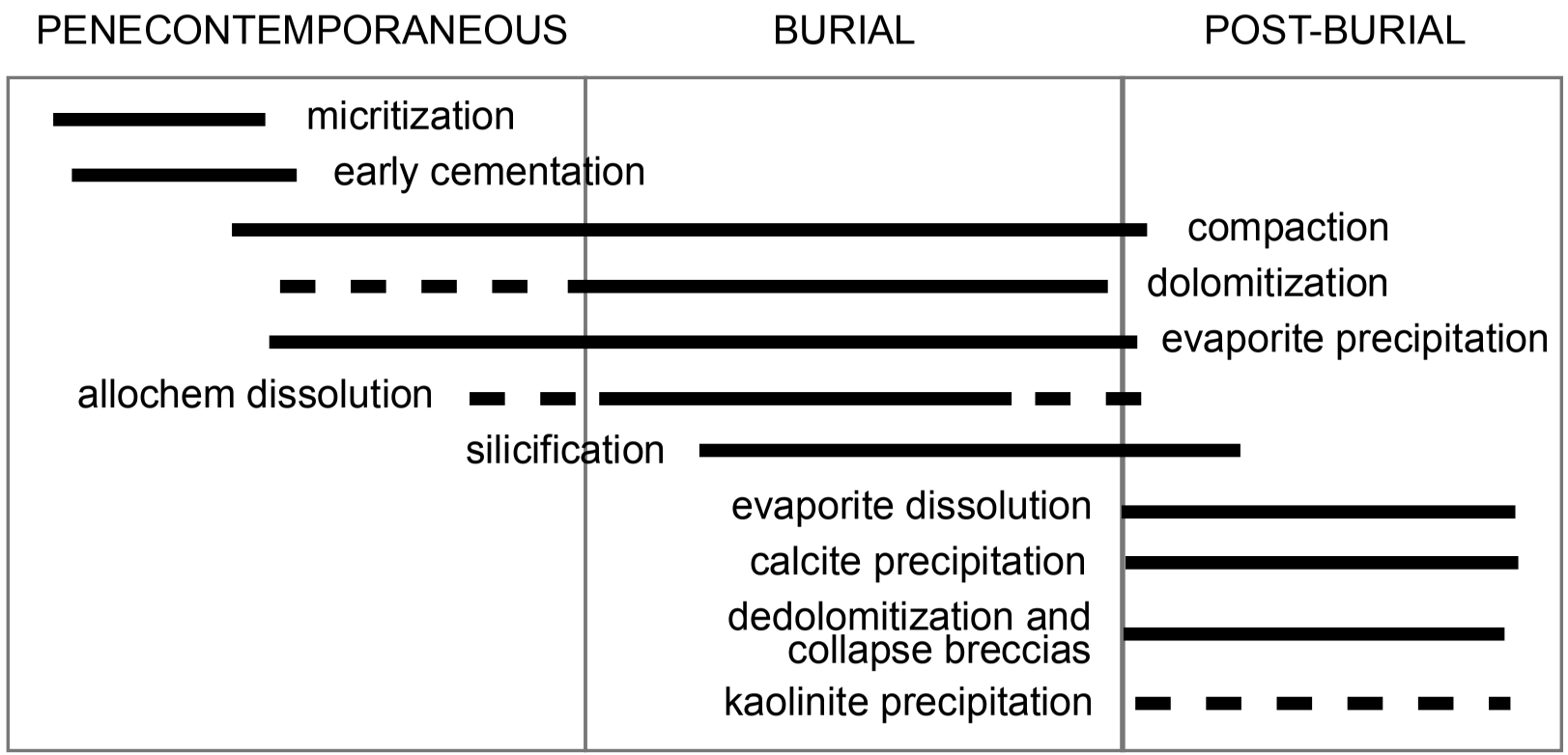

Figure 0.3: Diagenetic events in the San Andres Fm (after Colgan, 1990)

Chapter 1

OUTCROP AND SUBSURFACE COMPARISON OF LITHOLOGY DISTRIBUTION IN THE PERMIAN SAN ANDRES FORMATION: IMPLICATIONS FOR A DOLOMITIZATION MODEL

Abstract

This study presents a comparison of outcrop and subsurface lithologies in the Permian San Andres Formation. Outcrop and subsurface datasets provide comparable distributions of limestone, dolostone and siliciclastics. Additionally, anhydrite is also present in the subsurface but has been eroded away from the outcrop. Outcrop data will be used to construct a petrophysical model to be used in hydrogeological simulations of reflux dolomitization. Subsurface interpretations provide information to reconstruct parts of the outcrop that have been eroded away.

Prediction of dolostone patterns requires knowledge of the hydrology of dolomitizing fluids. Reflux seepage of evaporated seawater is one the mechanisms invoked to explain dolomitization in restricted carbonate settings. Although this conceptual model is broadly accepted, the hydraulics are poorly understood. I hypothesize that the source of

dolomitizing fluids was located in coastal carbonate depositional environments (tidal flats) and that a hydrologic model can be constructed on the basis of tidal-flat-related paleotopography and permeability distributions based on facies and rock types. This study focuses on the Permian carbonate/evaporite succession of the San Andres Formation because it is often presented as an example of reflux dolomitization.

The flat geometry of the San Andres platform suggests that the dolomitizing fluids sink a short distance under the intertidal zone then travel horizontally for long distances following the bedding. The low permeability of mud-rich facies dominating the limestone wedge or higher permeabilities of grainier facies in the middle to outer platform may be the cause of such dolomite distribution.

Introduction

King (1947) defined "Reflux action" as the seaward escape of dense brine generated in the inner platform by evaporation. Adams and Rhodes (1960) consolidated the "refluxion theory" by studying the bedded dolostones of the Permian Basin. On the basis of their association with evaporites, as well as regional mapping of depositional and diagenetic relationships, the authors concluded that restriction, evaporation, and seepage of brines on

a hypersaline lagoon was the mechanism by which calcium in aragonite and high-magnesium calcites was replaced by magnesium in these carbonate successions. Reflux dolomitization has withstood the test of time, unlike other dolomitization models. It has been widely invoked as the dolomitization mechanism of carbonate successions around the world spanning thought the Phanerozoic, especially, but not exclusively, when in association with evaporitic deposits. Theoretical and analytical studies have also been carried out for many decades. Hydrogeological numerical modeling is one of the more recent techniques used to approach this problem (e.g. Kaufman, 1994, Jones et al., 2003). Most of these numerical studies simulate dolomitization of the whole platform in one or limited number of steps and require large periods of time and large permeabilities or fluid rates.

This study analyzes reflux at the high-frequency cycle scale; it combines numerical models and petrographic analysis within a sequence stratigraphic framework. The object of the study is the San Andres Formation, which has often been invoked as an example of dolomitization by reflux and has been extensively studied.

The San Andres Formation

The San Andres Formation is a succession of carbonates and evaporites deposited in a broad, flat, and shallow marine setting, under arid climatic conditions. It spread over most of New Mexico and north and west Texas (Figure 1.1). Meissner's (1972) regional study describes the main depositional systems and lithologies (Figure 1.2). The most restricted areas of the platform were covered by salinas where halite, anhydrite, and carbonates were deposited. The Tucumcari and Palo Duro Basins (in New Mexico and Texas, respectively) are examples of this setting. Seaward of the evaporitic basin less restricted conditions gave way to development of a carbonate depositional environment, which is termed in this paper "the carbonate platform" or simply "the platform" and the focus of this study. Preliminary regional-scale hydrogeologic models showed no regional groundwater flow between the evaporitic basin and the carbonate platform that could have contributed dolomitizing fluids to San Andres carbonates.

The *type section* and *reference section* for the San Andres Formation were revisited and redescribed by Lindsay (1994). They are located in the San Andres Mountains, near Alamogordo, New Mexico, within the limits of the White Sands Missile Range, and are not readily accessible. Unfortunately, both sections are located in the evaporite-rich interior of the

carbonate platform and, thus, much of the formation has been eroded away. Inner platform to platform margin outcrops are beautifully exposed along the Algerita Escarpment, Brokeoff Mountains, and Western Escarpment of the Guadalupe Mountains and have been studied since the 1940's.

Understanding the sedimentology and sequence stratigraphy of the San Andres carbonate platform provides the high-resolution framework for numerical modeling of reflux and dolomitization in this formation. A preliminary field study of the lithology in the Algerita Escarpment, Brokeoff Mountains and Western Escarpment of the Guadalupe Mountains (Figure 1.3) showed dolostone/limestone relationships similar to those described by Meissner (1972). However, the anhydrite-rich peritidal deposits, allegedly the source of the dolomitizing brines, have been selectively eroded from outcrop. I have assembled an equivalent cross section from wire-line log data to reconstruct the part of the platform that is missing on outcrop.

Outcrop studies

World-class exposures of the San Andres Formation occur along the Western Escarpment of the Guadalupe Mountains, Last Chance Canyon,

Brokeoff Mountains, and Algerita Escarpment (Figure 1.4). They have been the subject of multiple studies in the last decades and the stratigraphy and sedimentology are very well constrained.

King (1948) produced one of the earlier descriptions of the Permian outcrops in the Guadalupe Mountains and correlated the lower San Andres Formation of the Algerita Escarpment with the upper Victorio Peak and Cutoff Formations of the Western Escarpment. This was followed by Boyd's (1958) study of the upper Victorio Peak and Cutoff Formations at the San Andres platform margin and their complicated relationship with the Cherry Canyon Tongue. Hayes (1964) carried out detailed regional mapping of the San Andres and Grayburg Formations and identified the principal unconformities. Sarg and Lehman (1986) developed the first comprehensive sequence stratigraphic study of the San Andres Formation in the Algerita Escarpment. Detailed descriptions and further studies of the formation in the outer platform to platform margin (Algerita Escarpment to Guadalupe Mountains) were carried out, among others, by Sonnenfeld (1991), Kerans and Ruppel (1994), Kerans and Fitchen (1995), Kerans and Tinker (1999), and Kerans and Kempter (2002) (Figure 1.5).

The present study adopts the sequence stratigraphic model described by Kerans and Fitchen (1995) and Kerans and Kempter (2002), which divides the San Andres Formation into lower and upper composite sequences of 1- to 2-Ma duration (Figures 1.4 and 1.5). The composite sequences are subdivided into six and two carbonate high-frequency sequences respectively. The lower composite sequence consists of the high-frequency sequences labeled Leonardian 6 and 7 and Guadalupian 1 through 4. L6, L7, and part of G1 form the transgressive systems tract of the lower San Andres composite sequence whereas G1-4 form the highstand systems tract. The top of G4, which is karst-modified, provided a bypass surface for lowstand siliciclastics into the basin during a major sealevel lowstand. The upper composite sequence includes the lowstand basinal high-frequency sequences of the Brushy Canyon Formation (G5-7) and the carbonate high-frequency sequences Guadalupian 8 and 9 (Figure 1.5). The geometry of the San Andres platform evolved from a distally steepened platform (L7 and L8), to a progradational sigmoid clinoform platform (G1-4), to oblique clinoform platform (G8), and finally a rimmed shelf (G9). The G9 high-frequency sequence has a siliciclastic-rich base, known as the Cherry Canyon Tongue, that passes into the basinal Cherry Canyon Formation.

Plate 1 shows outcrop lithologic relationships. This cross section is based on field descriptions by the author, as well as the data of Kerans and Fitchen (1995). The limestone-dolostone contact in the inner-platform wedge is sharp (Figure 1.6). Field mapping of the contact indicates that the stratigraphic position and facies at which it occurs varies from section to section and, thus, cuts time-lines and is facies independent.

Under closer inspection, the limestone/dolostone transition reveals a gradual character for approximately ten meters below the main contact. Dolomitized haloes around bedding planes suggest that bedding planes are conduits for dolomitizing fluids. Dolomitizing fluids could travel along bedding planes for large horizontal distances preventing the dolomitization of the lower San Andres formation in this part of the platform. Dolomitized pockets are also common below the main contact suggesting downward percolation of dolomitizing fluids (Figure 1.7). I hypothesize that these are formed by (1) free-convective vertical fluid flow driven by density differences between the dolomitizing plume and the formation pore fluids, or (2) fluid flow following a high-permeability zone such as, for example, a fossil debris accumulation. Grain-rich facies are more abundant in the middle portion of the carbonate platform (Kerans and Fitchen, 1995).

Concentration of high permeability facies may play an important role on the pervasive dolomitization of this part of the platform.

Subsurface cross section

An examination of subsurface data provides information about the along-strike distribution of lithologies in the San Andres Formation. It also allow to reconstruct the younger sequences of the inner platform that have been eroded from outcrop. The Permian section exposed in the Guadalupe Mountains dips eastward and quickly disappears in the subsurface (Figure 1.3). The transect runs as near the outcrop exposures as possible and extends from Carlsbad through Artesia and on to Roswell, New Mexico. The resulting cross section is shown in Plate 1.

The wireline logs selected are the gamma-ray radioactivity, neutron porosity, and density. The overlay between neutron porosity and density provides a simple tool for classifying main lithologies in the studied section: anhydrite, dolostone, limestone, and siliciclastic sands (Schlumberger, 1989). The gamma-ray helps to differentiate between clastics and carbonates and was key to identifying the bottom of the formation, which is characterized by a group of "hot" gamma-ray signals know as the Glorieta Formation.

Although most of the formation is composed of dolostone, other lithologies are distributed as follows. Bedded anhydrite is found on the upper portion of the formation. Its abundance and bed thickness decreases gradually from the inner platform towards the outer platform, and it is virtually absent at the platform margin. Some anhydrite can also be found below the Glorieta Sand, in the peritidal succession of the Yeso Formation.

Limestone is found in the inner platform, making up at least half of the section, the other half being interbedded anhydrite and dolostone. The amount of limestone decreases as a wedge towards the south and pinches out in the middle platform. Another limestone wedge is located below the platform margin.

The platform margin is composed of the upper Victorio Peak Formation limestones, overlain by a siliciclastic-rich succession. A thin sand, which extends landward for some distance from the margin, is known as the Lovington Sand (Cherry Canyon Tongue in outcrop).

Outcrop and subsurface comparison

Outcrop and subsurface lithologies are compared in Plate 1. Both cross sections show good agreement on geometries and dimensions of the

limestone wedges, peritidal anhydrite/dolostone cycles, the sandstone tongue in the G9 high-frequency sequence, and the position of the youngest platform margin. Breccias are often found in the uppermost part of the outcrop, within the shallowest facies successions. I interpret these breccias to have originated by the dissolution of evaporite beds and that the eroded interval coincides with the anhydrite/dolostone cycles observed in the subsurface (Figure 1.8). The interpreted anhydrite/dolostone cycles from the subsurface study can, thus, be used to reconstruct the eroded part of the outcrop.

Anhydrite/dolostone peritidal cycles

Understanding the sedimentology, petrography, and stratigraphy of the peritidal zone is indispensable to design a hydrologic model of the dolomitizing fluids that utilizes realistic hydraulic properties and time constraints (Lucia, 2007). The peritidal succession of the San Andres Formation is composed of cyclic dolostone and bedded anhydrite. Figure 1.9 shows representative images of the upper 150 meters of the San Andres Formation at four locations. The anhydrite/dolostone cycles become thinner and less abundant toward the outer platform (Figure 1.9A-C). Anhydrite is absent as we approach the platform margin (Figure 1.9D) and a thin sand bed can be correlated across for a few miles. Interestingly,

lack of anhydrite/dolostone cycles coincides with the pinch-out of the platform margin limestone wedge (Plate 1). Cycle thickness decreases upward, towards the top San Andres sequence boundary. And idealized anhydrite/dolostone cycle is shown in Figure 1.10.

I interpret that anhydrite/dolostone cycles at the top of the San Andres Formation were deposited subaqueously in very restricted shallow subtidal to supratidal environments. Single anhydrite beds can occasionally be correlated from well to well over distances of several kilometers, indicating that they were broad and occassionally continuous feature. Anhydrite was possibly deposited in isolated supratidal ponds that were occasionally recharged by seawater storm flooding. The dolostone part of the cycle is interpreted as an upward progression from subtidal to supratidal carbonate mudstones and most likely included cyanobacterial laminites. Scarce evaporite-removal breccias are the only outcrop expression of these cycles.

Implications for a dolomitization model

Previous studies demonstrated the suitability of reflux of dense, seawater-derived hypersaline brines to deliver the fluid and reactants necessary for dolomitization. Oceans are virtually an inexhaustible source of fluid and

seawater contains large amounts of magnesium. Thus, seawater is a viable candidate as the principal source of dolomitizing fluids (Land, 1985; Carballo et al., 1985). Lucia (1972), Montañez and Read (1992) and Fullmer (2005) demonstrated the importance of relative sealevel fluctuations and shoreline migration on dolomitization. Marine transgressions cause the landward migration of the shoreline and shift of depositional environments, flooding and shutting down of preexisting brine sources. Regressions, however, cause the seaward shift of depositional environments sourcing dolomitizing fluids. Fluid density increases with salinity and the specific configuration of density gradients play an important role in the transport of fluids and solutes. A denser fluid that overlies a less-dense fluid is gravitationally unstable and often results in downward movement (or free convection) of the denser fluid into the underlying less-dense fluid. Such circulation causes the mixing of fluids more rapidly and over longer distances than does diffusion alone (Simmons and Narayan, 1997).

I hypothesize that dolomitization of the San Andres Formation took place during the last half of San Andres time, which was characterized by a shallow inner shelf rimmed by cyanobacterial mats in the intertidal zone and broad saline ponds in the supratidal zone where evaporation was

intense (Figure 1.11). The ponds were recharged occasionally by seawater during storm flooding events. Flood recharge and evaporation rates were sufficient for deposition of bedded anhydrite. This supratidal complex experienced strong progradation at the end of the deposition of high-frequency sequence G4, a time of maximum sealevel drop and subaerial exposure of the platform (Kerans and Fitchen, 1995). Significant progradation is also observed during deposition of high-frequency sequences G8 and G9. Such shoreline migration, especially during progradation, results in the superposition of the high-salinity environments over subtidal sediments of normal marine salinity. This creates a density gradient that may lead to the free convection of the dense brines into the underlying sediments. I use numerical simulations to determine rates and volumes at which this mechanism can deliver fluids and magnesium resulting in dolomitization patterns observed today in the San Andres Formation.

On the basis of this conceptual model I am constructing a numerical model that will simulate density-driven flow as the peritidal succession is deposited. Such numerical simulations allow to evaluate volumes and fluxes of dolomitizing fluids, relative timing of dolomitization, and effects of superimposing dolomitization events.

Conclusions

The San Andres Formation provides a real-scale physical model to identify the sedimentologic and stratigraphic constrains on dolomitization by reflux seepage.

Peritidal cycles in the upper part of the San Andres Formation are hypothesized to be the sources of the dolomitization fluids. This part has been eroded away from the outcrop. I have built a subsurface cross section in the vicinity of the studied outcrops that allows to successfully reconstruct the missing outcrop.

Understanding the sedimentologic and stratigraphic constraints in a real example is indispensable for building a realistic model of dolomitization. It should provide the geometry, timing, and hydraulic properties for a numerical simulation of the hydrologic system that would lead to the dolostone/limestone patterns observed in San Andres outcrops.

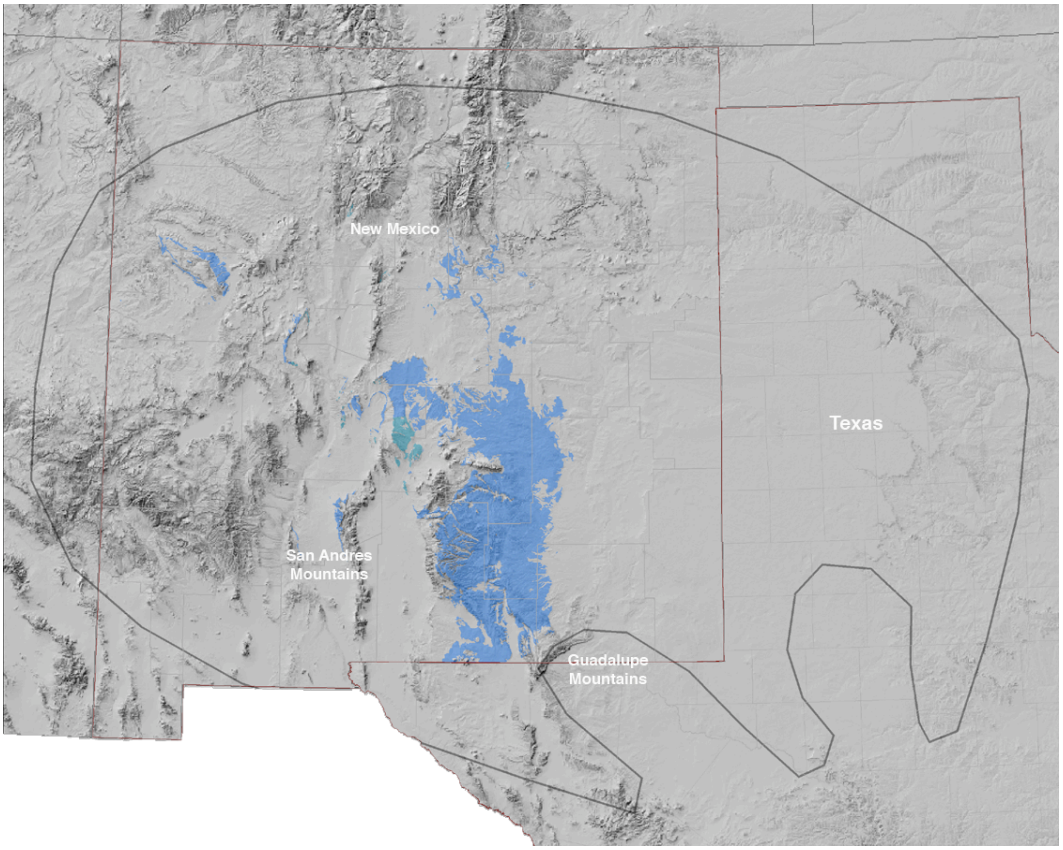

Figure 1.1: Approximate extent of the San Andres Formation in Permian time (after Kerans and Fitchen, 1995) and distribution of outcrop remains, in blue (source: New Mexico Bureau of Geology and Mineral Resources GIS Service).

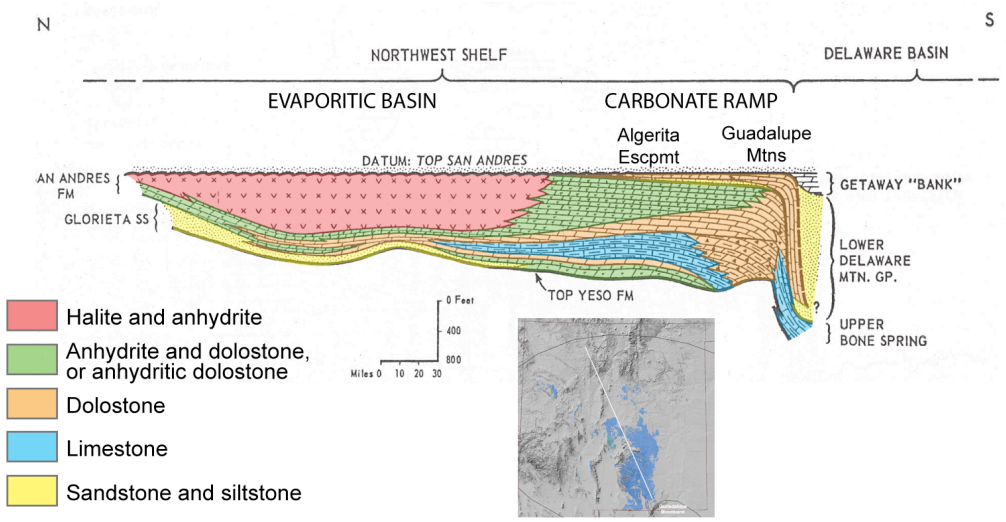

Figure 1.2: Regional cross section of the San Andres Formation. This study focuses on the carbonate ramp. Modified from Meissner (1972).

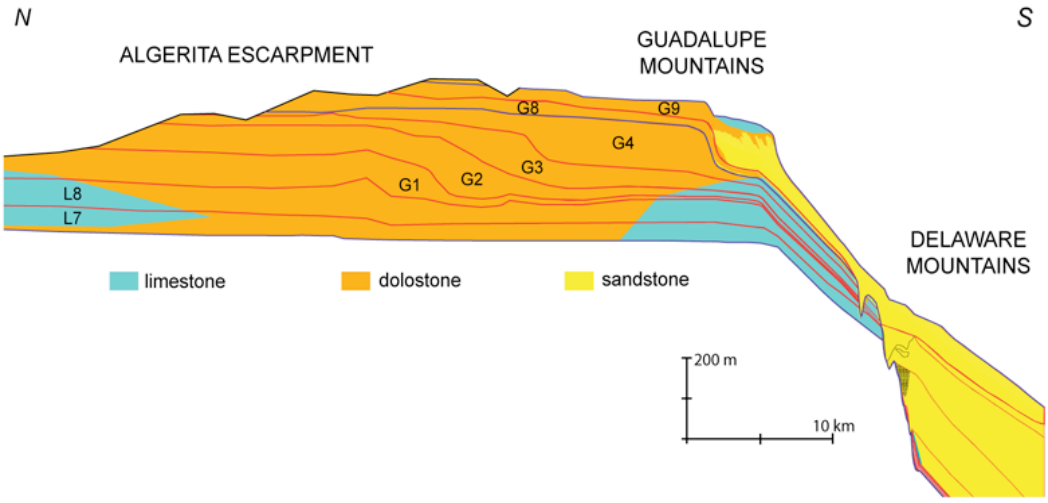

Figure 1.3: Preliminary mapping of lithologies along the Guadalupe Mountains and Algerita Escarpment.

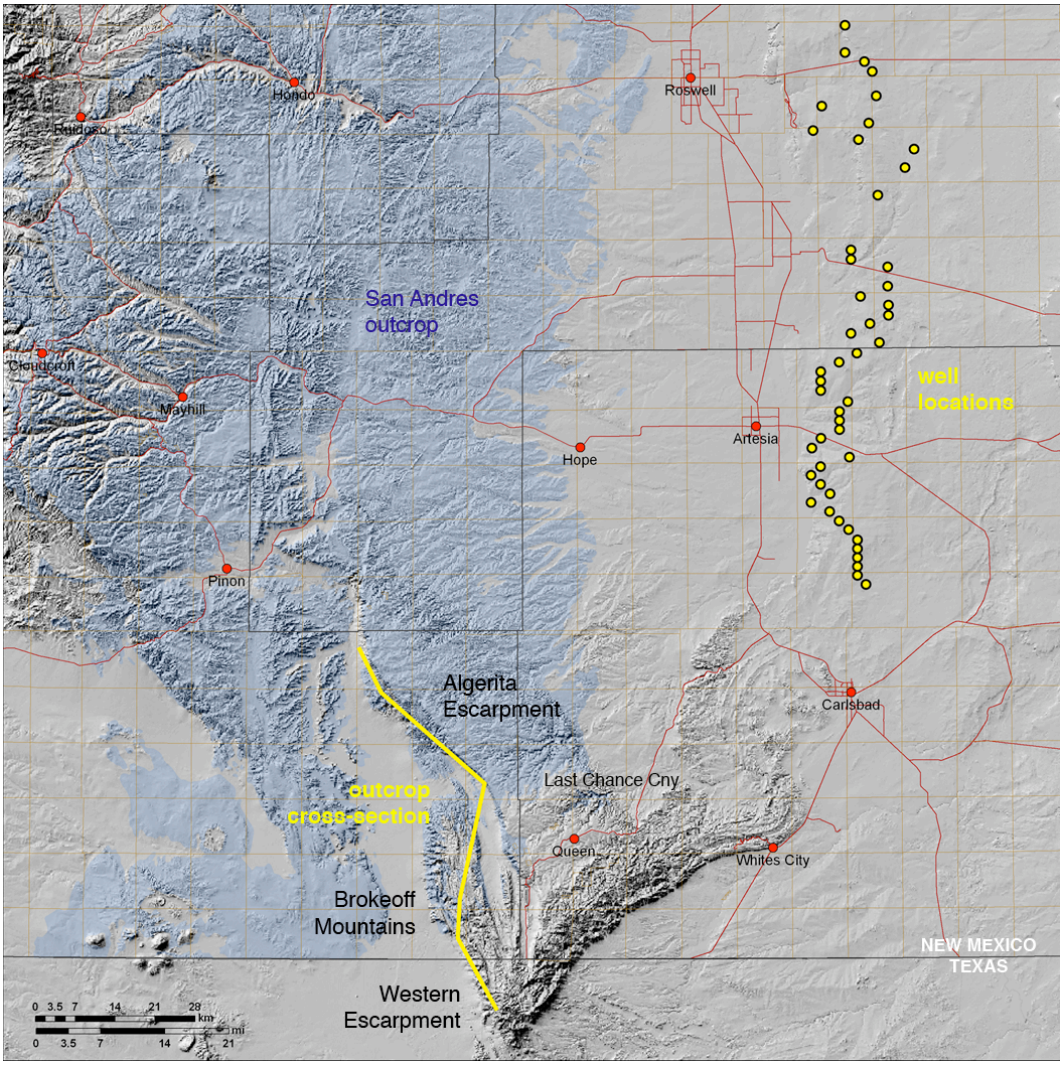

Figure 1.4: Location of outcrop and well locations used on cross sections. The subsurface cross section is a straight line upon which well locations are projected.

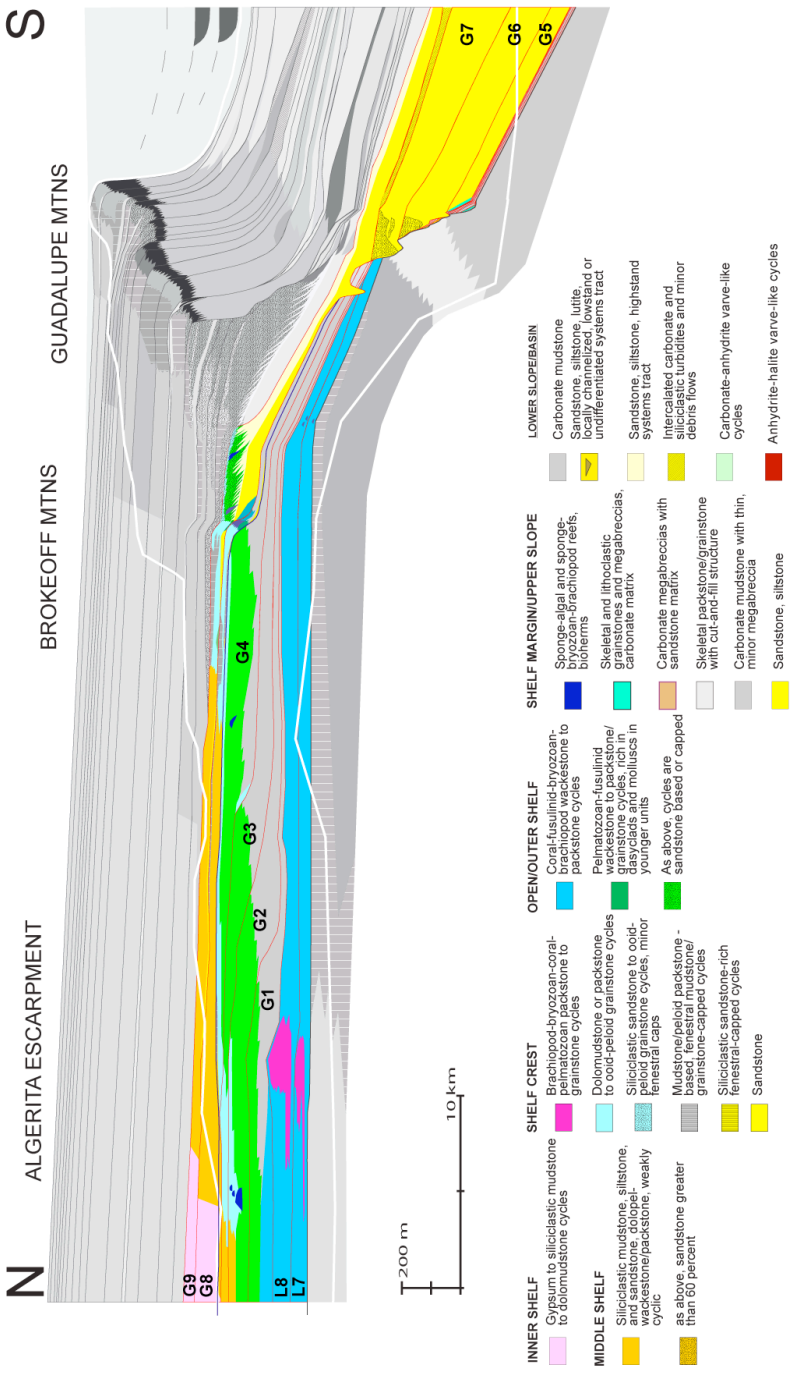

Figure 1.5: Permian section of the Guadalupe Mountains and Algerita Escarpment. San Andres Formation facies-tracts are shown in color (modified from Kerans and Kempter, 2002).

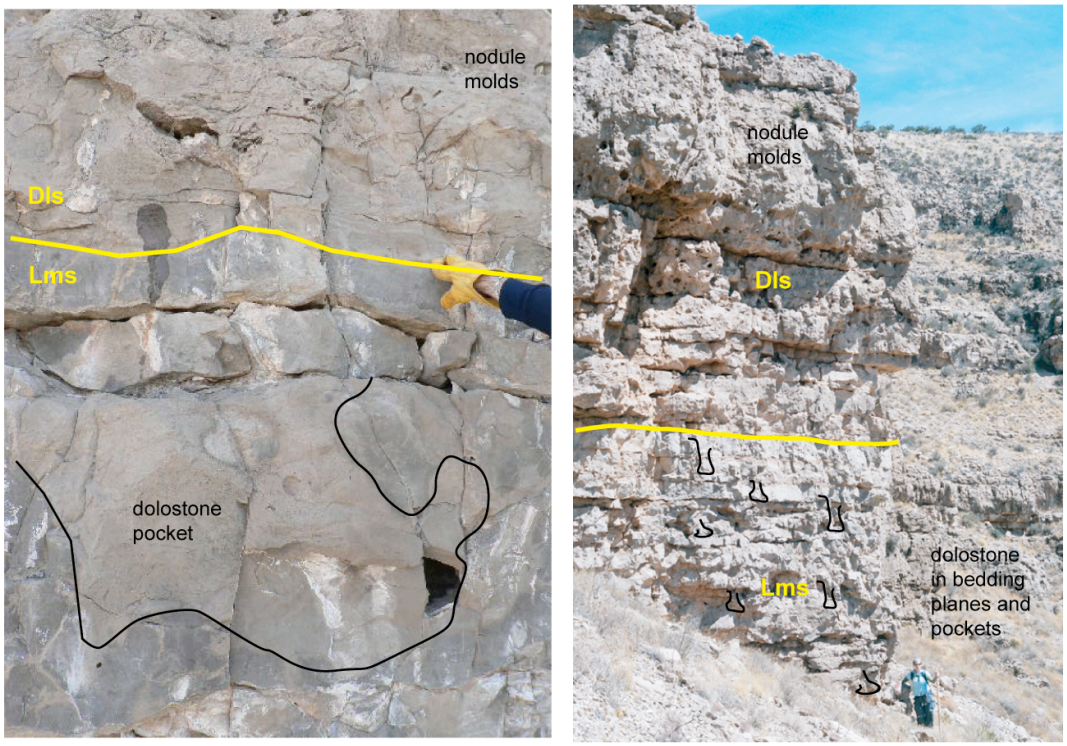

Figure 1.6: Limestone/dolostone contact at Pot Hole Tank section. Yellow line marks main lithology contact. Black lines outline dolomitized “pockets” within the limestone immediately below the contact. Dls = dolostone; Lms = limestone. Person for scale.

Figure 1.7: Detail of two dolostone pockets within the limestone. Pocket outline is easily identified by differential fizzing on contact with hydrochloric acid. Centimeter-scale vugs are common in pockets.

Figure 1.8: Evaporite-removal breccia on top of County Line section.

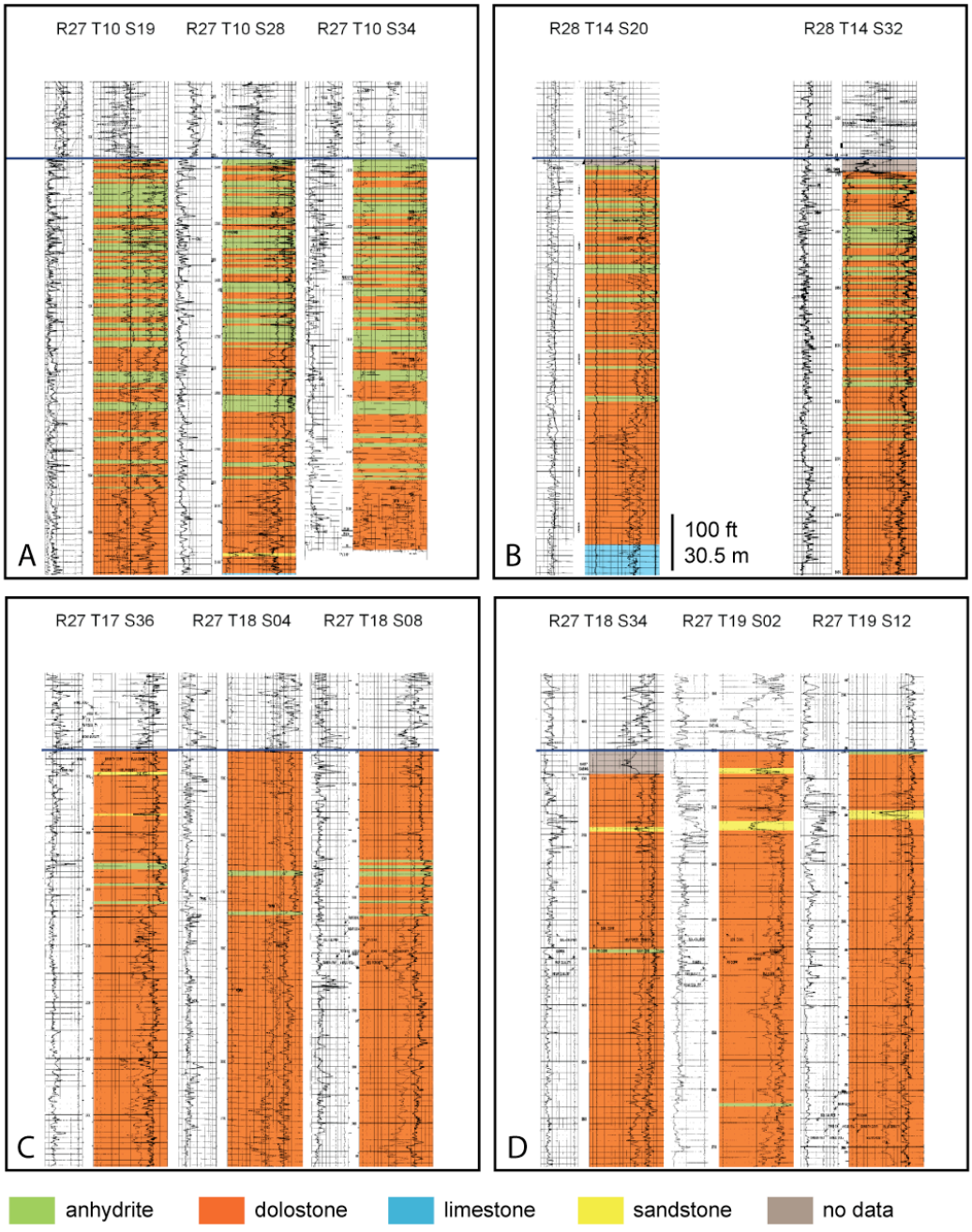

Figure 1.9: Dolostone/anhydrite cycles in the upper part of the San Andres Formation in four locations along the platform. Lithology was interpreted from density and neutron porosity overlay. Legend is the same as in Plate 1.

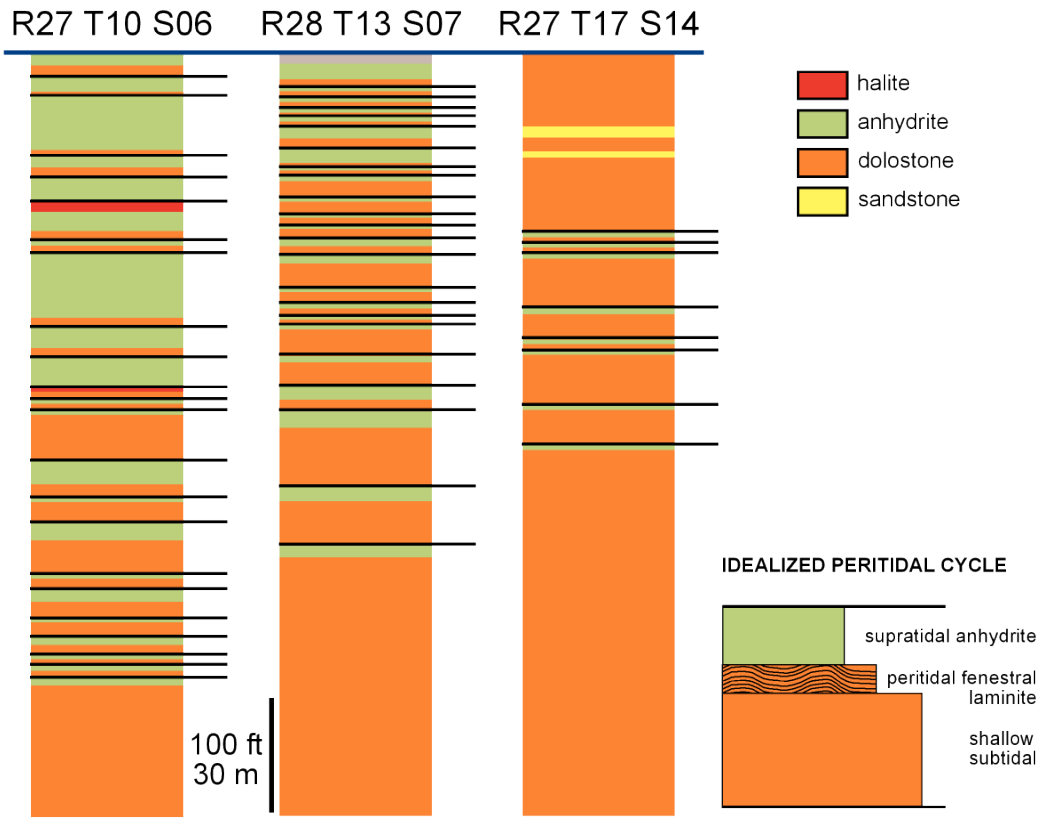

Figure 1.10: Examples of dolostone/anhydrite cycles from the upper part of the San Andres Formation and idealized upward-shallowing peritidal cycle. Anhydrite is interpreted to be deposited subaqueously in supratidal brine pans or salinas. Peritidal facies are interpreted as laminated fenestral mudstones overlying shallow subtidal mudstones.

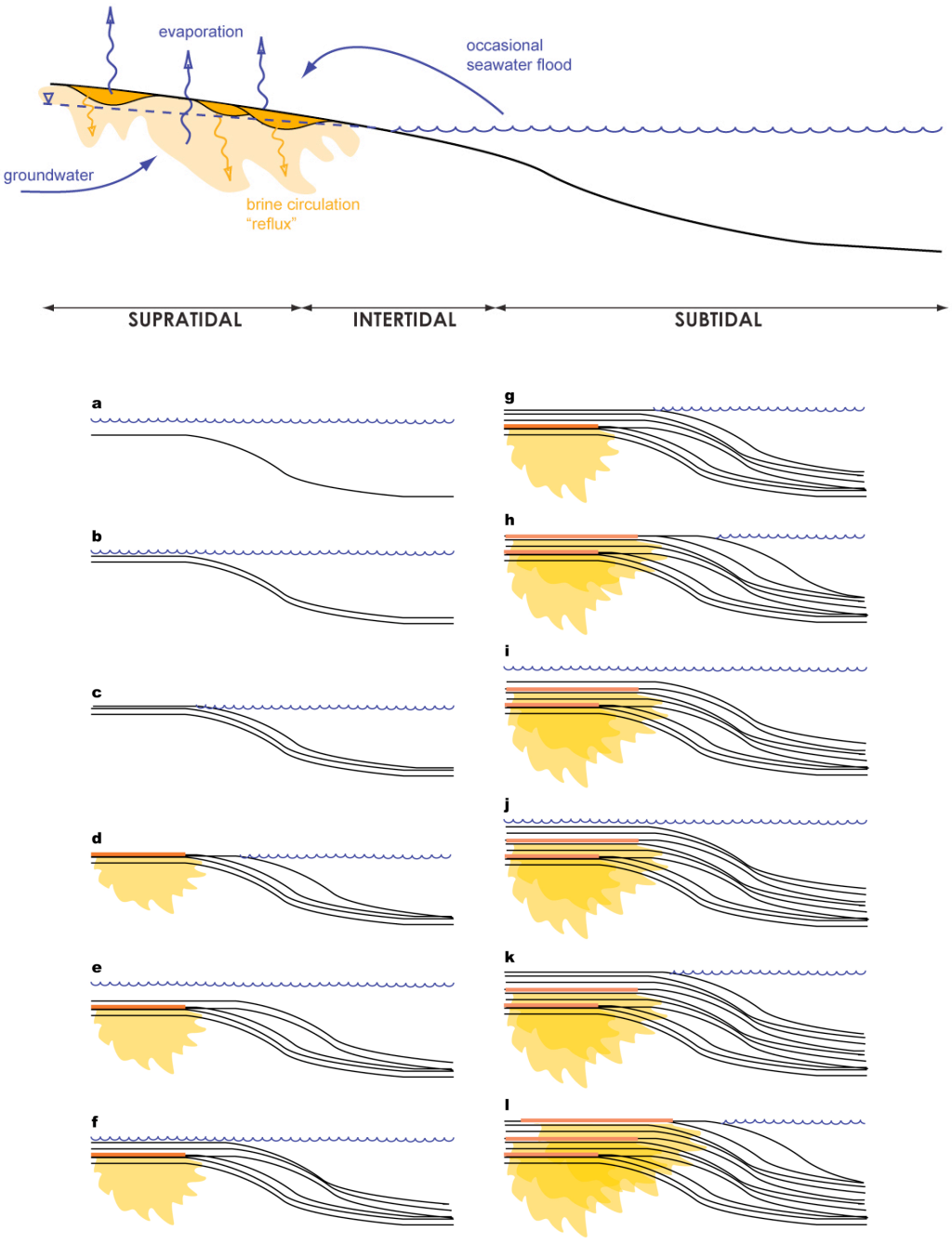

Figure 1.11: Above: idealized cross section of the peritidal zone and brine reflux below supratidal brine pans; orange shading corresponds to the zone of dolomitization. Length of cross-section is tens to hundreds of meters and vertically exaggerated. Below: sequence of relative sealevel fluctuations and cumulative dolomitization for three transgressive/regressive cycles (cycle 1: a-d; cycle 2: e-h; cycle 3: i-l).

PLATE 1

OUTCROP AND SUBSURFACE LITHOLOGY COMPARISON OF THE PERMIAN SAN ANDRES FORMATION

Guadalupe Mountains and Algerita Escarpment

W Texas and SE New Mexico

B. Garcia-Fresca and F.J. Lucia
Reservoir Characterization Research Laboratory
Bureau of Economic Geology
Jackson School of Geosciences
The University of Texas at Austin

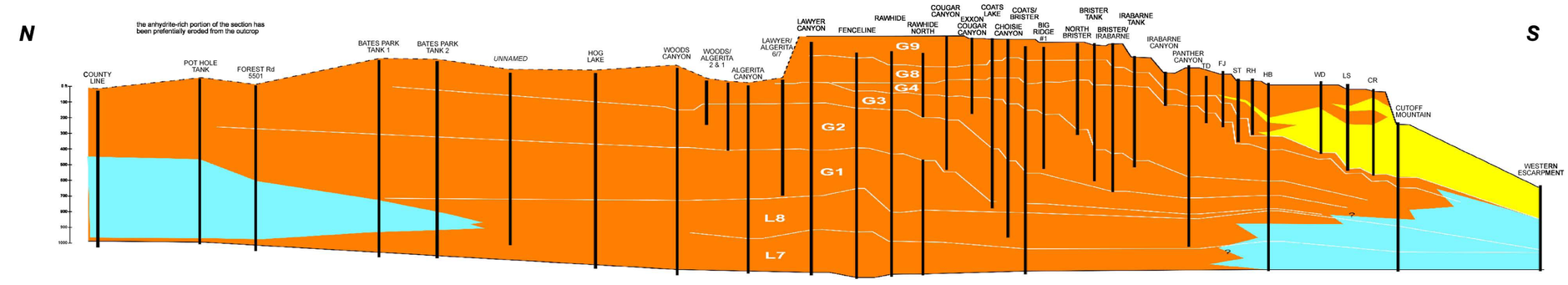

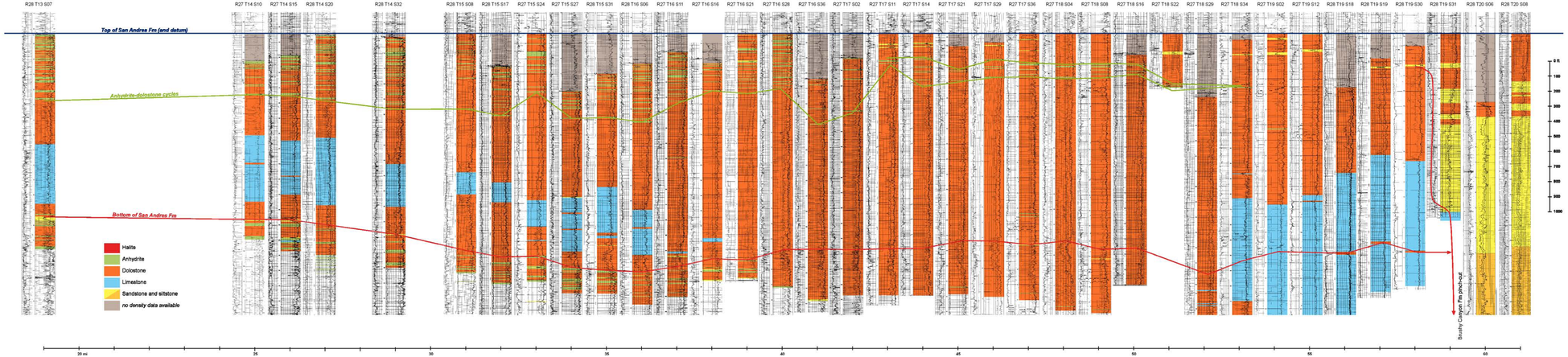

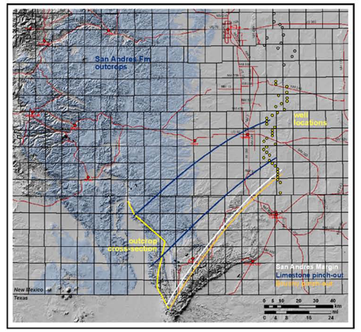

Well Logs
Gamma Ray, Neutron Porosity, Density
Source: New Mexico Energy, Minerals and Natural Resources

Outcrop Data
Beatriz Garcia-Fresca, unpublished
Kerans & Kempter (2002) Hierarquical stratigraphic analysis of a carbonate platform, Permian of the Guadalupe Mountains. AAPG Datapages Discovery Series no 5 (CD-ROM)

Chapter 2

OUTCROP-BASED PETROPHYSICAL MODEL OF THE PERMIAN SAN ANDRES FORMATION FOR STRATIGRAPHICALLY CONSTRAINED HYDROGEOLOGIC SIMULATIONS OF REFLUX

Abstract

I constructed a petrophysical model based on outcrop data of the partially dolomitized San Andres Formation to be used in hydrogeological simulations of synsedimentary fluid circulation and solute transport and to explore their implications for dolomitization of a carbonate platform. A practical petrophysical model should allow recognition of original stratigraphic and petrophysical features at the scale of interest and provide realistic porosity and permeability values that can be used to populate a grid for flow simulations. I translated outcrop facies descriptions into petrophysical parameters following the Lucia (2007) reservoir modeling approach. Steps included acquiring outcrop facies data and filling data gaps, translating facies descriptions into petrophysical properties, decompacting facies to depositional thicknesses, discretizing stratigraphy into modeling layers, upscaling petrophysical properties, and defining final rock types. The resulting model is ready for input into

hydrogeological simulations of synsedimentary dolomitization by brine reflux. Its sequence stratigraphic constraints provide transient boundary conditions such as platform geometry, timing of accumulation and reflux, and relative sea level and shoreline position. It also provides spatially distributed petrophysical properties that preserve the most relevant geologic features and heterogeneity in the formation.

Introduction and background

Fluid flow is a critical control in dolomitization and other diagenetic processes. Fluids deliver reactants and remove products of the reactions (Land, 1985), and different flow regimes result in different distributions and geometries of dolomite bodies (e.g., Machel, 2004). Significant progress has been made in studying the hydrodynamics of refluxing brines using numerical models (e.g., Kaufman, 1994; Jones et al., 2002; Whitaker et al., 2004). Such models place broad spatial and temporal constraints on reflux dolomitization but approach the system as a single fluid circulation event and use overly simplistic geological and petrophysical representations. A rigorous geologic model is important to the understanding of early diagenesis because only specific settings provide the necessary conditions for the processes involved. I used outcrop data to construct a stratigraphically constrained petrophysical model for input

into simulations of synsedimentary dolomitization of a carbonate platform by refluxing brines (Garcia-Fresca et al., 2008; Chapter 3). The Permian San Andres Formation is an excellent candidate for this exercise because its economic importance has resulted on a large volume of work on this unit, including a robust sequence stratigraphic framework. A detailed outcrop dataset (Figure 2.1) provides fundamental stratigraphic and lithologic constraints for hydrogeological modeling, platform geometry, relative sea-level and shoreline position, location of restricted environments where brines may have been sourced, relative timing of events, and distribution of facies and burial history –all of which can be used to estimate petrophysical properties.

A successful petrophysical model should (1) allow recognition of original stratigraphic and petrophysical features at the scale of interest and (2) provide realistic porosity and permeability values that can be used to populate a grid for flow simulations. I converted the outcrop into petrophysical parameters following the Lucia (2007) carbonate reservoir modeling approach. Lucia (2007) postulated that an effective petrophysical model for reservoir performance simulations should incorporate a chronostratigraphic framework, as well as information on the processes that form and modify petrophysical properties. He proposed the

following steps for constructing such a model: (1) relating rock fabrics to porosity and permeability, (2) identifying the geological processes that generated those fabrics, (3) describing a sequence stratigraphic framework based on high-frequency cycles, and (4) distributing petrophysically significant rock-fabric bodies within the stratigraphic framework.

Heterogeneity and anisotropy in the permeability field greatly affect flow and transport in porous media (e.g., Schincariol and Schwartz, 1990; Kerans et al., 1994; Jennings, 2000; Simmons et al., 2001; Jones and Xiao, 2005; Shi, 2005). These parameters cause flow paths to deflect with respect to hydraulic gradients, generate complex circulation patterns, and disperse the transport of solutes. Heterogeneity in a carbonate formation is the consequence of various fabrics of sedimentary facies (Lucia, 1995). Kerans et al. (1994) showed that inverting the direction of flow in a reservoir model with a heterogeneous permeability field results in different flow patterns. Simmons et al. (2001) showed that the onset, growth, and decay of saline fingers are closely related to the structure of heterogeneity in the permeability field. A critical cause of anisotropy is the stratigraphic layering of fabrics, which imposes strong permeability contrasts on vertical flow. In the case of density-driven flow, layered heterogeneity may cause

saline plumes to pond at permeability contrasts, forcing them to flow downdip along the contact, whereas lenticular permeability heterogeneity may disperse saline plumes (Schincariol and Schwartz, 1990). Heterogeneity in the permeability field occurs at all scales of observation. Sudicky (1986) proposed that large-scale heterogeneity is important in controlling convective flow, whereas small-scale heterogeneity controls dispersion. Thus, values should be estimated at scales appropriate to the particular problem.

Estimating new values for a property at increasing scales is known as *upscaling*. Sudicky (1986) highlighted the relevance of incorporating geological data when characterizing heterogeneity and flow in aquifers. This concept was sufficiently proven in studies that combine outcrop observations of permeability distributions (facies variations and bedding) into reservoir performance simulations (e.g., Hinrichs et al., 1986; Eisenberg et al., 1992; Lucia et al., 1992; Eisenberg et al., 1994; Grant et al., 1994; Kerans et al., 1994; Wang et al., 1994; Jennings et al., 1998; Jennings, 2000). These studies present statistical analyses on high-resolution outcrop permeability measurements that show several scales of heterogeneity of permeability data in two dimensions. They conclude that rock fabric bodies are the representative elementary volume (Bear, 1972)

at the reservoir scale. This study uses a similar approach at the platform scale.

This study focused on construction of a petrophysical model to be used in hydrogeologic simulations. The model is based on measured sections of the San Andres Formation in west Texas and New Mexico (Figure 2.1) and a well-established stratigraphic framework (Kerans and Kempter, 2002). Depositional facies were described in terms of rock fabrics and assigned values of petrophysical properties from modern carbonate sediments. Outcrop thicknesses were decompacted to depositional values. Because petrophysical properties based on facies descriptions at the submeter scale required significant upscaling, a vertical permeability profile was built for each measured section. Facies were grouped according to vertical successions of similar permeability, while maintaining significant sequence stratigraphic surfaces. These groups of similar permeability were correlated laterally to define modeling layers. Next, porosity and permeability were averaged within each layer, and average horizontal permeabilities were used to define six rock types. This approach resulted in a petrophysical model that respects the chronostratigraphic framework and preserves a degree of petrophysical

heterogeneity appropriate for hydrogeologic simulations at the platform scale.

The following sections describe the outcrop dataset and how gaps in the data were managed, translation of facies descriptions into petrophysical properties, decompaction of facies to depositional thicknesses, discretization of stratigraphy into modeling layers, upscaling of petrophysical properties, and definition of final rock types to be used as input in hydrogeological simulations.

Geologic model

This analysis examines the widespread Permian San Andres and equivalent formations that crop out in west Texas and New Mexico (Figure 2.1). World-class exposures occur along the Western Escarpment of the Guadalupe Mountains, Last Chance Canyon, Brokeoff Mountains, and Algerita Escarpment. Remarkably continuous and undeformed outcrops record the evolution of a carbonate platform in an arid climatic setting. The formation dips to the east and goes into the subsurface, where it is a prolific oil producer (e.g. Ward et al., 1986; Kerans et al., 1994).

In this section I summarize relevant previous studies of San Andres Formation outcrops, describe the outcrop dataset and sequence stratigraphic framework developed by Kerans and Fitchen (1995) and Kerans and Kempter (2002), introduce new measured sections in the restricted inner platform where limestone has been preserved, and describe procedures for filling gaps in the outcrop dataset, including a well-log-based reconstruction of the evaporite-rich succession in the inner platform.

Previous work

The San Andres Formation has been the subject of many studies, and its stratigraphy and sedimentology are well constrained. Lee and Girty (1909) first described the San Andres Formation in the San Andres Mountains, New Mexico. Needham and Bates (1943) described the type section and Kottlowsky et al. (1956) a reference section, which were revisited by Lindsay (1994). Unfortunately, both sections are located in the evaporite-rich platform interior, where much of the formation has been eroded away, as first pointed out by Kerans and Ruppel (1994). King (1948) produced one of the early descriptions of the Permian outcrops in the southern Guadalupe Mountains and correlated them to the basinal siliciclastics of the Delaware Mountains. Subsequent important stratigraphic studies in

the Guadalupe Mountains and Algerita Escarpment include those of Boyd (1958) and Hayes (1964). Incomplete inner platform outcrops of the lower San Andres Formation occur along the Rio Hondo valley and U.S. Highway 82 and were described by Kelly (1971) and Beserra and Dorobeck (1994). Sequence stratigraphic and sedimentologic studies were carried out by Sarg and Lehman (1986) and Sonnenfeld (1991). Kirkby (1982) and Harris (1982) studied the upper Victorio Peak and Cutoff Formations, respectively, along the western escarpment of the Guadalupe Mountains, which are currently interpreted to be equivalent to the lower San Andres Formation (Kerans and Fitchen, 1995).

Sequence stratigraphic framework

The most recent and comprehensive studies of the outer platform to the platform margin (Algerita Escarpment to Guadalupe Mountains) were carried out by Kerans and Ruppel (1994), Kerans and Fitchen (1995), Kerans and Tinker (1999), and Kerans and Kempter (2002). The present study is based Kerans and Fitchen (1995) and Kerans and Kempter (2002), that provide a robust chronostratigraphic framework and a detailed description of the spatial and temporal variability of facies across the different platform settings (Figure 2.2). I present five new measured sections that expand the composite cross section of Kerans and Kempter

(2002) 30 kilometers northward. Such a continuous and detailed outcrop dataset provides a unique opportunity to build a detailed geologic model of the San Andres Formation and its equivalents.

The San Andres platform accumulated in 2 to 4 million years and records part of a second-order supersequence (Kerans and Fitchen, 1995). The chronostratigraphic units defined by Kerans and Kempter (2002) are composite sequences, high-frequency sequences, and high-frequency cycles (Figure 2.2). Two composite sequences are subdivided into six and five high-frequency sequences, respectively.

Evolution of the platform geometry and depositional styles interpreted by Kerans and Kempter (2002) can be summarized as follows:

1. Leonardian 7 and 8 high-frequency sequences: Transgressive systems tract of the lower San Andres composite sequence, open-marine carbonates deposited in a distally steepened ramp.
2. Guadalupian 1 through 4 high-frequency sequences: Highstand systems tract of the lower San Andres composite sequence of sigmoid clinoform geometry. The maximum flooding zone of G1 coincides with the second-order maximum flooding zone. The

composite sequence boundary at the top of G4 is a karst-modified bypass surface.

3. Guadalupian 5 through 7 high-frequency sequences: Lowstand systems tract of the upper composite sequence consisting of eolian siliciclastic sediments that bypassed the platform top and were deposited in the basin (not shown in Figure 2.2).
4. Guadalupian 8 high-frequency sequence: Transgressive systems tract of the upper composite sequence, with a transitional geometry from sigmoid clinoforms to rimmed shelf.
5. Guadalupian 9 high-frequency sequence: Highstand systems tract of the upper composite sequence, sigmoid to oblique clinoform-ramp to rimmed-shelf geometry, has a siliciclastic-rich base known as the Cherry Canyon Tongue, which passes into the basinal Cherry Canyon Formation.

Kerans and Fitchen (1995) defined the different depositional environments across the platform in terms of the following lithostratigraphic units: lithofacies, vertical facies successions, and facies tracts. Lithofacies are defined by allochem types, fabrics, and sedimentary structures, and they record discrete depositional events in specific depositional environments. Vertical facies successions record upward-shallowing events as the

platform grows to fill the accommodation space during a high-frequency sea-level fluctuation. The main facies tracts of the inner platform, middle platform, platform crest, open platform, and distal outer platform are summarized in Figure 2.3. During early San Andres deposition (L7 and L8), open marine conditions prevailed, and grainstone shoals developed in the ramp crest in the vicinity of the *Fenceline* section. During deposition of G1–4, conditions become more variable, from restricted lagoonal facies, an open marine to high-energy platform crest, to a muddy slope. During deposition of the upper San Andres, composite sequence conditions ranged from very restricted evaporitic inner platform, high-energy open marine margin, to siliciclastic-rich slope.

Five new measured sections, *County Line* through *Hog Lake*, document the transition from open marine to restricted inner-platform conditions (Figure 2.4). Facies in this part of the platform are predominantly mud-rich and weakly cyclic. However, successions of progressively deepening and shallowing facies can be recognized and correlated to Kerans and Kempter's (2002) high-frequency sequences. This outcrop record most of the lower San Andres composite sequence, from L7 through the beginning of G3. Interbedded peritidal dolostones and siliciclastic sands of the Glorieta Formation represent the earliest steps of a second order marine

transgression that continues until the beginning of Guadalupian time. L7 is mainly composed of coral-brachiopod-crinoid wackestones and packstones that indicate open marine conditions. A gradual upward progression to deeper facies and thinner bedding, the presence of ammonoids, and a wispy-laminated zone with intense horizontal burrowing (planolites) represent the deepest water conditions found in the San Andres Formation and coincide with the maximum flooding zone of high-frequency sequence G1 (Kerans and Fitchen, 1995). The highstand of G1 records transitional facies between open platform, middle platform and platform crest (Figure 2.3). Facies become more peloidal and mud-rich on high-frequency sequences G2 and G3, indicating a progressive shallowing into middle platform facies. The highstand of G2 and limited exposures of G3 are composed of peritidal mud-rich cycles where stratiform breccias can be found (Figure 2.5). These breccias are interpreted to be the outcrop expression of evaporite dissolution and, thus, signal the transition into the inner platform evaporitic facies tract, which is mainly eroded away from the outcrop.

The inner platform is composed of interbedded dolostone and anhydrite eroded from outcrop (Figures 2.3, 2.6). I used well log data from a cross section between Carlsbad and Roswell to reconstruct this part of the

platform (Figure 2.6; Garcia-Fresca and Lucia, 2007). I interpret these deposits as upward-shallowing peritidal cycles ranging from shallow subtidal carbonates to supratidal evaporites. I also think that anhydrite was deposited as gypsum in hypersaline intertidal or supratidal salinas. Some anhydrite beds are very continuous and can be correlated for distances of several kilometers. The relative proportion between carbonate and sulfate varies: anhydrite becomes relatively thicker with increasing restriction, both toward the top of the San Andres and in the inner platform to the north. Similarly, anhydrite becomes progressively thinner and sparser toward the less restricted parts of the platform to the south. Cycle thicknesses that can be resolved from log data range from 2 to 10 m and appear to decrease toward the top of the San Andres Formation. Dissolution caused by removal of evaporites occurred after several phases of outcrop uplift and exhumation of the formation that reached a maximum in the early Miocene (Zoback, 1981; Hill, 1996). Evaporite removal caused collapse, brecciation, and preferential erosion of this part of the formation (Figure 2.6). Anhydrite precipitated as gypsum in supratidal brine pans or salinas, which I interpreted as the source of dolomitizing fluids for hydrogeological simulations of reflux dolomitization. Interbedded carbonate represents relative sea-level transgressions in which the brine source is shut off.

Lithology

Although most of the San Andres Formation is pervasively dolomitized, some areas are preserved as limestone (Figure 2.6). Such lithologic relationships were also described by Meissner (1972), Cowan and Harris (1986), and Garcia-Fresca and Lucia (2007). The vertical transition between limestone and dolostone is sharp, passing from one lithology to the other in just a few centimeters (Figures 2.4, 2.5). The contact is flat between *County Line* and *Pot Hole Tank* sections, where it approximately coincides with the maximum flooding zone of high-frequency sequence G1. Farther south, the dolomitization front descends rapidly and crosscuts timelines and facies boundaries until the limestone pinches out near the *Cantrell Lake 2* section. In detail, the dolomitization front is irregular with decimeter-scale dolomitized pockets or fingers that can be found as far as 25 m below the main limestone/dolostone contact (Figure 2.5). I hypothesize that such fingering responds to centimeter-scale preferential permeability pathways and, perhaps, patterns resulting from free-convecting brines.

Data-gap reconstruction

So that a complete dataset could be assembled, gaps in the measured sections had to be interpreted using geomorphological and outcrop

weathering criteria. Gaps in the data include: (1) areas poorly exposed or covered by vegetation, (2) gaps interpreted to be caused by faulting, and (3) karstification related to platform exposure events. Meter-scale gaps where the rocks are covered by vegetation or poorly exposed were interpreted to represent mudstone facies because mud-dominated dolostones tend to weather recessively relative to grain-rich fabrics. These gaps occur mainly within the peritidal successions of the upper San Andres Formation, where mudstones and wackestones are abundant. Some gaps occurring within the mud-rich slope deposits of the G1–4 high-frequency sequences (also know as the Cutoff Formation) were interpreted as mudstones. In the *Lawyer/Algerita* section, bioclastic wackestones (Kerans and Kempter, 2002) were assigned to gaps in a succession of fusulinid peloidal wackestone/packstone on the basis of their resemblance to contiguous sections to the north and south. I reconstructed the *Choisie Canyon* section by interpreting a fault within the mud-rich Cutoff Formation facies of high-frequency sequences G2 and G3. Approximately 50 meters were added to the middle part and populated with facies on the basis of adjacent sections.

Eroded inner platform high-frequency sequences G3 through G9 were reconstructed based on the subsurface interpretation by Garcia-Fresca

and Lucia (2007) as thinly bedded dolomite-anhydrite cycles (Figure 2.6). The carbonate part was interpreted as subtidal mudstones and tidal flat fenestral laminites on the basis of outcrop peritidal successions with evaporite-removal breccias (Figure 2.5). Sequence boundaries in the reconstructed succession were interpreted by extrapolating horizontally from outer platform outcrops.

Much of the G4 high-frequency sequence is broadly affected by erosion and karstification during bypass of the G5–7 lowstand deposits and is completely missing updip of *Lawyer Canyon*. I reconstructed the eroded top of G4 to a relatively flat surface, with respect to *Coats Lake* and *Choisie Canyon* sections, by adding a few meters to platform-crest facies. Updip of *Lawyer Canyon* I assumed that G4 had a constant thickness of 10 m. I also reconstructed the top of G8 in the Rawhide to Cougar Canyon interval by adding a few meters as necessary to achieve a flat surface. Localized, minor karstification was assumed not to have reduced the thickness of the sequences significantly and was disregarded in the reconstruction.

From facies to petrophysical properties

The goal of this exercise is to transform outcrop information into gridded data that can be input in hydrogeological simulations of brine reflux. Once the geologic model was completed, the next step involved assigning values of porosity, permeability, and decompaction coefficients to the facies. Outcrop descriptions provide the current appearance of lithofacies and spatial distribution of heterogeneity. Since deposition, the rocks have undergone compaction and a variety of diagenetic processes. However, the goal of this study was to build a hydrogeologic model that simulates fluid circulation in the formation at the time of deposition. Therefore, petrophysical parameters used in the model must reflect values at the time of accumulation. I accomplished this goal by assigning porosity and permeability values of modern sediments and decompaction coefficients to the facies.

Porosity and Permeability

Porosity and permeability values for most of the facies were assigned on the basis of rock fabrics (Lucia, 1995), as summarized in Figure 2.7. Enos and Sawatsky (1981) measured porosity and permeability of modern carbonate sediments. Their data display a general trend of increasing permeability and decreasing porosity following the transition from muds to

sands. I grouped different rock fabrics based on Enos and Sawatsky (1981) descriptions of sediment textures and the Lucia (1995) porosity-permeability cross-plot (shaded in gray in Figure 2.7). I identified plot regions for six broad fabrics: grainstone, grain-dominated packstone, mud-dominated packstone, wackestone, fenestral mudstone, and mudstone. On Lucia's (1995) plot, grain-dominated fabrics lie in the class 2 field, mud-dominated fabrics in the class 3 field, and pure muds lay outside these fields. Rock fabric/facies descriptions by Kerans and Fitchen (1995) and Kerans and Kempter (2002) were plotted within these regions (Figure 2.7). Further subdivisions within each of these regions were qualitatively established on the basis of fabric elements such as allochem type and pore structure. For example, a fabric composed of well-sorted, spherical ooids should have lower porosity and higher permeability than one composed of irregular, elongated skeletal fragments and mud.

Petrophysical values for other fabrics were given estimated values. Boundstone/bafflestone fabrics were assigned best-judgment values, assuming they may undergo early cementation. Karst-related breccias occur near the platform margin in the upper composite sequence and were formed during San Andres time. Karst-related breccias represent a small fraction of the total volume of the outcrop and were assigned values

that are the average of all the other facies. Evaporite-removal breccias in the restricted inner platform (Figure 2.5) were formed during uplift and exhumation of the formation and, thus, would not have been present during Leonardian-Guadalupian time. Siliciclastics are abundant in the youngest Guadalupian sequences (Figure 2.2). Values of well-sorted, fine to medium siliciclastic sand are based on Beard and Weyl (1973).

Estimating depositional porosity and permeability of evaporites was problematic. I interpret that the anhydrite beds were originally deposited as subaqueous gypsum in supratidal salina environments because gypsum is the most common sulfate in modern depositional environments. Inversion from gypsum to anhydrite is a function of temperature and salinity (e.g., Hardie, 1967; Warren, 2006), and inversion probably takes place under several hundred meters of burial. In these simulations, the oldest sulfate facies were buried to a maximum depth of 150 m and, thus, were not submitted to the overburden or high temperatures needed for inversion to occur. According to Lucia (1968), subaqueous gypsum deposits can be quite coarse and porous. Porosity and permeability values for gypsum are estimated following the works of Murray (1964), Hardie (1967), Lucia (1968), Hovorka (1991), and Warren (2006).

A plot of permeability of modern sediments applied to San Andres Formation facies (Figure 2.8) shows some of the same features identified as facies tracts (Figure 2.3). However, this petrophysical model has too much variability to be effectively implemented in a flow simulation and requires upscaling as described below.

Decompaction

Decompaction coefficients were assigned to different facies on the basis of rock fabrics (Figure 2.7) to allow reconstruction of sedimentary thickness. Determining original sedimentary thickness is accompanied by uncertainty, but it is paramount in describing the evolution of porosity and permeability throughout the burial history of a formation. Detailed discussions about this topic were presented by Schmoker and Halley (1982), Goldhammer (1997), and Hunt and Fitchen (1999). Understanding the role and extent of compaction is especially difficult when dealing with carbonate sediments because of their susceptibility to early cementation, which influences subsequent compaction. Mud-rich carbonate sediments have higher depositional porosity and compact faster than grain-rich sediments. However, grain-rich sediments are more prone to early cementation, which inhibits mechanical compaction and yet contributes to reducing their porosity (Budd, 2001). Moreover, it is often hard to

differentiate between mechanical and chemical compaction. Goldhammer (1997) compiled empirical data and constructed curves of porosity versus depth for carbonate muds and carbonate sands. He also presented analytical and graphical methods of decompacting carbonate muds and sands. Despite limitations mentioned by Goldhammer (1997), the graphical method allows approximation of depositional thicknesses from outcrop thicknesses, provided the maximum burial depth of the formation is known.

The San Andres Formation was deposited over a broad region, and its burial history varies for different areas. In the area covered by this study, the Northwestern Shelf, discontinuous sedimentation took place through the Cretaceous and finished with Laramide-related uplift in Late Cretaceous to early Tertiary time (King, 1948). For most of the Cenozoic, no significant sedimentation took place in the study area other than localized accumulations of extrusive rocks. In the late Cenozoic, the Basin and Range phase began, uplifting the area and resulting in the shedding of gravel and sand toward the east, which accumulated to form the Ogallala Formation. According to King (1948) and Hill (1996), no significant late Tertiary sediments accumulated in the vicinity or west of the Guadalupe Mountains. According to Lloyd's (1929) data, the Glorieta

Formation (at the base of the San Andres Platform) of east-central New Mexico was buried to approximately 1,524 m (5,000 ft). Thus, using the Goldhammer (1997) graphical approach, an outcrop thickness of 1 m would have had an initial thickness of about 2.5 m for a mud-rich layer and 1.1 m for a grain-rich layer. Values of each facies were interpolated between these end-member values (Figure 2.7).

Model layers and property upscaling

The next step in model construction consists of subdividing the stratigraphic section into layers and then computing average petrophysical properties within each model layer. According to the Lucia (2007) method, high-frequency cycles should be divided into mud- and grain-rich fabrics. These rock-fabric packages are correlated laterally to define flow units, responding to the fact that facies change abruptly in the vertical dimension (of the submeter scale) and gradually in the horizontal scale (over tens to hundreds of meters). Petrophysical properties for each flow unit are averaged vertically at each well and interpolated between wells. This method guarantees preservation of petrophysical variability during upscaling and results in more effective reservoir flow simulations.

Although this approach is useful at the reservoir scale, correlating high-frequency cycles at the platform scale is impractical. Hydrologic simulations, however, require stratigraphic resolution higher than that of the high-frequency sequences of Kerans and Kempter (2002). Thus Lucia's (2007) approach was modified and the stratigraphy discretized into layers that may contain several high-frequency cycles, while preserving high-frequency sequence boundaries and maximum flooding surfaces.

Because permeability is one of the principal controls on fluid flow, permeability was used to subdivide the stratigraphy. I plotted permeability profiles for each section (Figure 2.8), following the facies/petrophysical relationship illustrated in Figure 2.7. I divided each section into packages of similar permeability and correlated such packages across the platform (Figure 2.10). Each high-frequency sequence is divided into 4 to 6 modeling layers, for a total of 39 layers. Modeling layers have variable thicknesses, but I assume that they are bound by timelines. They are labeled based on the Kerans and Kempter (2002) nomenclature for San Andres Formation high-frequency sequences, followed by a digit indicating the position of the layer within the high-frequency sequence (e.g., G3.1 is the oldest layer of four within the Guadalupian 3 high-frequency sequence). I assumed that the environment in which the

dolomite/anhydrite cycles had been deposited was probably very flat in the horizontal dimension, and I defined the layers by extending them as straight horizontal lines from the middle platform.

After defining modeling layers, I upscaled the values by averaging porosity, permeability, and decompaction coefficients within each of the layers. The horizontal component of permeability and porosity are approximated by the arithmetic average, and the vertical permeability by the harmonic average .

The next step was to populate incomplete sections with petrophysical properties, which was carried out by interpolating between adjacent sections on either side. *Rawhide Canyon North* and *Rawhide-Cougar Lower San Andres* sections are treated as one single section, with a large gap in G2, which was filled by interpolation. Slope deposits of the Cutoff Formation were interpreted as mudstone where missing.

Results: rock types for hydrogeological modeling

Properties were upscaled one more time to obtain single values for rock types to be used as input in hydrogeological simulations of synsedimentary fluid flow and solute transport on the San Andres Platform

(Garcia-Fresca et al., 2008; Chapter 3). I did so by plotting the spatial distribution of average permeabilities and porosities. The plots were visually analyzed and grouped so that they would best preserve the most relevant stratigraphic features in the San Andres Formation. Figure 2.11 shows the selected horizontal permeability cutoffs that define six rock types, RT1 through RT6. This arrangement separates mud-rich (RT1–4) and grain-rich (RT5, 6) fabrics, emphasizes low permeabilities of pure muds (RT1), and highlights the inner ramp succession of interbedded sulfate/carbonate (RT4). Values of petrophysical properties in each group (Figure 2.11) were averaged to obtain a single value for each rock type. Final values of porosity (phi), horizontal permeability (k_H), vertical permeability (k_V), anisotropy, and decompaction coefficients for rock types are summarized in Table 1. The permeability anisotropy factor was computed as the ratio between horizontal and vertical permeability (k_H/k_V or k_V/k_H, according to usage in hydrogeology and petroleum geology, respectively).

The resulting petrophysical model is displayed in Figure 2.12, which shows (a) the final distribution of horizontal permeability, (b) vertical permeability, and (c) the porosity for modeling rock types to be used as input in hydrogeological simulations. This model reduces variability while

maintaining the principal heterogeneity observed in outcrop. Rock Type 1 (RT1) includes mostly mudstones and coincides with slope deposits of the Cutoff Formation. RT2 represents mud-rich fabrics elsewhere. Both RT1 and RT2 have low average permeabilities. RT3 groups mud-rich fabrics with a large proportion of mud-dominated packstones. RT4 mainly includes carbonate/sulfate cycles of the restricted inner platform, which are thinly bedded. Both RT3 and RT4 have intermediate average permeabilities, but RT4 has a very low k_V/k_H because the facies are thinly bedded and, thus, have low average k_V values. RT5 and RT6 represent the grainier fabrics of the platform crest and have high average permeabilities. Porosity shows a decreasing trend, from RT1 to RT6, which reflects the progression from mud-rich to grain-rich fabrics.

Discussion

I describe the process of transforming field descriptions into a quantitative porosity and permeability model to be used in hydrogeological simulations or reflux circulation and dolomitization (Figure 2.12). The resulting petrophysical model preserves the principal stratigraphic features observed in San Andres outcrops, while significantly reduces petrophysical variability (compare Figures 2.3, 2.8 and 2.12). Construction of the petrophysical model was based on the method of building a

reservoir model devised by Lucia (2007) that relies on core descriptions and a sound sequence stratigraphic framework. In the process, I used measured sections of San Andres outcrops instead of core and well log data generally used in a subsurface hydrocarbon reservoir, and the spacing between measured sections is comparable to well spacing in a reservoir. However, there are some significant differences between this model and a reservoir model. With a lateral extent of 70 km and a decompacted thickness of approximately 600 m, the San Andres Platform is larger than most hydrocarbon fields. The model is designed so that it can be used in simulations of natural fluid circulation through the platform at the time of deposition, whereas a reservoir model is used to predict the performance of a reservoir during development of a hydrocarbon field.

Some of the most significant sources of uncertainty introduced into this model-building process include (1) assumed concordance of current outcrop facies and depositional texture of sediments, prior to compaction, lithification, and diagenesis; (2) ignoring effects of chemical compaction, early cementation and other synsedimentary diagenetic processes on sediment thickness, porosity, and permeability; (3) using simplistic decompaction coefficients; (4) anhydrite/dolomite cycles interpreted from

well logs that may not reflect the actual character of this interval; and (5) ignoring small-scale karsting and early fracturing.

This dataset allows interpretation of the evolution of the San Andres Platform over time, its geometry, relative sea level, location of brine sources, and spatial distribution of facies and petrophysical properties. Such critical parameters are required to constrain simulations of fluid circulation and the implications for synsedimentary dolomitization of the formation. Restricted depositional environments, such as tidal flats, are a source of concentrated fluids capable of dolomitizing carbonate sediments (Deffeyes et al., 1965; Patterson, 1972; Patterson and Kinsman, 1982). Lucia (1972) and Lucia and Major (1994) proposed that the migration of such environments in response to relative sea-level fluctuations allows for these fluids to sweep across the platform and dolomitize broad successions. Studies of the rock record show that certain stratigraphic settings are prone to dolomitization. For instance, dolomite is often more abundant in restricted platform environments and falling sea-level stages than in environments with open ocean circulation and rising relative sea level (e.g., Montañez and Read, 1992).

Principal controls on the circulation of early diagenetic fluids are time, location and extent of fluid source, hydraulic potential, chemical potential, and petrophysical properties. All of these controls are, in turn, subject to sequence stratigraphic parameters such as relative sea-level position, rate of sea-level rise and fall, shoreline position, sedimentation rate, topography of the platform top, and depositional environments. The complex combination and interdependence of these factors produce transient fluid circulation regimes that generate intricate diagenetic bodies over time. Results of hydrogeological simulations of the San Andres Formation using this petrophysical model are described in Chapter 3.

Conclusions

I converted a regional-scale outcrop dataset and sequence stratigraphic framework into a petrophysical model following a reservoir characterization method. The model serves as input into hydrogeologic simulations for studying the role of fluid flow and solute transport in early dolomitization by refluxing brine. A robust sequence stratigraphic framework and a detailed petrophysical model are important to the understanding of spatial and temporal distribution of diagenesis because they can be used to constrain the transient hydrologic, stratigraphic, and geochemical boundary conditions that controlled the flow of diagenetic

fluids during accumulation of the carbonate platform. The model successfully displays the petrophysical heterogeneity of the San Andres Formation at the platform scale, while maintaining the most relevant stratigraphic and depositional features. It provides spatially distributed values of porosity and permeability to input into hydrogeologic simulations described in Chapter 3.

New outcrop descriptions of the San Andres Formation are located in the inner platform and span the outcrop cross section of Kerans and Fitchen (1995) into the platform interior, where restricted evaporite-rich deposits were a significant element. The lower part of the inner platform remains undolomitized. The sharp limestone-dolostone contact cuts timelines and facies boundaries, suggesting that its position is controlled mainly by timing, source area, and hydrodynamics of dolomitizing fluids. Outcrop evidence shows that the restricted platform was composed mainly of shallow subtidal carbonates to supratidal carbonates and sulfates, which I interpret as the source of dolomitizing fluids. A well log study of lithologies in the subsurface supports outcrop observations.

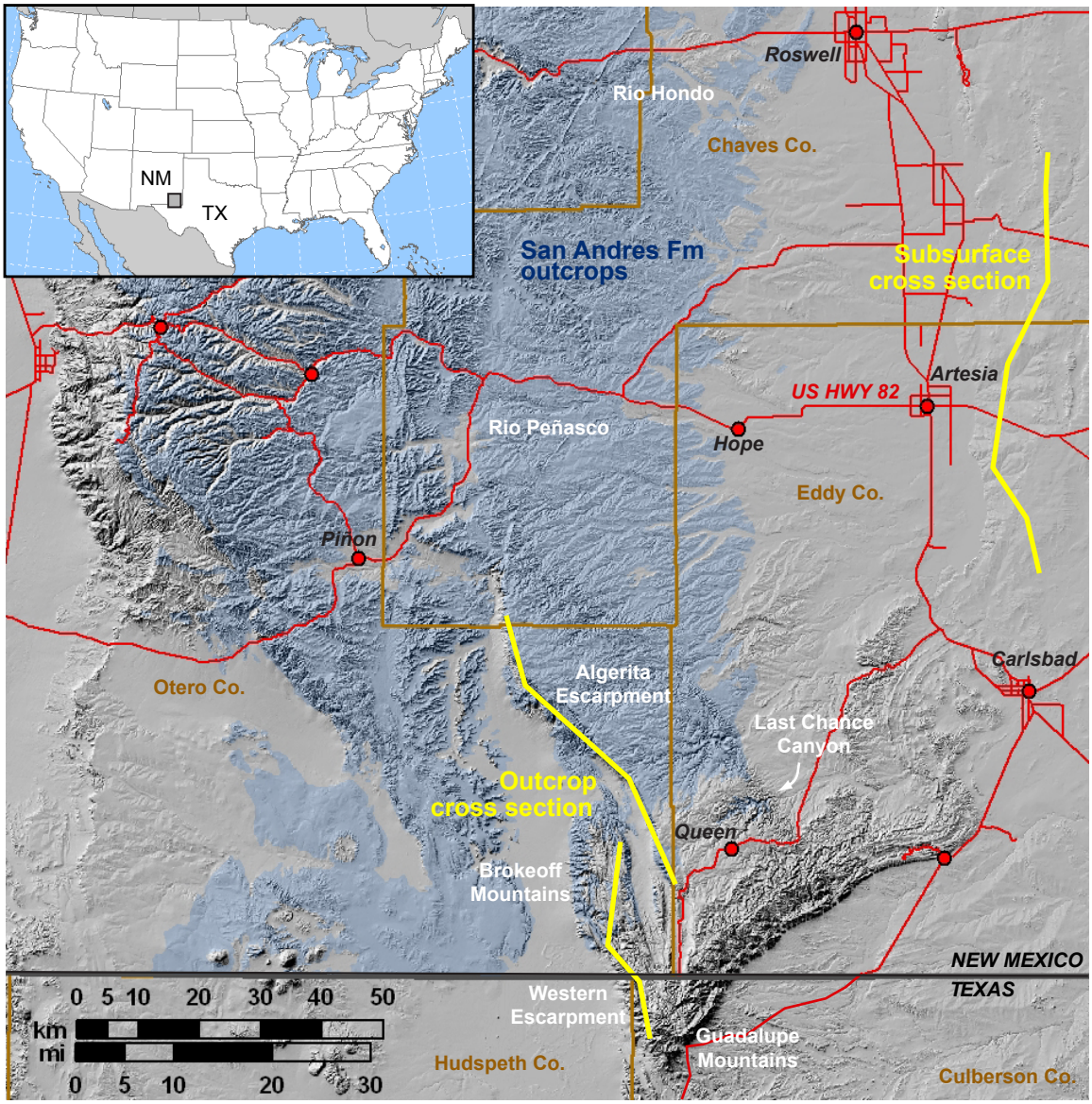

Figure 2.1: Map of San Andres Formation outcrops in Texas and New Mexico. In yellow are locations of outcrop and subsurface cross sections, subject of this study (Figures 2.2 and 2.6, respectively). (Sources of GIS public access data: U.S. Geological Survey and New Mexico Resource Geographic Information System).

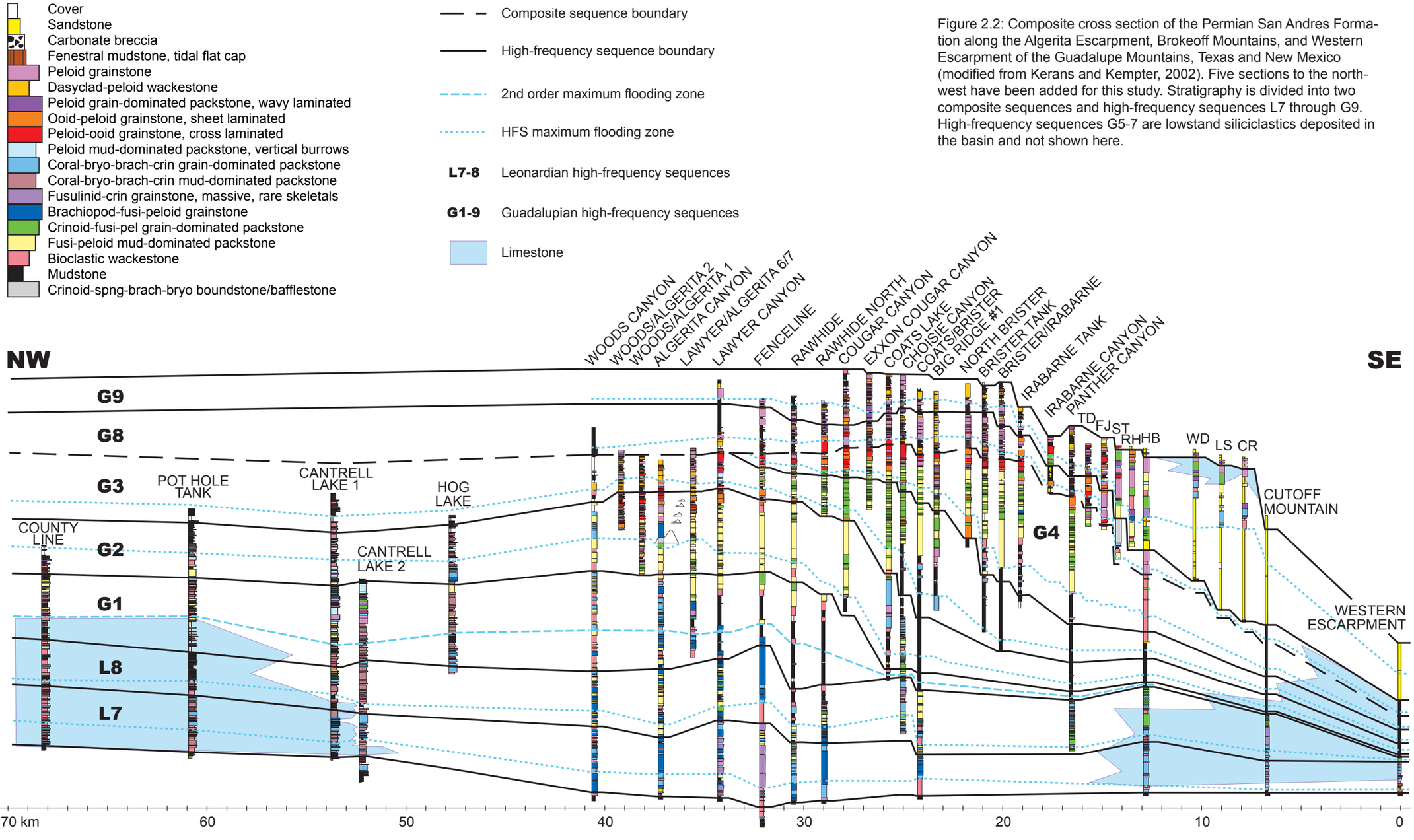

Figure 2.2: Composite cross section of the Permian San Andres Formation along the Algerita Escarpment, Brokeoff Mountains, and Western Escarpment of the Guadalupe Mountains, Texas and New Mexico (modified from Kerans and Kempter, 2002). Five sections to the northwest have been added for this study. Stratigraphy is divided into two composite sequences and high-frequency sequences L7 through G9. High-frequency sequences G5-7 are lowstand siliciclastics deposited in the basin and not shown here.

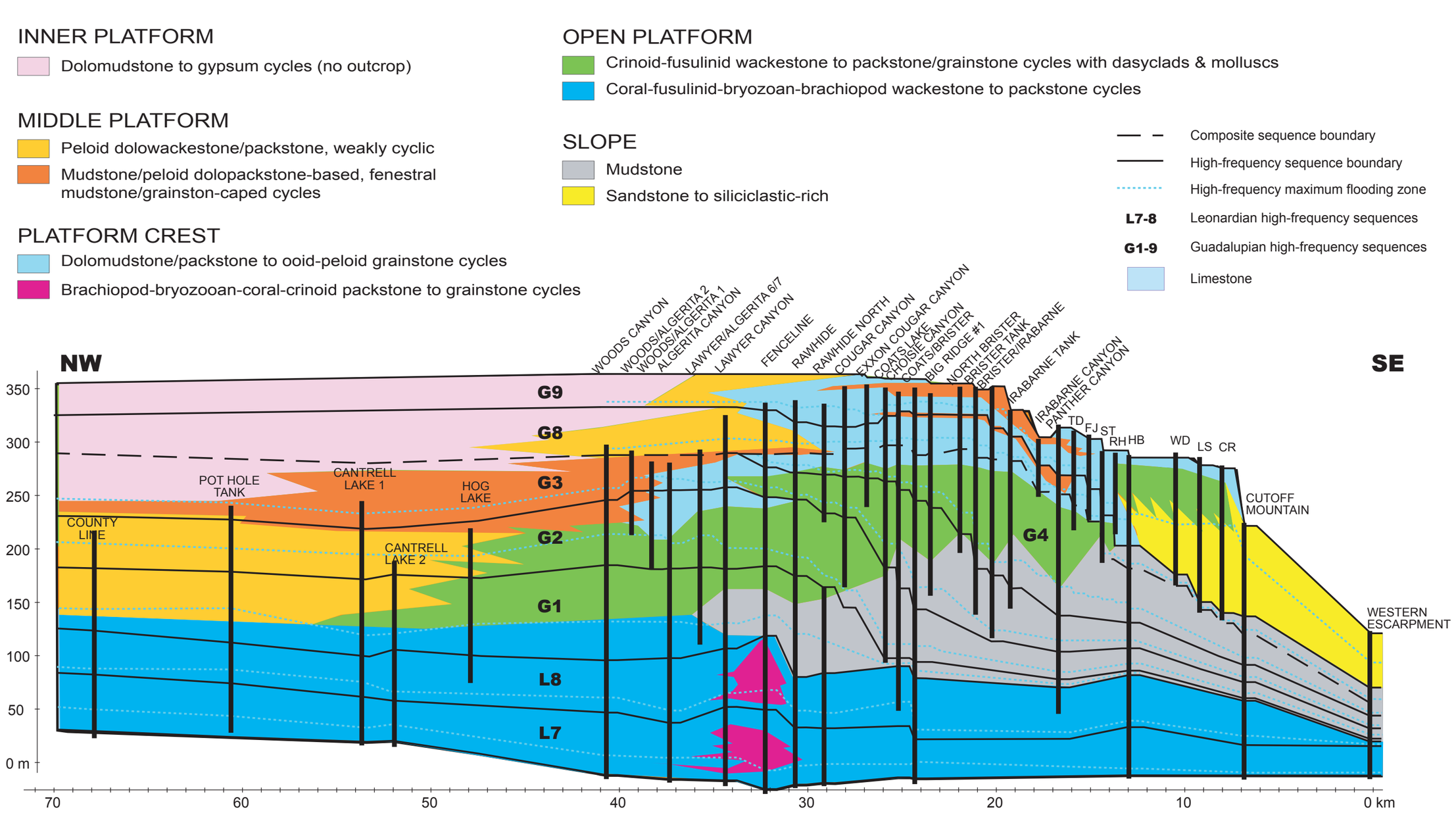

Figure 2.3: Facies tracts of the San Andres Formation reflect the evolution of conditions and depositional environments across the platform (modified from Kerans and Kempter 2002). Vertical lines are locations of measured sections.

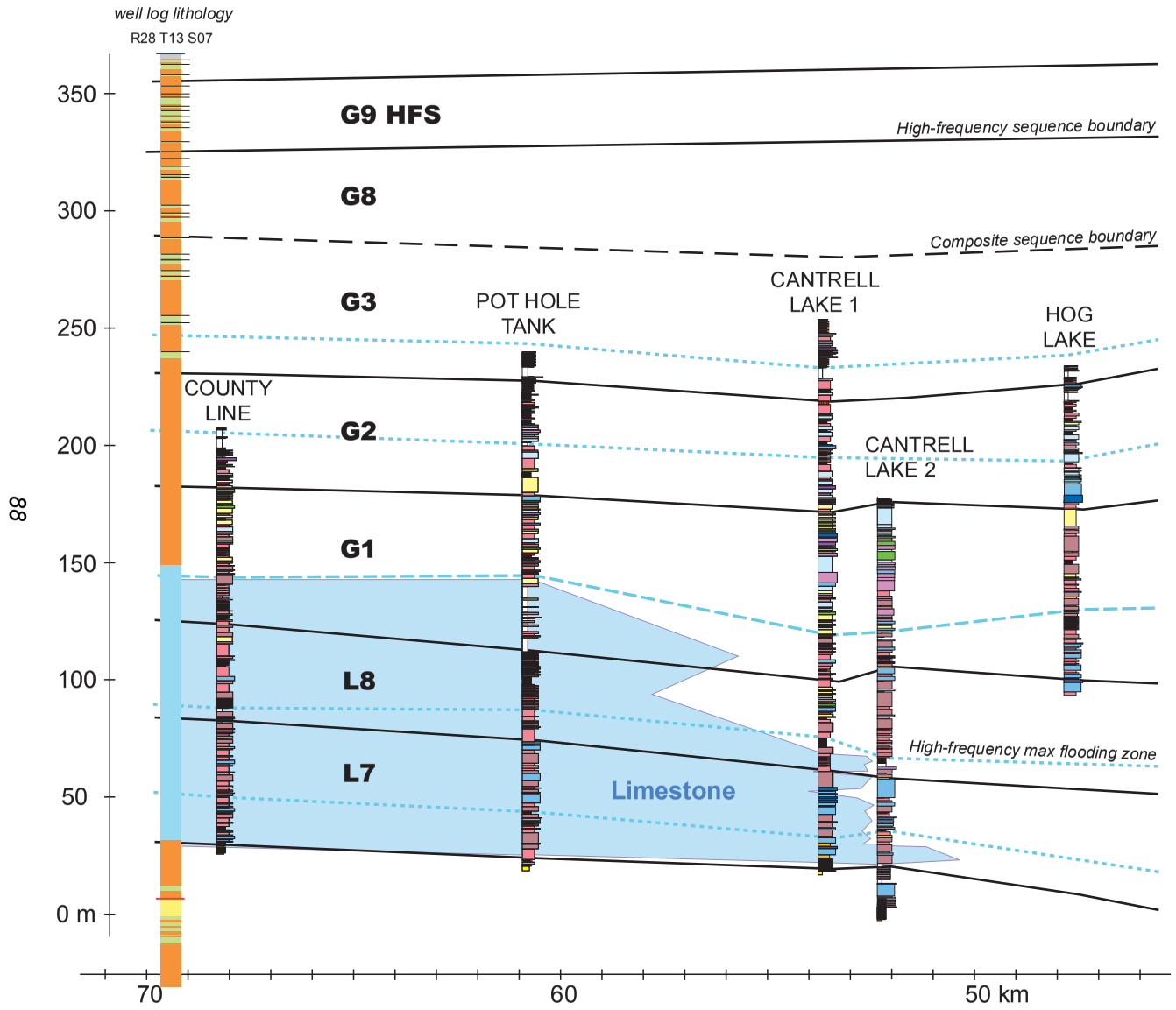

Figure 2.4: Five new sections in the far north-west end of the Algerita Escarpment (see Figure 2.2 for legend). These sections record the transition from an open marine ramp to a restricted inner platform and are dominated by mud-rich facies. Log interpretation from a well located in section 7, township 13, range 28 shows strong agreement between outcrop and subsurface lithologies (see Figure 2.6 for legend). Subsurface data also show that the eroded part of the outcrop is composed of interbedded anhydrite and dolostone.

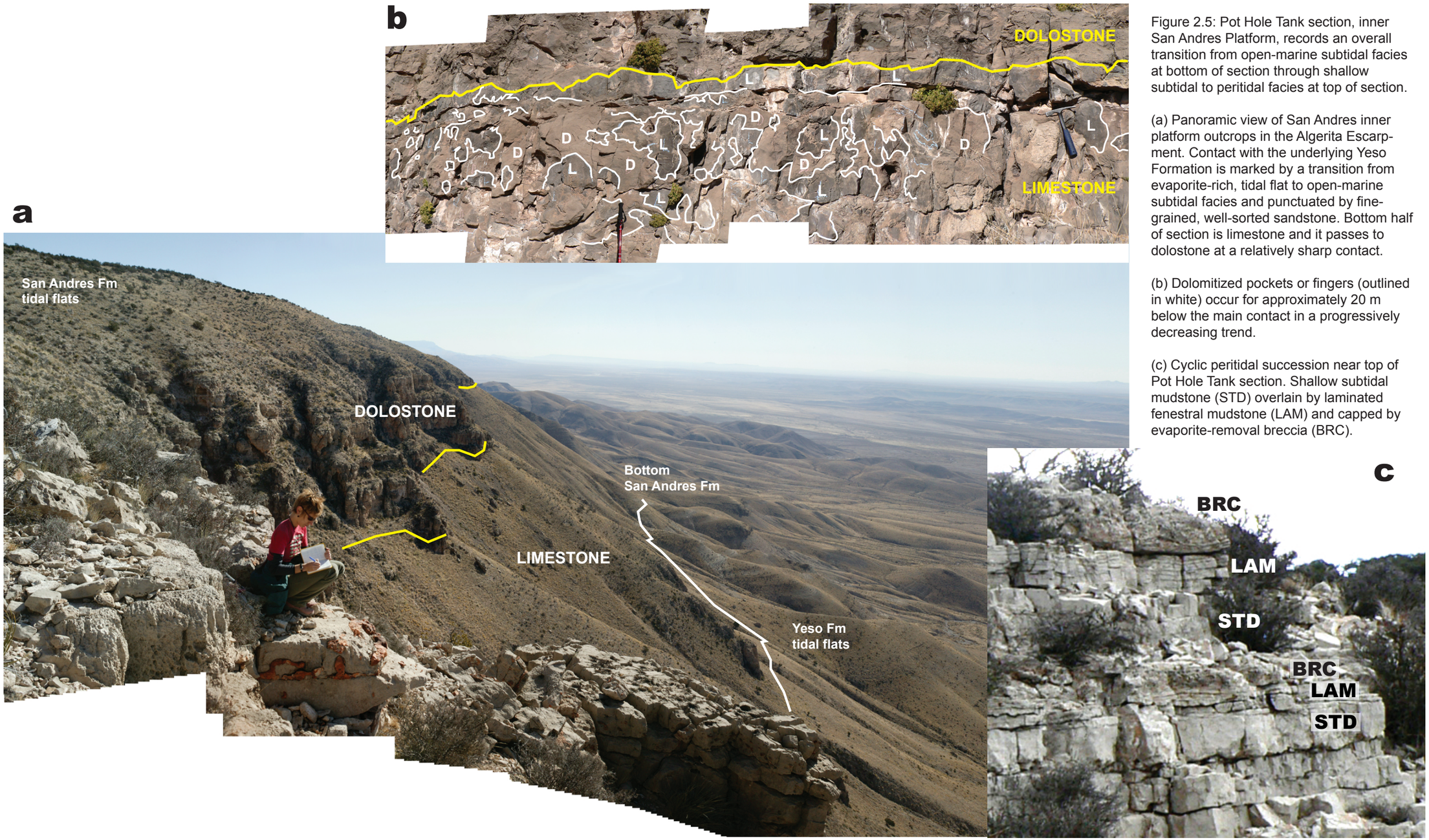

Figure 2.5: Pot Hole Tank section, inner San Andres Platform, records an overall transition from open-marine subtidal facies at bottom of section through shallow subtidal to peritidal facies at top of section.

(a) Panoramic view of San Andres inner platform outcrops in the Algerita Escarpment. Contact with the underlying Yeso Formation is marked by a transition from evaporite-rich, tidal flat to open-marine subtidal facies and punctuated by fine-grained, well-sorted sandstone. Bottom half of section is limestone and it passes to dolostone at a relatively sharp contact.

(b) Dolomitized pockets or fingers (outlined in white) occur for approximately 20 m below the main contact in a progressively decreasing trend.

(c) Cyclic peritidal succession near top of Pot Hole Tank section. Shallow subtidal mudstone (STD) overlain by laminated fenestral mudstone (LAM) and capped by evaporite-removal breccia (BRC).

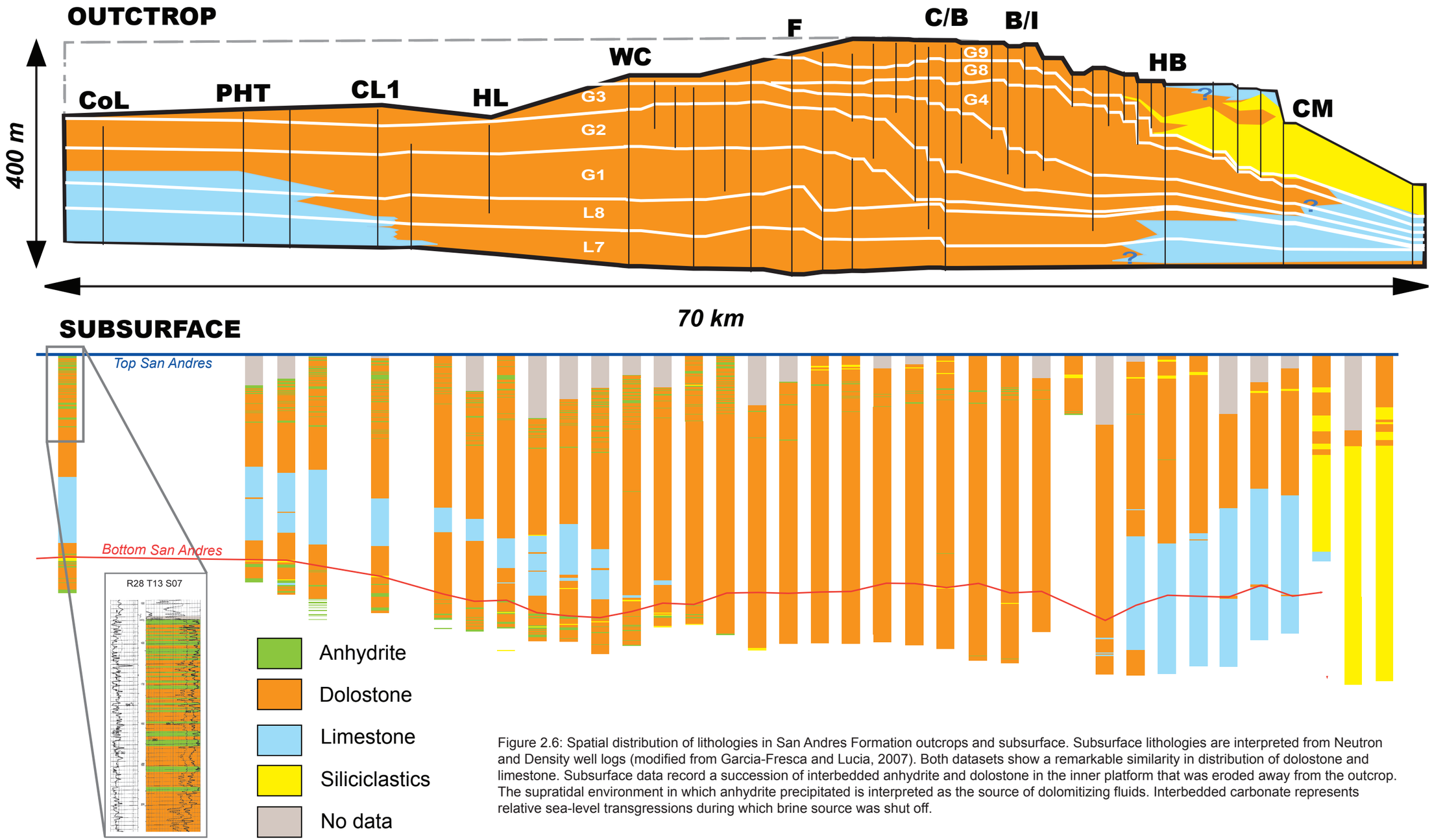

Figure 2.6: Spatial distribution of lithologies in San Andres Formation outcrops and subsurface. Subsurface lithologies are interpreted from Neutron and Density well logs (modified from Garcia-Fresca and Lucia, 2007). Both datasets show a remarkable similarity in distribution of dolostone and limestone. Subsurface data record a succession of interbedded anhydrite and dolostone in the inner platform that was eroded away from the outcrop. The supratidal environment in which anhydrite precipitated is interpreted as the source of dolomitizing fluids. Interbedded carbonate represents relative sea-level transgressions during which brine source was shut off.

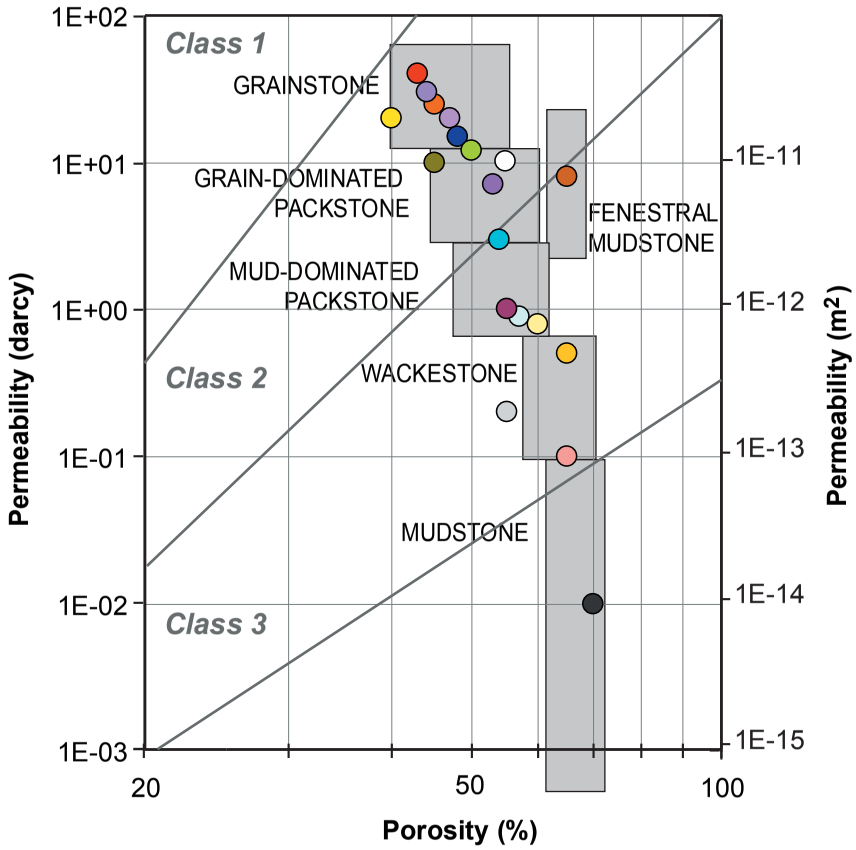

Decptn coeff	Poro (%)	Perm (darcy)	
1.1	43	40	Pel-ooid grainstone, cross laminated
1.1	44	30	Fusi-crin grainstone, massive, rare skeletals
1.1	45	25	Ooid-peloid grainstone, sheet laminated
1.1	40	20	Sandstone
1.2	47	20	Peloid grainstone
1.2	48	15	Brach-fusi-peloid grainstone
1.2	50	12	Crin-fusi-pel grain-dominated packstone
1.5	55	10.2	Carbonate breccia with sandstone-rich matrix
3	45	10	Gypsum
2	65	8	Fenestral mudstone, tidal flat cap
1.3	53	7	Peloid grain-dominated packstone, wavy laminated
1.4	54	3	Coral-bryo-brach-crin grain-dominated packstone
1.5	55	1	Coral-bryo-brach-crin mud-dominated packstone
1.5	57	0.9	Peloid mud-dominated packstone, vertical burrows
1.5	60	0.8	Fusulinid-peloid mud-dominated packstone
1.5	65	0.5	Dasyclad-peloid wackestone
1	55	0.2	Crin-spong-brach-bryo boundstone/bafflestone
2	65	0.1	Bioclastic wackestone
2.5	70	0.01	Mudstone

Measurements on recent carbonate sediments by Enos and Sawatsky (1980)

Figure 2.7: Petrophysical property values assigned to San Andres Formation facies of Kerans and Kempter (2002). Porosity and permeability values of carbonate fabrics based on Enos and Sawatsky (1981) measurements of modern carbonate sediments (shaded grey), except for boundstone/bafflestone and carbonate breccia. Values for gypsum based on Murray (1964), Hardie (1967), Hovorka (1991), and Warren (2006). Values of well-sorted, fine to medium sand from Beard and Weyl (1973). Decompaction coefficients based on Goldhammer (1997).

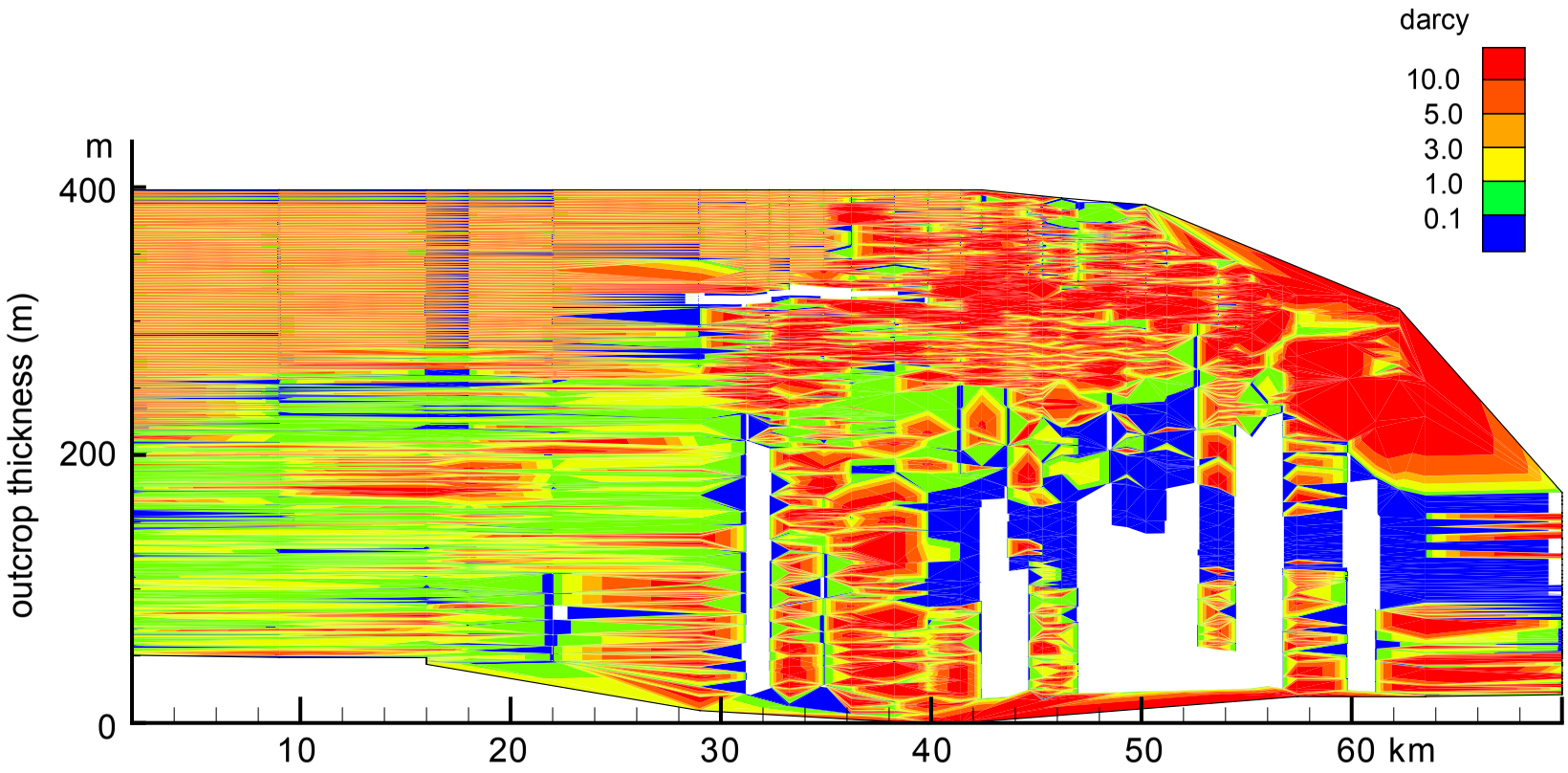

Figure 2.8: Plot of permeability of modern carbonate sediments applied to San Andres Formation facies based on rock fabrics, prior to upscaling. Facies tracts represented in Figure 2.3 can be recongnized. Inner platform succession reconstructed based on subsurface data (Figure 2.6). In white are areas with no outcrop data available.

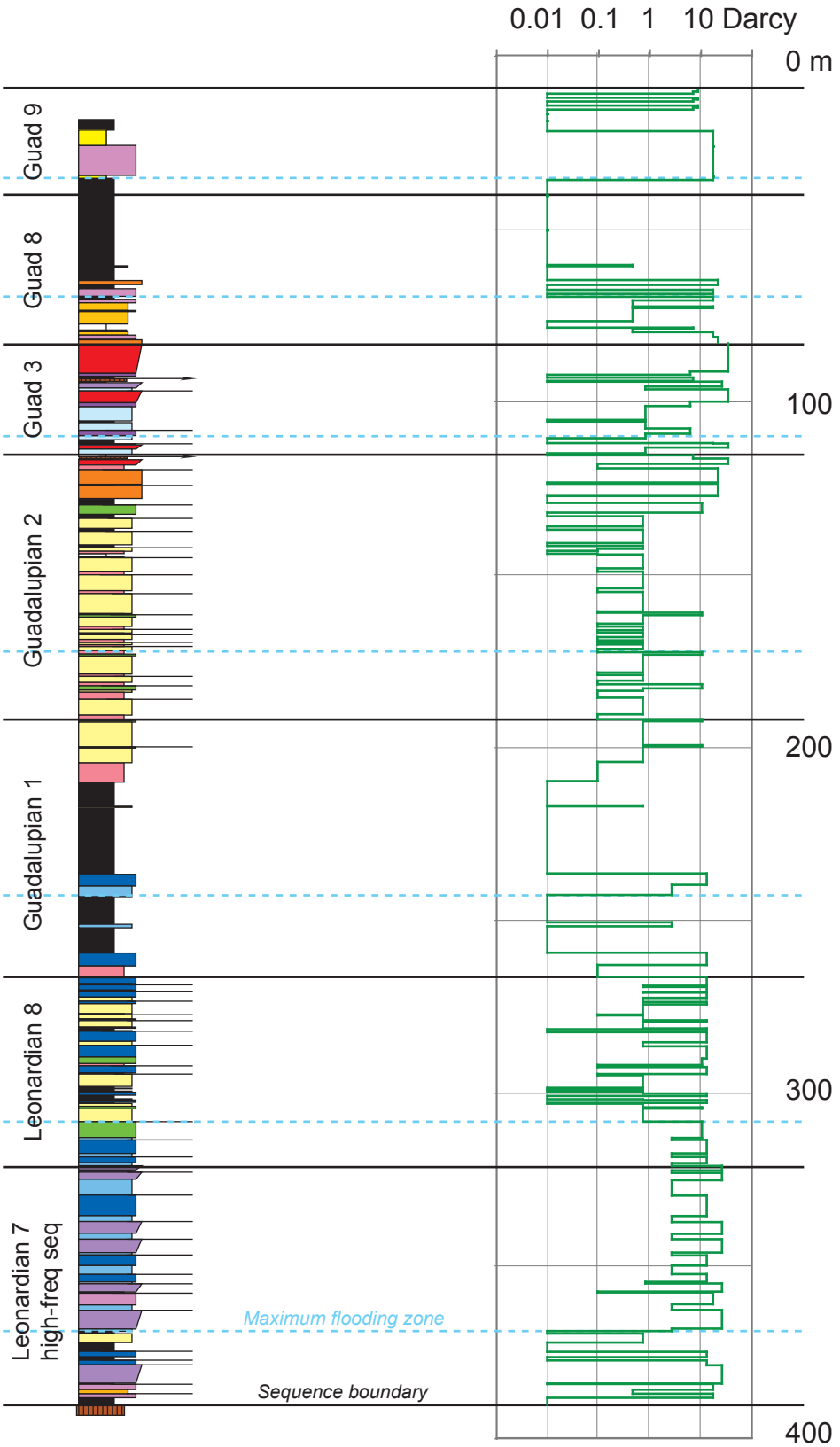

Figure 2.9: Example of permeability profile at Lawyer Canyon section (Figure 2.2). Permeability values based on rock fabrics and measurements from modern carbonate sediments by Enos and Sawatsky (1981), as shown in Figure 2.7.

Figure 2.10: Modeling layers (shaded alternately gray and white) built on the basis of sequence boundaries (black), maximum flooding zones (blue), and vertical permeability profiles (green). Vertical successions of muddy and grainy fabrics were grouped into a modeling layer to preserve heterogeneity of original outcrop dataset into the petrophysical model. Restricted carbonate/evaporite cycles in the inner platform, eroded away from outcrop, were reconstructed on the basis of well log data and flow layers extrapolated horizontally from outer-platform measured sections.

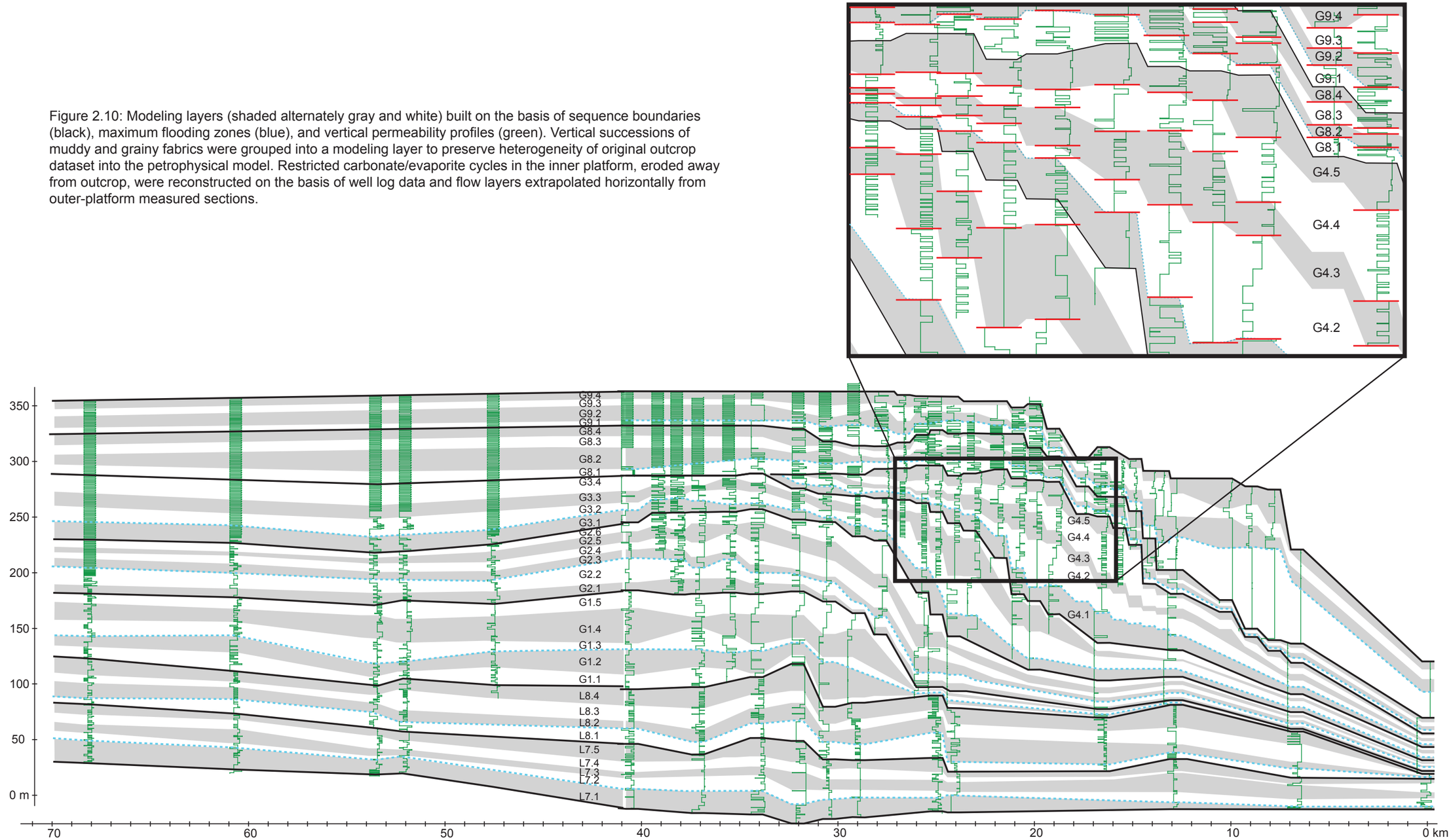

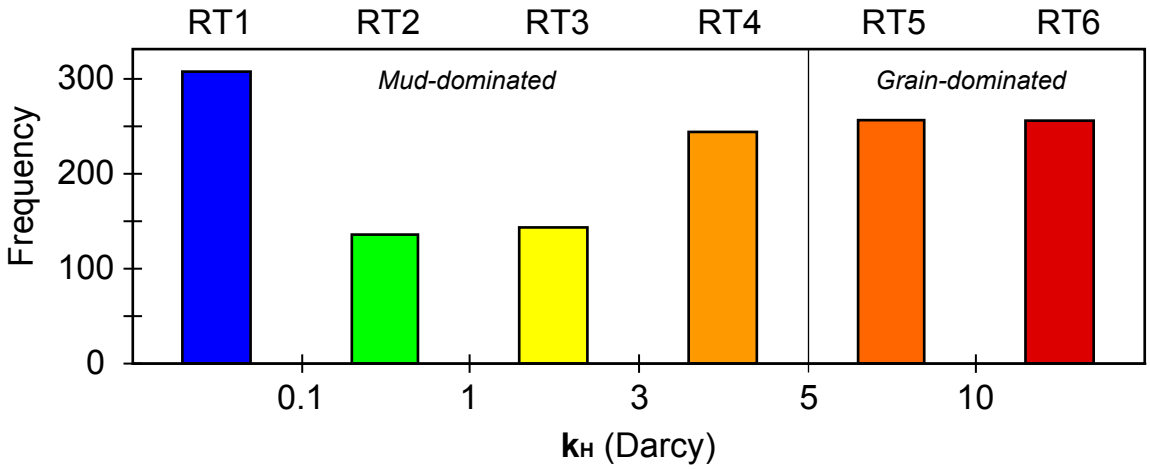

Figure 2.11: Histogram of average horizontal permeability (kH) values. Bins correspond to cutoffs that define six rock types.

Table 2.1: Petrophysical properties of modeling rock types (RT): decompaction coefficients, average porosity (phi), average horizontal permeability (kH), average vertical permeability (kV), and permeability anisotropy coefficients (kH/kV and kV/kH).

	Decomp coeff	**Phi**	**k_H** (Darcy)	**k_V** (Darcy)	**k_H/k_V**	**k_V/k_H**
RT1	2.47	0.70	0.02	0.01	1.11	0.90
RT2	1.86	0.63	0.57	0.19	2.97	0.34
RT3	1.81	0.61	2.02	0.43	4.70	0.21
RT4	2.11	0.61	4.20	0.45	9.41	0.11
RT5	1.53	0.56	7.39	2.30	3.21	0.31
RT6	1.30	0.49	18.07	10.73	1.68	0.59

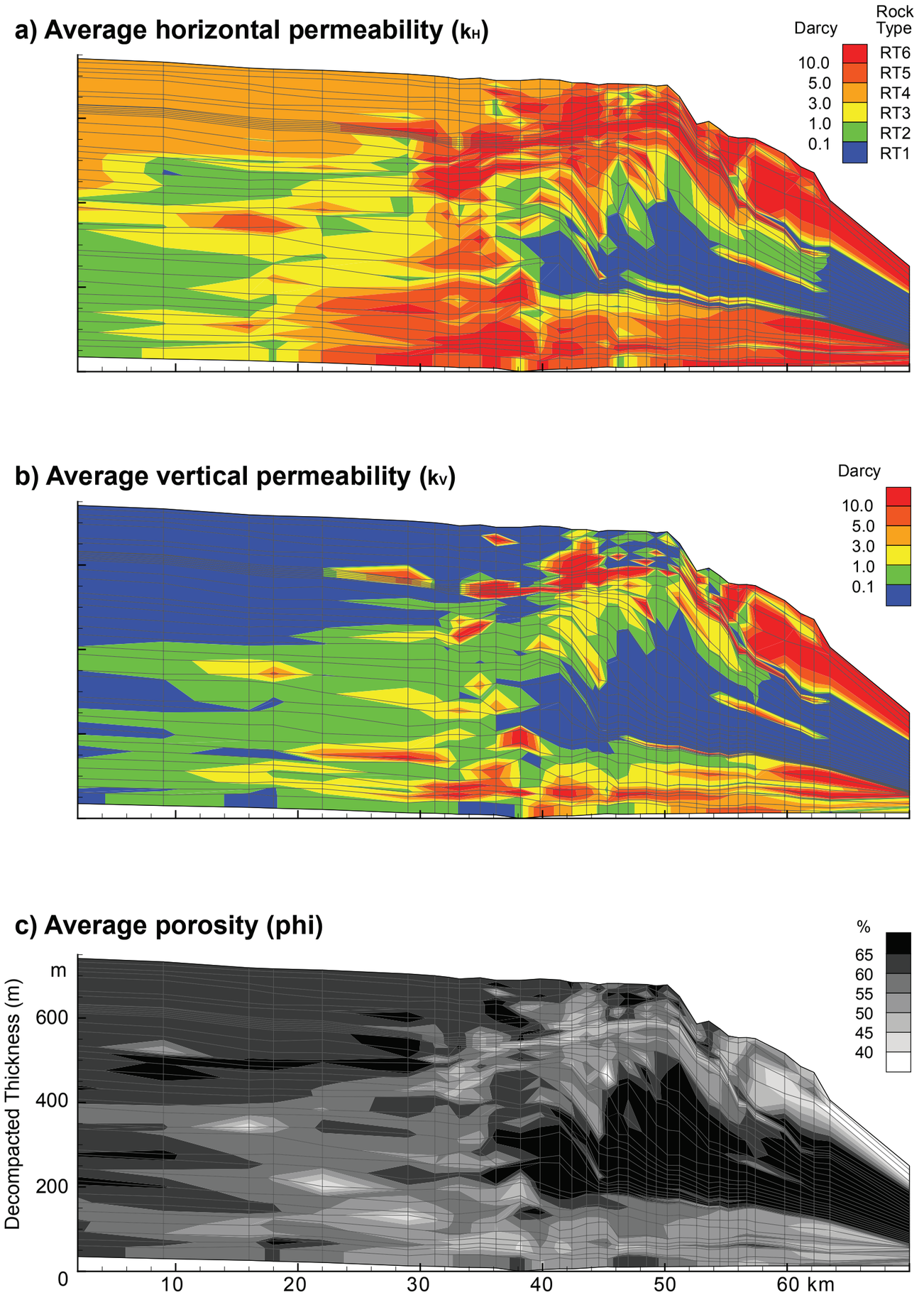

Figure 2.12: Upscaled petrophysical model based on outcrop facies and properties of newly deposited carbonate sediments. This data is the input intial conditions for the hydrogeological simulations described in chapter 3.

(A) Average horizontal permeability (kH) and rock types (RT); kH was computed as the arithmetic mean.

(B) average vertical permeability (kV), computed as the harmonic mean.

(C) average porosity (phi)

Chapter 3

OUTCROP-CONSTRAINED HYDROGEOLOGICAL SIMULATIONS OF BRINE REFLUX AND IMPLICATIONS FOR EARLY DOLOMITIZATION OF THE PERMIAN SAN ANDRES FORMATION

Abstract

A hydrogeologic model tests the effectiveness of brine reflux as the mechanism for early dolomitization of the Permian San Andres Formation. Brine circulation is constrained by sequence stratigraphic parameters and a heterogeneous distribution of petrophysical properties based on outcrop data. It simulates the accumulation of the San Andres platform and calculates fluid flow and solute transport in response to relative sealevel fluctuations. It tracks porosity loss due to compaction and the concomitant permeability feedback. The amount of dolomite that can potentially be formed is calculated by means of a magnesium mass balance between brine and rock. Results show that: (1) brine reflux is an effective mechanism to deliver magnesium to dolomitize large carbonate successions; (2) relative sealevel-controlled transient boundary conditions result in intricate flow patterns and salinity distributions and can generate irregular dolomite bodies of complex spatial distribution; (3) pervasive

dolomitization can be the result of several short-lived reflux events by the amalgamation of brine plumes sourced in different locations and times; and (4) the model successfully recreates the dolostone/limestone patterns observed on San Andres outcrops.

Introduction

Here I present a numerical simulation of brine circulation and solute transport in a carbonate platform with implications for dolomitization. The model design and boundary conditions are constrained by outcrop data of the Permian San Andres Formation along the Algerita Escarpment, Brokeoff Mountains and Western Escarpment of the Guadalupe Mountains (Figure 3.1). The model simulates the accumulation of the carbonate platform with boundary conditions that change over time.

Fluid flow is the mechanism that delivers reactants and removes products of diagenetic reactions (Land, 1985) and is a critical rate-controlling parameter in dolomitization. Different fluid circulation regimes and geochemical systems can generate different distributions and geometries of diagenetic bodies (e.g. Machel, 2004; Wilson et al., 1990). This study focuses on dolomitization by brine reflux. Reflux is a broadly accepted dolomitization model and is supported by field and core descriptions,

petrographic observations, geochemical analyses, and numerical modeling (e.g. Pray and Murray, 1965; Zenger et al., 1980; Zenger and Mazzullo, 1982; Shukla and Baker, 1988; Purser et al., 1994; Warren, 2000; Braithwaite et al., 2004). In this paper, the term reflux is referred to as the general process by which seawater is restricted in peritidal/supratidal environments, concentrates by evaporation, flows downward driven by density gradients, and dolomitizes underlying sediments.

Significant progress has been made in studying the hydrodynamics of refluxing fluids using hydrogeological models, analytical (e.g. Simms, 1984; Shields and Brady, 1995) and numerical (e.g. Kaufman, 1994; Jones et al., 2002; Whitaker et al., 2004; Jones and Xiao, 2005). Such models estimated flow rates and patterns of dolomitization for a variety of platform geometries and boundary conditions; demonstrated the suitability and effectiveness of the reflux mechanism to deliver reactants; and placed broad spatial and temporal constrains on this process. However, in these studies reflux was approached as a single or limited number of fluid circulation events that do not fully represent the transient nature of boundary conditions, which are the consequence of sealevel fluctuations,

and the concomitant migration of depositional environments and brine sources.

Reflux is principally driven by density gradients. Density-dependent fluid flow has the potential to transport solutes faster and farther than advective flow alone (Simmons et al., 2001). Field studies of variable density fluid flow show that these flow regimes are transient and short-lived, and respond to seasonal changes in boundary conditions (Fenstemaker et al., 2001, Stevens et al., in press). As a result, earlier numerical models of reflux demanded long temporal scales and/or high permeability values. In some of these models, petrophysical properties were treated as homogeneous and isotropic, which does not reflect the variability observed in carbonates and the critical role of heterogeneity on fluid flow (e.g. Sudicky, 1986; Hinrichs et al., 1986; Lucia et al., 1992; Eisenberg et al., 1994; Grant et al., 1994; Kerans et al., 1994; Jennings, 2000). Some models prescribed specific brine flow rates rather than determining them based on thermohaline gradients.

Garcia-Fresca and Jones (in review; Chapter 4) used reactive transport modeling to demonstrate that a discrete dolostone body may be generated by the cumulative action of several brines sourced in different stratigraphic

locations and times. This study revealed the importance of a well-constrained sequence stratigraphic framework for understanding early diagenesis. Parameters controlling dolomitization (time, location and extent of fluid source, hydraulic potential, chemical potential, and petrophysical properties) depend on sequence stratigraphic controls such as relative sealevel position, the rate of sealevel rise and fall, shoreline position, sedimentation rate, topography of the platform top, and depositional environments. Depositional environments prone to restricted marine circulation and evaporation, such as tidal flats, are the source of concentrated fluids capable of dolomitizing carbonate sediments (Deffeyes et al., 1965; Patterson, 1972; Patterson and Kinsman, 1982). Lucia (1972) proposed that the migration of such environments in response to relative sealevel fluctuations allows these fluids to sweep across the platform top and dolomitize broad successions. Studies of the rock record show that certain stratigraphic settings are more prone to dolomitization. Lucia and Major (1994) and Saller and Henderson (1998) showed that the degree and style of dolomitization is a function of location within the platform and distance to the brine source along a flow path. In the Ordovician Upper Knox Group, dolomite is more abundant in restricted platform environments and falling sealevel stages than in environments with open ocean circulation and rising relative sealevel (Montañez and Read, 1992).

In the Mississippian Madison Formation, hypersalinity and concomitant dolomitization developed during sealevel rises associated with the formation of restrictive barriers to marine circulation (Sonnenfeld, 1996; Smith et al., 2004).

I propose that reflux dolomitization is a process that progresses simultaneously with platform accumulation. It may appear to be a continuous process on large time scales (> 10^4 years) and yet be intermittent in shorter scales. In this model, relative sealevel ultimately controls conditions necessary for reflux, such as hydraulic gradients, the location and extent of the brine source, brine chemistry, and brine residence time. Sealevel fluctuations drive sedimentation and the migration of environments and, thus, result in transient boundary conditions for reflux circulation. This model is based on a well-established sequence stratigraphic framework used to constrain the deposition of a carbonate platform and evolving boundary conditions driven by relative sealevel fluctuations. Saline convection is used to determine flow rates and salinity distributions across the platform. A petrophysical model represents the heterogeneity observed on San Andres outcrops. Dolomitization takes place when and where a combination of appropriate conditions occur, such as simultaneous high fluid flow rate and salinity. I

hypothesize that many reflux events over time and space result in the pervasive dolomitization of the platform and are responsible for the complex limestone/dolostone distributions observed in carbonate formations.

Below I present the San Andres Formation outcrop dataset and the petrophysical model derived from it that is used as model input. I describe the hydrogeological model design and the results of the simulations, especially flow rates and salinity distributions. Finally, a magnesium mass-balance addresses the implications of the model results for dolomitization of the San Andres platform.

Geological and petrophysical models

The model is based on outcrop descriptions and well logs of San Andres Formation in west Texas and New Mexico (Figure 3.1). Outcrop and subsurface studies show that San Andres carbonates were dolomitized by refluxing brines shortly after deposition (Bein and Land, 1982; Ruppel and Cander, 1988; Leary and Vogt, 1990; Colgan, 1990). Extensive outcrop studies and a robust stratigraphic framework by Kerans and Fitchen (1995) and Kerans and Kempter (2002) make this formation a good candidate for this model. The outcrop dataset (Figure 3.2) provides

fundamental stratigraphic and lithologic constraints for hydrogeological modeling: timing of sediment accumulation, platform geometry, relative sealevel and shoreline position, location of restricted environments where brines may be sourced, and the distribution of facies, lithologies and petrophysical properties across the platform. Facies descriptions were converted into a porosity and permeability model (Chapter 2) and used as input data.

The San Andres platform accumulated during the middle Permian near the equator and under arid conditions (Kerans and Fitchen, 1995). Biostratigraphic and radiometric studies indicate a duration for the accumulation between 2 and 4 million years, from late Leonardian to early Guadalupian (Cooper and Grant, 1972-77; Wilde, 1986; Ross and Ross 1987; Harland et al., 1989; Wardlaw and Grant, 1990). According to Kerans and Kempter's (2002) interpretation, the formation consists of two composite sequences recording two consecutive 3rd order relative sealevel rises and falls (Figure 3.2A). Platform deposits can be further subdivided into eight carbonate high-frequency sequences, 4th order of cyclicity (L7 and 8, G1-4, and G8 and 9). The platform was flooded through the Leonardian high-frequency sequences with a sealevel maximum coincident with the Guadalupian 1 high-frequency sequence

maximum flooding zone. Relative sealevel dropped progressively through G4. The platform was exposed and the aeolian siliciclastics (G5-7) were deposited in the basin, and are not part of this model. Significant erosion happened on the platform top during this period of exposure and clastic bypass. G8 and G9 record another composite sequence deepening and shallowing cycle. Each high-frequency sequence also records a relative sealevel rise and fall, which are reflected in the hydrogeological model. A higher frequency signal is recognizable in most measured sections but the lateral correlation of such cycles is problematic, and such level of resolution is excessive for the scale of this model.

Depositional environments in the San Andres Formation can be recognized based on facies tracts (Kerans and Kempter, 2002; Figure 3.3). Inner platform facies are represented by dolomudstones and evaporites and are eroded from the outcrop and is best developed in the younger, regressive San Andres high-frequency sequences. Garcia-Fresca and Lucia (2007) reconstructed this tract based on lithologies interpreted from well logs (Figure 3.2B) and scarce brecciated outcrop successions (Figure 3.2C). Middle platform facies consist mainly of peloidal packstones and tidal flat cycles. Unrestricted areas of the platform are composed of wackestones, packstones, and grainstones with open

marine fauna. The platform crest is composed of peloidal and skeletal packstones and grainstones. Slope facies can be found in the Guadalupian high-frequency sequences and consist of mudstones and siliciclastic sand. Although most of the San Andres Fm is composed of dolostone, some areas remain undolomitized as shown in Figure 3.2A.

Construction of the petrophysical model is described in detail in Chapter 2 and it is summarized below. Because brine circulation occurs simultaneously with platform accumulation, the petrophysical properties in the model must reflect those of recently deposited sediments. Petrophysical values are assigned to the different outcrop facies based on rock fabrics and measurements of modern carbonates by Enos and Sawatsky (1981; Figure 3.4). On outcrop, facies change abruptly in the vertical dimension (of the sub-meter scale) and gradually in the horizontal scale (over tens to hundreds of meters). Based on these observations, Lucia (2007) suggests that high-frequency cycles are the optimal stratigraphic element to construct a petrophysical model for reservoir performance simulations. Given the regional scale of this study, I subdivide the stratigraphy into layers that may contain several high-frequency cycles. Following Lucia's (2007) method, the stratigraphy is subdivided into layers (Figure 3.5) based on vertical permeability profiles

constructed for each measured section. Vertical intervals of similar permeability are grouped and correlated between sections. High-frequency sequence boundaries and maximum flooding surfaces are preserved to maintain chronostratigraphic succession in the layering. The remaining layer boundaries are assumed to also represent time lines. Outcrop thicknesses are decompacted to depositional values based on Goldhammer's (1997) approach as portrayed in Figures 3.5A and 3.5B. Properties are averaged in each measured section, within each modeling layer. Horizontal permeability is computed as the arithmetic average, and vertical permeability as the harmonic average. Porosity and permeability values are upscaled again, based on permeability ranges, to define six rock types to be used as input in the hydrogeological model (Figure 3.4). Figure 3.6 shows plots of horizontal permeability (kH), vertical permeability (kV), porosity (phi0), and rock types (RT). The resulting petrophysical model reduces variability, preserves facies tracts and relevant stratigraphic features, and provides time constraints for the hydrogeological modeling. Note that this petrophysical model is more heterogeneous and certainly more realistic than previous models that used homogeneous and isotropic permeability fields.

The hydrogeological model based on this dataset tests the stratigraphic and petrophysical controls on brine circulation. The model allows simulation of the dolostone/limestone patterns observed on outcrop, based on the timing of brine reflux, the location within the platform with respect to the brine source, and the distribution of petrophysical properties.

Model design and boundary conditions

The model consists of 39 layers derived from the petrophysical model (Figure 3.5). Layers are assumed to be bound by timelines that are deposited consecutively. Boundary and initial conditions are different for each layer, (i.e. thickness, geometry, relative sealevel position, distribution of petrophysical properties, and source of dolomitizing fluids). Fluid flow, solute transport, and compaction equations are solved for each layer. The numerical code used on the simulations is Basin2 (Bethke et al., 2002), a software that simulates the evolution of groundwater flow regimes within sedimentary basins through time. This basin simulator was previously used to simulate fluid flow in carbonate platforms by Kaufman (1994) and Jones and Xiao (2006). Basin2 allows the design of the arrangement of strata along a two-dimensional cross-section, including deposition and erosion, and to distribute physical and hydrologic properties. Program

output relevant to this study includes: (1) fluid flow through the basin in response to buoyant forces, topographic relief, and sediment compaction; (2) groundwater salinity, accounting for advection, diffusion, hydrodynamic dispersion, and the presence of evaporites; and (3) porosity and permeability of materials across the basin, as calculated from overburden stress, fluid pressure, and stress history. Additional capabilities include: (4) temperature distribution by heat conduction, groundwater advection, and crustal heat flux; (5) mineral precipitation and dissolution along flow paths; (6) pore fluid pressure, accounting for burial compaction and unloading rebound, topographic relief, thermal expansion, and fluid flow; (7) distribution of radioactive and radiogenic isotopes in basin groundwater; and (8) thermal maturation of organic matter, including the timing of oil and gas generation and the distribution of mature petroleum sources through time.

Platform topography and relative sealevel position affect hydraulic gradients across the domain. The geometry of the platform evolves from a very low angle ramp, sigmoidal ramp, to a platform with a relatively steep margin (Figures 3.2 and 3.5B). The two-dimensional grid is designed based on outcrop measured sections and the petrophysical model layers. It consists of 2652 cells, 1 km in length and of variable thicknesses from 0

to 50 m, when sediment accumulate, and up to -10 m, when strata are eroded (Figure 3.5C). Cells accumulate layer by layer, coinciding with the layering of the petrophysical model. Layers are labeled according to Kerans and Kempter's (2002) nomenclature for San Andres Formation high-frequency sequences followed by a digit indicating the position of the layer within the high-frequency sequence (e.g. G3.1 is the oldest layer of four within the Guadalupian 3 high-frequency sequence).

Hydraulic properties vary across the platform based on the petrophysical model discussed in Chapter 2 (Figure 3.6). Rock Type 1 (RT1) includes mostly mudstones and coincides with the slope deposits of Guadalupian 1-4 high-frequency sequences. RT2 represents mud-rich fabrics elsewhere. Both RT1 and RT2 have low average permeabilities. RT3 groups mud-rich fabrics with a large proportion of mud-dominated packstones. RT4 mainly includes the carbonate/sulfate cycles of the restricted inner platform, which are thinly bedded. Both RT3 and RT4 have intermediate average permeabilities but RT4 has a high anisotropy ratio (kH/kV) because the facies are thinly bedded and, thus, have relatively low kV values. RT5 and RT6 represent the grainier fabrics of the platform crest and have high average permeabilities. Porosity (phi0) shows a

decreasing trend from RT1 to RT6, which reflects the progression from mud-rich to grain-rich fabrics.

Table 1 summarizes the most relevant hydraulic properties of rock types. Initial porosity ranges between 49 and 70% (after Enos and Sawatsky, 1981) as discussed in Chapter 2. Lowest porosity values are found in grain-rich fabrics whereas maximum values are found in pure carbonate mud. Changes in porosity (phi) at each time step are determined based on initial porosity (phi0), irreducible porosity (phi1), depth (z) and coefficient of burial compaction (bpor) as follows:

$$phi = phi0 \exp(-bpor * z) + phi1 \quad (1)$$

Initial horizontal permeability (kH or perm_max) values range between 0.02 and 18.07 darcy (1.9×10^{-14} to 1.9×10^{-11} m^2). Changes in permeability (k) are computed from porosity based on a semi-logarithmic transform of the form:

$$\log k = A\ phi + B \quad (2)$$

Porosity-permeability transforms are adjusted through parameters A and B to approximate Lucia's (1995) log-log transforms for carbonate rocks (Figure 3.7A).

Permeability anisotropy is determined as the ratio between horizontal and vertical permeabilities (kH/kV).

Initial layer thicknesses are based on decompacted outcrop values and change over the course of the simulation as a function of burial compaction (compare Figures 3.5B, and C). The coefficient of burial compaction (bpor) controls the shape of compaction curves (Table 1). Compaction curves for each rock type (Figure 3.7B) are assigned as function of depth and rock fabric, according to the studies by Schmoker and Halley (1982) and Goldhammer (1997).

Field-scale hydrodynamic dispersion is a function of heterogeneity of the porous medium and, perhaps, scale of observation (Dagan, 1986; Gelhar et al., 1992; Schulze-Makuch, 2005; Niemann and Rovey, 2009). I prescribe values based on a numerical modeling rules-of-thumb that suggest longitudinal dispersivity should be about an order of magnitude smaller than the modeling domain (68 km), and larger than one-fourth the

length of the cell (1 km). Transverse dispersivity is often an order of magnitude smaller than longitudinal dispersivity (Gelhar et al., 1992). Thus, I prescribe a longitudinal dispersivity of 25 m and a transverse dispersivity of 2.5 m. However, the magnitude of dispersivity affects the spread of the solute but not necessarily its median travel time (Fernandez and Gomez, 2007) and, thus, it is not deemed a critical parameter in this study. Other parameters, such as diffusivity and density of rock grains, default to Basin2 values for a generic carbonate (Bethke et al., 2002).

Initial fluid pressure through the domain is hydrostatic and the initial fluid composition in newly deposited sediment is that of modern seawater (0.5 NaCl molality).

Model boundary conditions are summarized in Figure 3.8. The bottom boundary is impermeable and closed to flow and solute flux, justified by the low-permeability evaporite-rich succession of the underlying Yeso Formation. Pressure is hydrostatic at the top boundary where submerged below sealevel; where exposed, it has a pressure distribution equivalent to the elevation head and the head due to the density brine. Salinity is approximated as NaCl molality (i.e. 0.5 molal for seawater). Where the platform is exposed, a constant concentration boundary is specified, of

salinity of 1.5 molal as NaCl, simulating a brine source based on seawater concentrated to gypsum saturation. The right and left boundaries are open to advective transport and the concentration gradient across it is fixed at zero, which prevents diffusive transport. Boundary conditions change during the course of the simulation, as relative sealevel fluctuates and new layers of sediment accumulate (Figure 3.9). The system is isothermal. Geothermal heat fluxes affect fluid density gradients and fluid flow but, in the shallow subsurface, these gradients are small compared to density gradients due to salinity contrasts generated by brine reflux (Jones et al., 2003; Jones et al., 2004).

Given the uncertainty in the timing of San Andres accumulation described above, I assume it to span three million years, an intermediate duration value. Layers have variable thickness but are assumed to record constant sedimentation rates. Thus the duration of the accumulation of each layer varies from 37,000 to 98,000 years. Because reflux is a transient and ephemeral process (Stevens et al., in press), I assume brine is available only 10% of the time for each layer, and no other fluid circulation takes place between reflux events. Therefore, the total duration of the flow simulation is 300,000 years.

Simulation results

The simulations begin with the deposition of layer L7.1; there is a long period of non-sedimentation, exposure, and erosion during G5-7; and sedimentation resumes until the deposition of layer G9.4. Basin2 calculates a variety of parameters but only the most relevant to dolomitization are described below. Fluid flow and solute transport is calculated for each of the layers and its specific boundary conditions. Figure 3.10 illustrates the results for the transgressive-regressive cycle of high-frequency sequence G3, following a relative sealevel rise and fall (Figure 3.10A).

Fluid flow shows complex patterns due to the evolving geometric configuration and boundary conditions, and mixed-convective circulation under the saline source (Figure 3.10B). Highest flow rates are found immediately below the hypersaline source, near the shoreline (Figures 3.10B and C), and in high-permeability zones that are below the brine source (Figures 3.10C and F). Flow rates increase towards each Guadalupian high-frequency regression, and progressively in younger high-frequency sequences. Flow rates are negligible during Leonardian time, as the platform was submerged below sealevel and no hypersaline environment existed. Maximum flow rates in high-frequency sequence G1

are near 1 m^3/yr; 2 m^3/yr in HFSs G2 and 3; and 5-6 m^3/yr in HFSs G4, 8 and 9.

Salinities vary over time and space in response to sealevel fluctuations and related shrinking and expanding of the hypersaline environment (Figure 3.10D). Although the salinity of the fluid at the source remains constant throughout the simulation, the size of the source varies considerably throughout each 4^{th} order relative sealevel rise and fall (Figure 3.10B), and progressively larger over the course of the simulation, in response to 3^{rd} and 2^{nd} order sealevel cycles (Figure 3.9). Salinity values range between seawater (0.5 molal) and brine (1.5 molal). Highest salinities are found immediately below the brine source. However, high salinities remain at depth even when the source has been shut off in response to a relative sealevel rise and shrinking of the hypersaline environment (Figure 3.10D).

Basin2 calculates porosity and permeability as a function of burial compaction following equations 1 and 2. Figures 3.10E and F show the subtle porosity and permeability loss during the deposition of G3 high-frequency sequence. Figure 3.11 shows a comparison between the initial porosity used as model input and the porosity distribution at the end of the

simulation. The largest porosity changes occur in the deepest parts of the platform and progressively decrease towards the top. Porosity changes in L7 HFS range from 5-20 percentage points, in comparison to 0-5 in G9. Areas with abundant mud-rich facies, represented by RT1 also show large porosity losses, even with modest degrees of burial.

Magnesium mass balance and potential dolomitization

The potential amount of dolomite that could be formed during deposition of the San Andres Formation is estimated based on the two-dimensionally distributed flow rates, salinities and porosities calculated from Basin2 simulations. This is accomplished with a magnesium mass-balance between the brine and the rock (e.g., Shields and Brady, 1995; Jones et al., 2003). In previous studies a magnesium mass balance was computed from average flow rates, whereas in this study it is carried out for each grid cell and each time step to estimate the spatial and temporal distribution of dolomite. The volume of dolomite is computed as follows:

$$V_{dls} = \frac{cMg_{fluid} \times Q \times t}{cMg_{rock}} \times eff$$

Where, *Vdls* (m^3) is the potential volume of dolostone that could be formed during each time step; *cMgrock* (kg/m^3) is the concentration of magnesium in dolostone composed of 100% stoichiometric dolomite, and is a function of porosity; *cMgfluid* (kg/m^3) is the magnesium concentration in the fluid; *Q* (m^3/yr) is the volumetric flow rate of brine; *t* (yr) is the amount of time of brine circulation for each layer; and *eff* (-) is the efficiency coefficient of the magnesium-calcium exchange reaction. The volumes of dolostone generated during the deposition of each layer (Figure 3.10G) are summed after each time step to obtain a cumulative volume and distribution of dolostone (Figure 3.10H).

Dolomite distributions were estimated for a range of magnesium/calcium replacement efficiencies from 10 to 100% (e.g., Shields & Brady, 1995; Jones et al., 2000; Jones et al., 2003). Figure 3.12 shows model results for the progressive formation of dolostone during the deposition of the San Andres platform, for a 50% efficiency. During late Leonardian and beginning of Guadalupian time the platform was submerged and no dolomite formed, according to the model. First exposure and hypersaline conditions developed during the late highstand of high-frequency sequence G1 and dolostone began to form. Dolomite formation came nearly to a halt during 4^{th} order transgressions and progressed quickly

during regressions. The size of the hypersaline environment became progressively larger for each consecutive highstand resulting in the formation of progressively increased volumes of dolostone. The platform top was exposed and eroded for an extended period during the lowstand that separates both composite sequences (G5-7). No hypersaline environment was prescribed on the simulations during this period. In the event of moderate flushing by meteoric water, the brine saturating the formation continued to dolomitize during this time. Large amounts of dolostone formed during the strongly regressive high-frequency sequences, G4, G8 and 9. By the end of San Andres deposition the platform was almost pervasively dolomitized, with a few remaining undolomitized areas.

The potential volume of dolostone formed varies for different magnesium exchange efficiencies (Figure 3.13). A 100% efficiency creates pervasive dolomitization of the whole platform whereas a 25% efficiency creates a patchy pattern. Limestone/dolostone relationships observed in outcrop can be approximated with reduced efficiencies (compare Figures 3.13A and C). Undolomitized areas respond to locations within the platform that have not experienced much brine circulation, because of the combined effects of the location with respect to the brine source, distance along flow paths,

and the hydraulic properties of the rocks. Figure 3.13D illustrates how dolostone bodies in different locations within the platform are generated by different combinations of favorable dolomitizing conditions. Some dolostone bodies were generated by their proximity to the brine source and the shoreline, which provides high salinities and flow rates (e.g. Figure 3.13D1). Areas immediately underneath the brine source that have low flow rates could remain undolomitized (e.g. Figure 3.13D2). Areas of high permeability and prevailing high salinities are also preferentially dolomitized, even if they were never located immediately below the brine source (e.g. Figure 3.13D3). Permeability contrasts also appear to favor dolomitization (e.g. Figure 3.13D4; this particular example may be an artifact of grid configuration, but illustrates the effect of permeability contrasts wherever they may exist in nature). Finally, areas that have never experienced high salinity and seldom high flow rates also remain undolomitized (e.g. Figure 3.13D5).

Discussion

A robust sequence stratigraphic and petrophysical framework is critical for defining the transient and intertwined boundary conditions of early reflux dolomitization. The principal controls on the circulation pattern and volume of early diagenetic fluids are: time, location and extent of brine source,

hydraulic potential, chemical potential, and petrophysical properties. All of these controls are, in turn, controlled by sequence stratigraphic parameters such as relative sealevel position, the rate of sealevel rise and fall, shoreline position, sedimentation rate, topography of the platform top, and depositional environments. For instance, hydraulic gradients are controlled by relative sealevel position, topographic relief on the platform top, and fluid density contrasts. Fluid composition and concentration are controlled by the degree of restriction across the platform top, which are a function of relative sealevel position, topography and the nature of the source of fluids (marine, meteoric, connate). The duration of the flow regime is a function of the relative sealevel position, the rate of change of sealevel and the rate of sediment accumulation. Porosity and permeability of the sediments depend on their depositional fabric, which is a function of the depositional environment, ecological system and, ultimately, of relative sealevel position. The complex combination and interdependence of these factors produces transient fluid circulation regimes that generate intricate diagenetic geobodies over time. These results support the hypothesis by which a platform may be dolomitized by the cumulative effect of many short-lived reflux events and is in agreement with findings discussed in Chapter 4 (Garcia-Fresca and Jones, in review), such that a dolostone body may be generated by several pulses of brine that are sourced at

different times and locations. Unraveling the hierarchy of such interdependent controls should be accomplished by detailed sensitivity studies.

Results illustrate the importance of physical heterogeneity in hydrogeological modeling and dolomitization. Areas of high permeability focus the flow of diagenetic fluids, when and where these are available. High flow rates can deliver larger volumes of magnesium and result in more dolomitization and areas with lower permeability show a relative paucity in the formation of dolomite (Figure 3.10). Results also show that high salinities within the platform can be long-lived, even when the brine source has been shut off (Figure 3.10D). This phenomenon was called “latent reflux” by Jones et al., (2002) and implies that dolomitization may progress at depth at times when the source of refluxing brines is not present.

Although most of the San Andres dolomite is interpreted as formed by refluxing fluids soon after deposition, other dolomitizing mechanisms could have acted simultaneously or postdating the platform accumulation, contributing to the current distribution of dolomite in the formation.

Petrographic and geochemical studies could contribute to unravel the complexity of superimposed brine circulation events and continuous recrystallization of reflux dolomite. Such studies should address the spatial distribution of crystal sizes and habits, crystal zonations and overgrowths, stoichiometry, isotopic and trace element trends and fluid inclusions (Kupecz et al., 1993; Banner, 1995).

As in any model, there are sources of uncertainty and limitations to this model. A critical factor in the simulations involves the duration of San Andres accumulation, constrained by biostratigraphy to be between 2 and 4 million years, and assumed to be 3 million years in the simulation. This has a large implication on the assumed sedimentation rates and brine residence times. The residence time of the brine source and duration of the flow regime on each time step is another source of uncertainty, although studies on modern reflux settings indicate these are small in comparison with depositional processes (Stevens et al., in press). I limited flow circulation to 10% of sediment accumulation time. Sedimentation rates are assumed constant and modeling layers assumed bound by time lines. The exact composition, salinity and density of brines are unknown, and simulations do not account for reactive transport along flow paths that could resolve some of the chemical feedbacks between different

diagenetic phases. Thus, this model uses salinity as a proxy to determine the magnesium concentration but does not account for magnesium depletion along flow paths, as dolomitization progresses. Most importantly, the kinetics of dolomitization at surface temperatures are poorly known (Land, 1998; Arvidson and Mackenzie, 1999; Wilson et al., 2001); thus, the efficiency of the magnesium/calcium exchange, a critical control, is large source of uncertainty as shown by these results. Some parameters contributing to the efficiency factor include the amount of synsedimentary dolomite present in the system (seed effect), the effective reactive surface area of dolomite, the stoichiometry of early formed dolomite, and permeability feedbacks related to mineral dissolution/precipitation. Basin2 boundary conditions on the left and right sides of the model may allow some regional groundwater to flow into the model from the left. However, it is not unfeasible that some regional flow may have existed that could have affected the resulting dolomitization patterns in the San Andres platform. However, preliminary modeling efforts suggested that regional groundwater flow was almost negligible in such thin and flat carbonate environment.

Conclusions

The hydrodynamic analyses show that brine reflux can be an effective mechanism to dolomitize large carbonate successions. I illustrate how predicting the distribution of early diagenetic products can be accomplished by sequence stratigraphically-constrained synsedimentary hydrogeological simulations. I constructed a hydrogeological model based on outcrop data of the Permian San Andres Formation to estimate flow rates and salinity distributions over time and the potential amount of dolomite that may be generated. The resulting limestone/dolostone distribution generally approximates the pattern observed on outcrops of the San Andres Formation.

I show that relative sealevel-controlled transient boundary conditions result in intricate flow patterns and salinity distributions, and can generate irregular dolomite bodies of complex spatial distribution. Dolostone bodies across the platform may be generated by different combinations of favorable conditions, such as proximity to the brine source, zones of relatively higher permeability, and permeability contrasts.

These findings support the hypothesis that pervasive dolomitization can occur as the cumulative action of many short-lived reflux events by the

amalgamation of successive dolostone bodies sourced in different locations and times. This model contrasts with previous studies that approached dolomitization of a carbonate platform as a single or limited number of reflux events.

The model also reveals critical controls on brine reflux and subsequent dolomitization. These include: time, fluid flow rate, brine chemistry, and permeability which are, in turn, a function of sequence stratigraphic factors such as relative sealevel and depositional environments. The efficiency of magnesium/calcium exchange, which represents the net chemical and biological controls, is also a critical control on this process. The model confirms the relevance of “latent reflux”, or brines that may continue to dolomitize in the subsurface, after the source has been shut off.

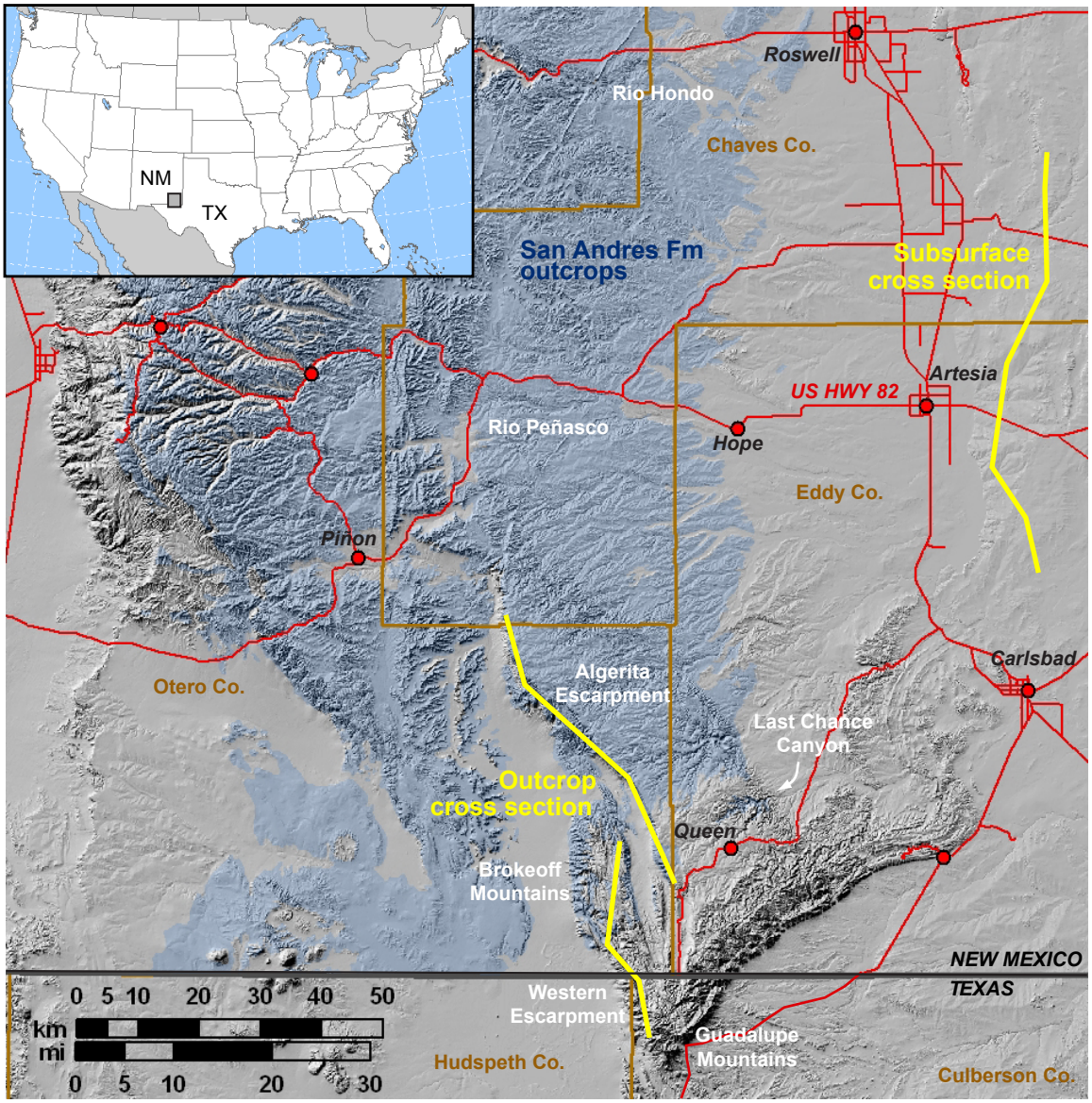

Figure 3.1: Location map of San Andres Fm outcrops in west Texas and southeastern New Mexico (Sources of GIS public access data: US Geological Survey and New Mexico Resource Geographic Information System). Yellow lines show the approximate location of outcrop and well log cross-sections used on this study.

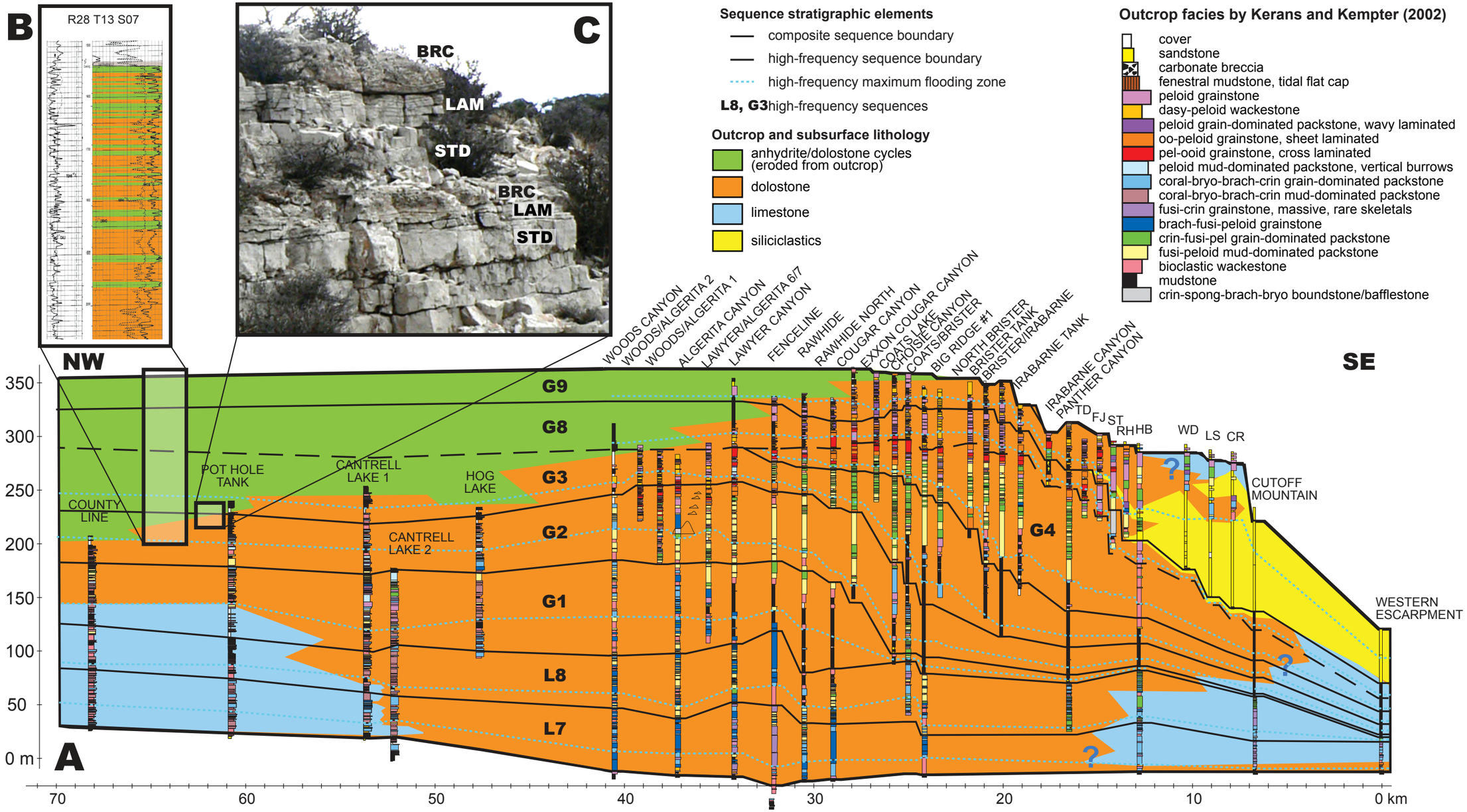

Figure 3.2: Outcrop dataset of the Permian San Andres Formation. A) Measured sections, sequence stratigraphic framework, and lithology. The restricted inner platform (green) is composed of interbedded evaporites and carbonates and interpreted as the source of dolomitized fluids. B) Example of well log used to infer lithology in eroded areas (Garcia-Fresca and Lucia, 2007). C) The inner platform is sparsely represented on outcrop by peritidal cycles of subtidal mudstone (STD), laminated fenestral mudstone (LAM), and evaporite removal breccia (BRC).

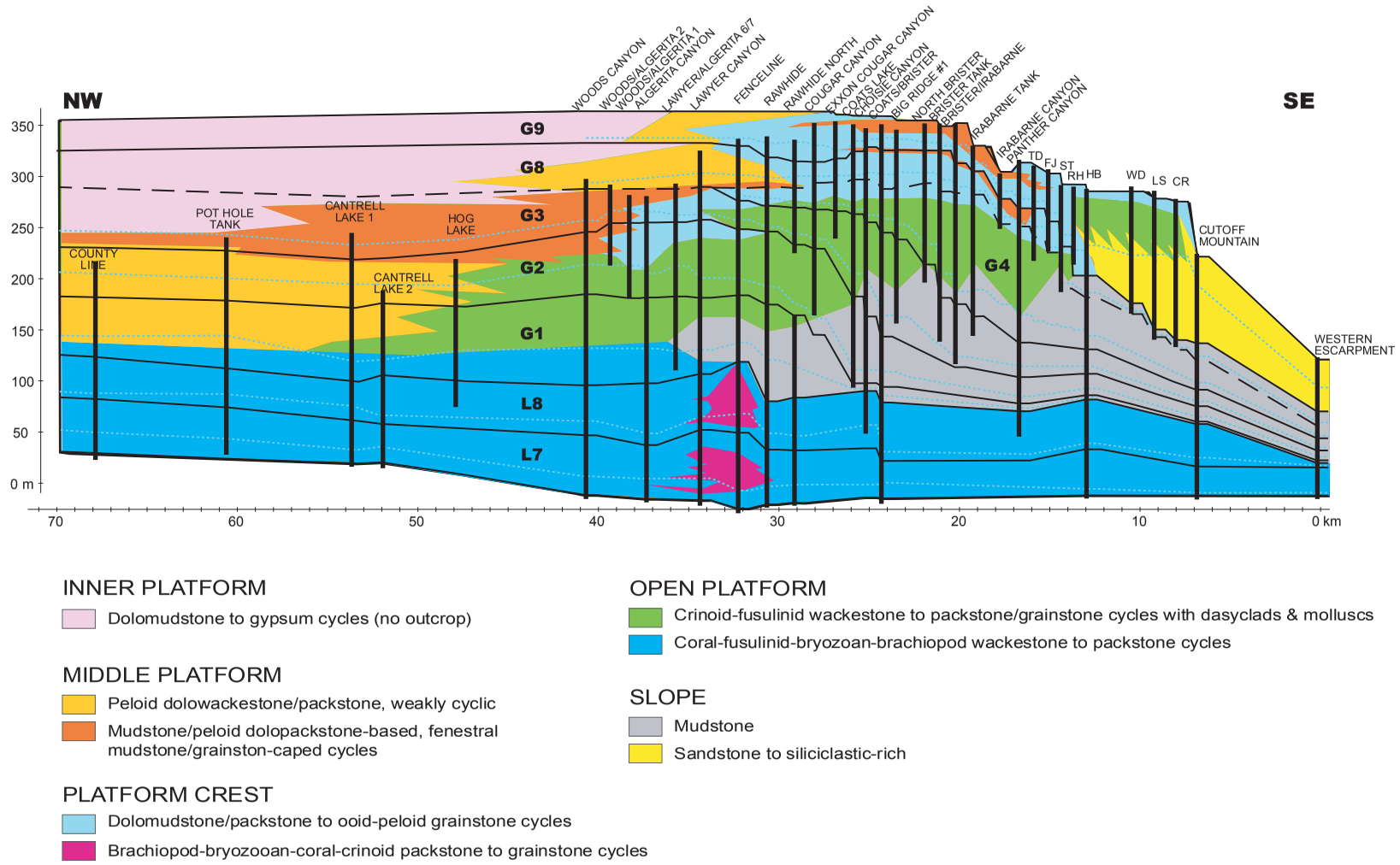

INNER PLATFORM

- Dolomudstone to gypsum cycles (no outcrop)

MIDDLE PLATFORM

- Peloid dolowackestone/packstone, weakly cyclic
- Mudstone/peloid dolopackstone-based, fenestral mudstone/grainston-caped cycles

PLATFORM CREST

- Dolomudstone/packstone to ooid-peloid grainstone cycles
- Brachiopod-bryozooan-coral-crinoid packstone to grainstone cycles

OPEN PLATFORM

- Crinoid-fusulinid wackestone to packstone/grainstone cycles with dasyclads & molluscs
- Coral-fusulinid-bryozoan-brachiopod wackestone to packstone cycles

SLOPE

- Mudstone
- Sandstone to siliciclastic-rich

Figure 3.3: Facies tracts of the San Andres Formation reflect the evolution of conditions and depositional environments across the platform (modified from Kerans and Kempter, 2002). Horizontal lines are high-frequency sequence boundaries and maximum flooding zones. Vertical lines are locations of measured sections.

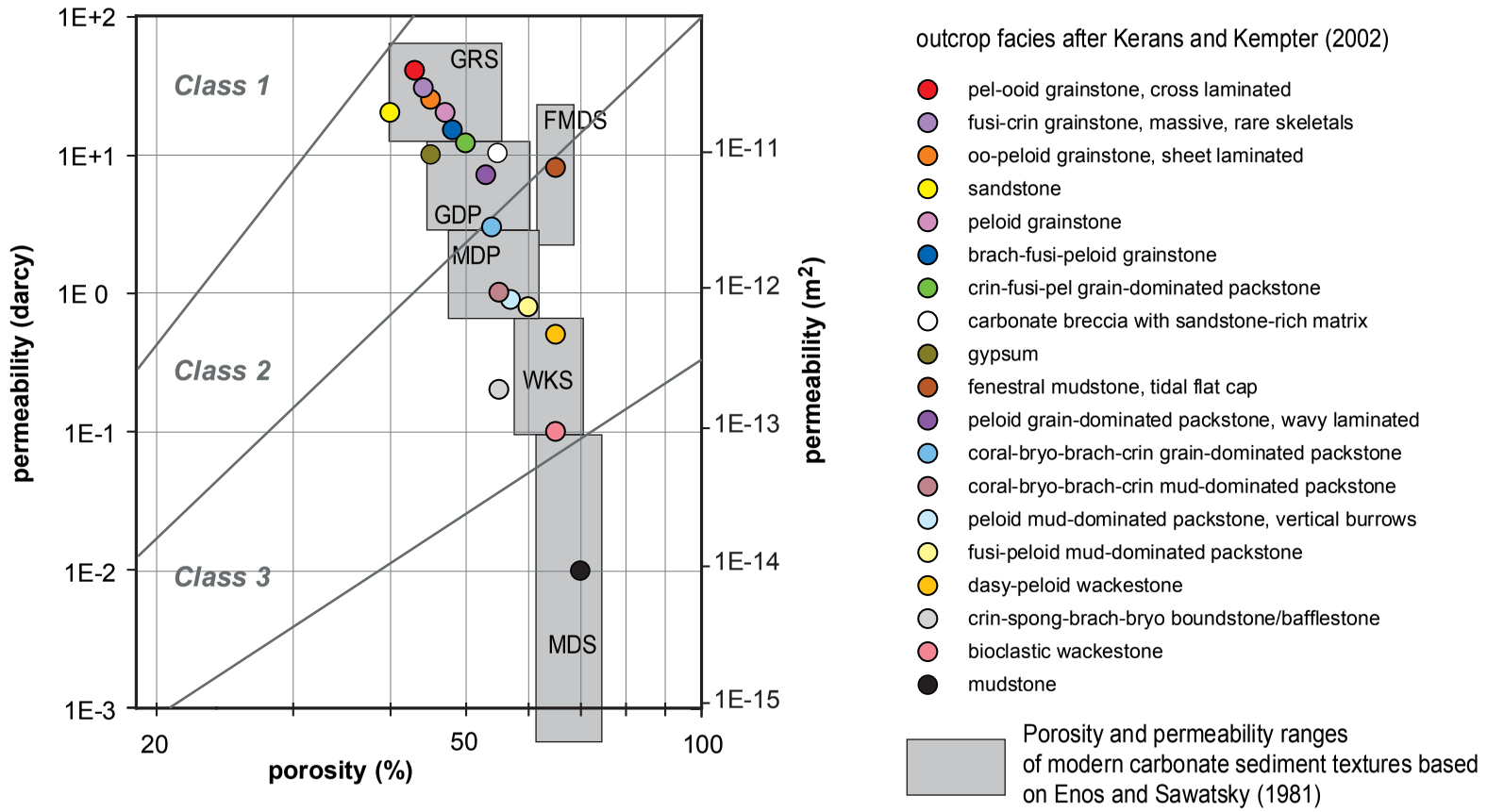

Figure 3.4: Porosity and permeability values of modern carbonate sediments after Enos and Sawatsky (1981; gray shading) are used to assign values to facies of Kerans and Kempter (2002; circles) based on their fabric. Newly deposited carbonates plot as class 2 and 3 of Lucia's (1995) classification of carbonate fabrics, with the exception of pure mud. GRS: grainstone; GDP: grain-dominated packstone; MDP: mud-dominated packstone; FMDS: fenestral mudstone; WKS: wackestone; MDS: mudstone.

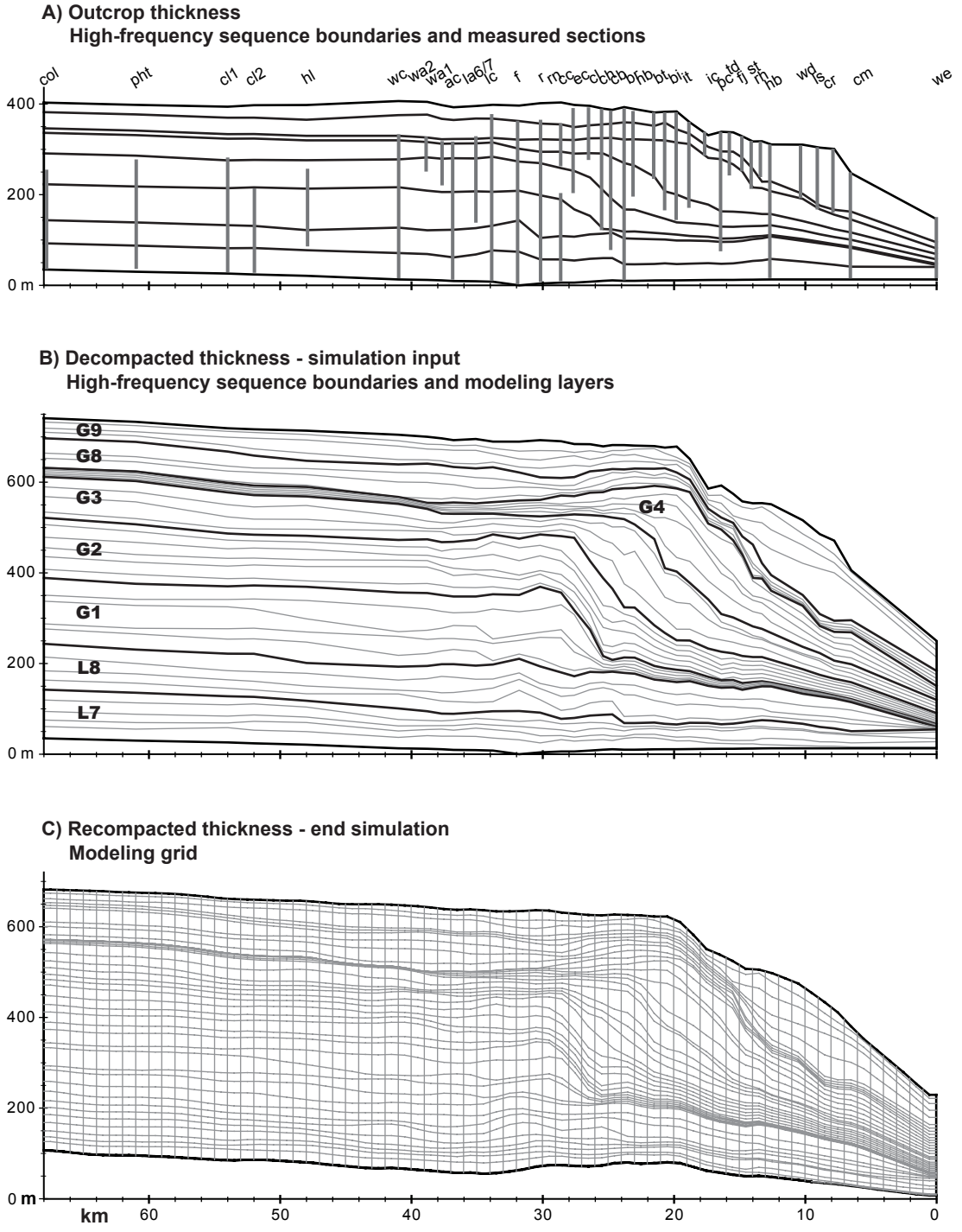

Figure 3.5: Comparison of outcrop, decompacted and recompacted thicknesses of the San Andres platform model. A) Outcrop thicknesses and location of measured sections. B) Decompacted thicknesses used as input in the hydrogeological simulations (after Garcia-Fresca et al., in preparation; Chapter 2) and high-frequency sequence boundaries (after Kerans and Kempter, 2002). C) Model grid and mechanically recompacted thicknesses at the end of the simulation.

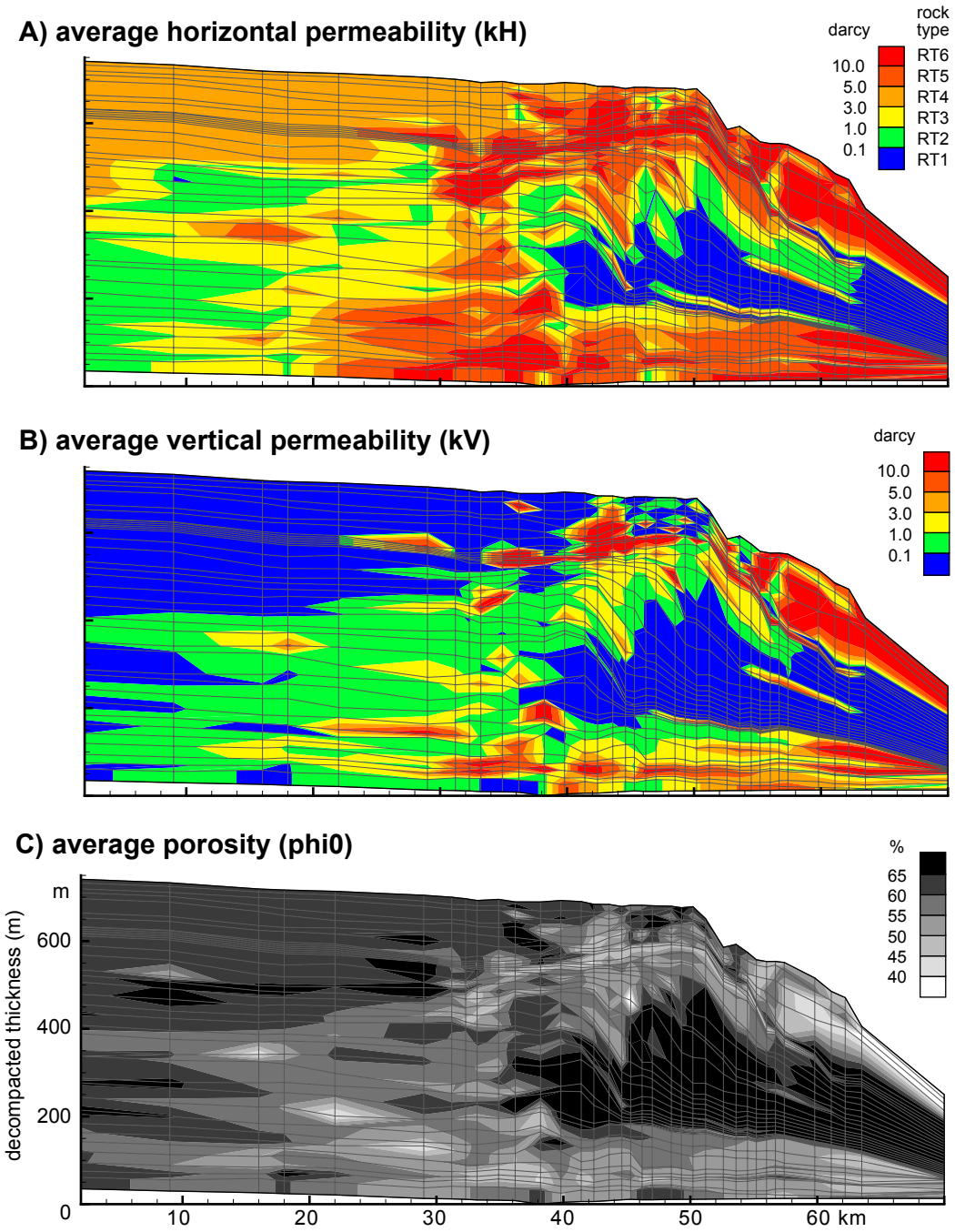

Figure 3.6: Petrophysical model based on upscaled outcrop descriptions of the San Andres Fm (Garcia-Fresca et al., in preparation; Chapter 2) used as initial values in hydrogeological simulations (Figure 3.4, Table 3.1). A) Average horizontal permeability (kH or perm_max) and modeling rock types (RT); highest values are associated with the grainstone-rich platform crest; lowest values can be found in the slope mudstones of high-frequency sequences G1-4. B) Average vertical permeability (kV); lowest values correspond to slope mudstones of G1-4 and thinly interbedded sulfate/carbonate cycles of the restricted inner platform. C) Average porosity (phi0); depositional porosity increases with increasing mud content.

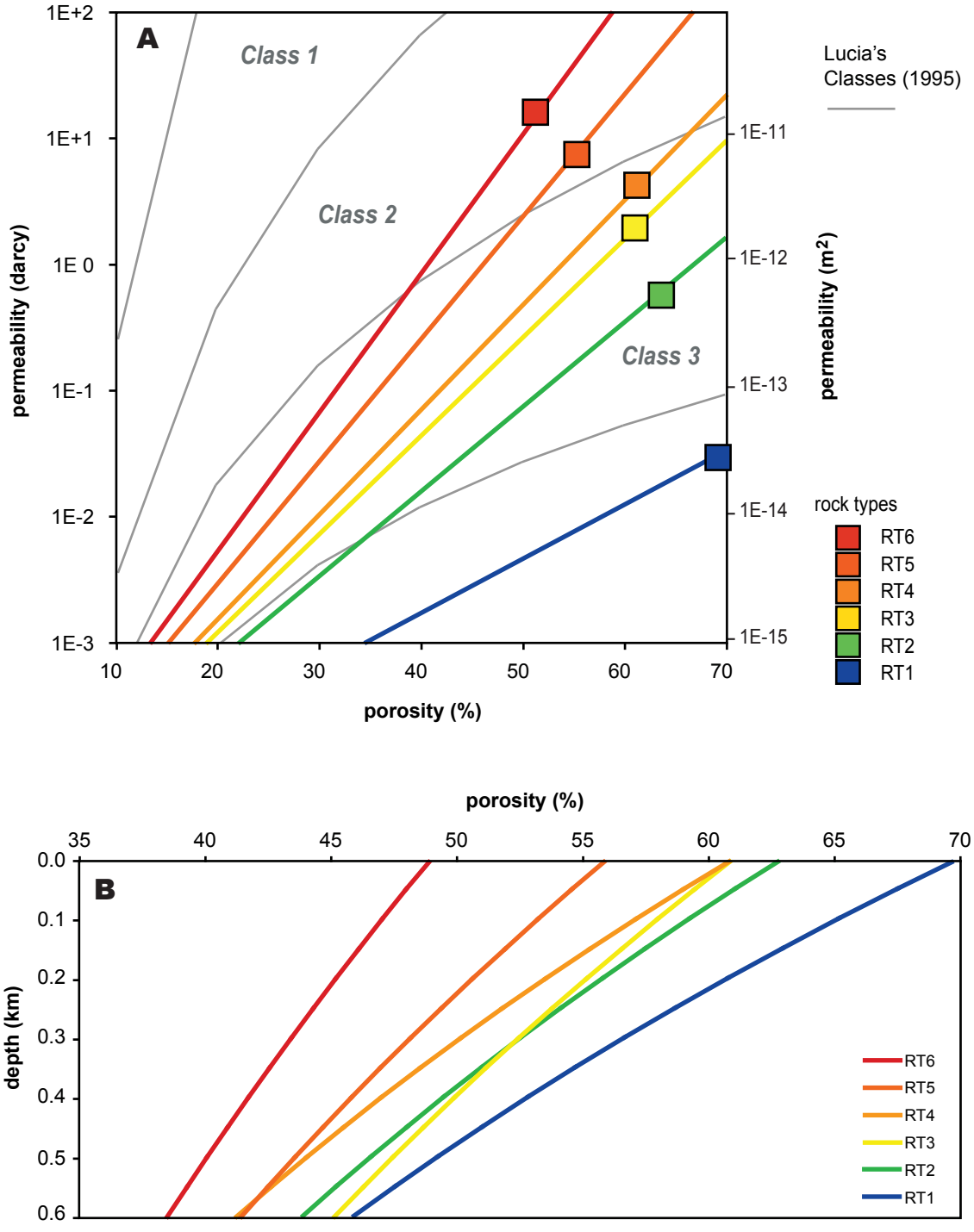

Figure 3.7: Petrophysical properties of rock types. A) Porosity and permeability values, and transforms describing the relationship between the two, compared to Lucia's 1995 log-log transforms. B) Compaction curves based on Schmoker and Halley (1982) and Goldhammer (1997).

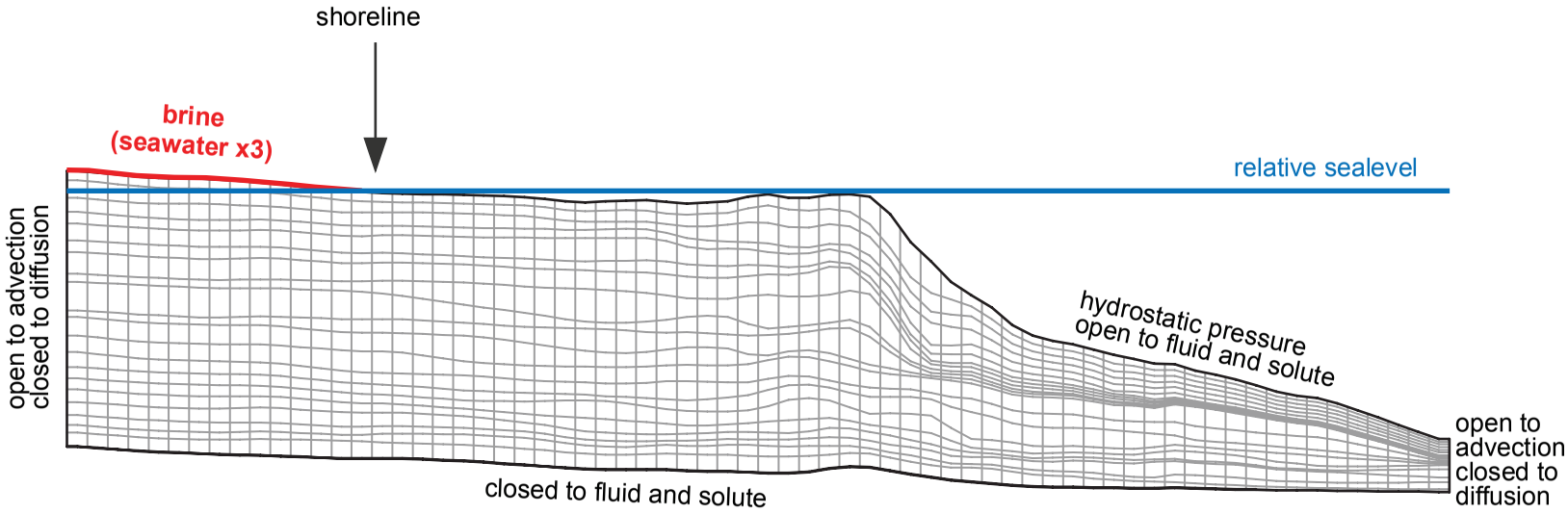

Figure 3.8: Boundary and initial conditions at the deposition of layer G2.6. The new layer is initially saturated with seawater whereas the rest of the layers have salinities inherited from previous time steps. The position of the shoreline varies for each layer, as relative sealevel rises and falls resulting in the expansion and contraction of the brine source in the exposed part of the platform. Fluid circulation is estimated to last 10% the time (approximately 5,000 yrs per layer)

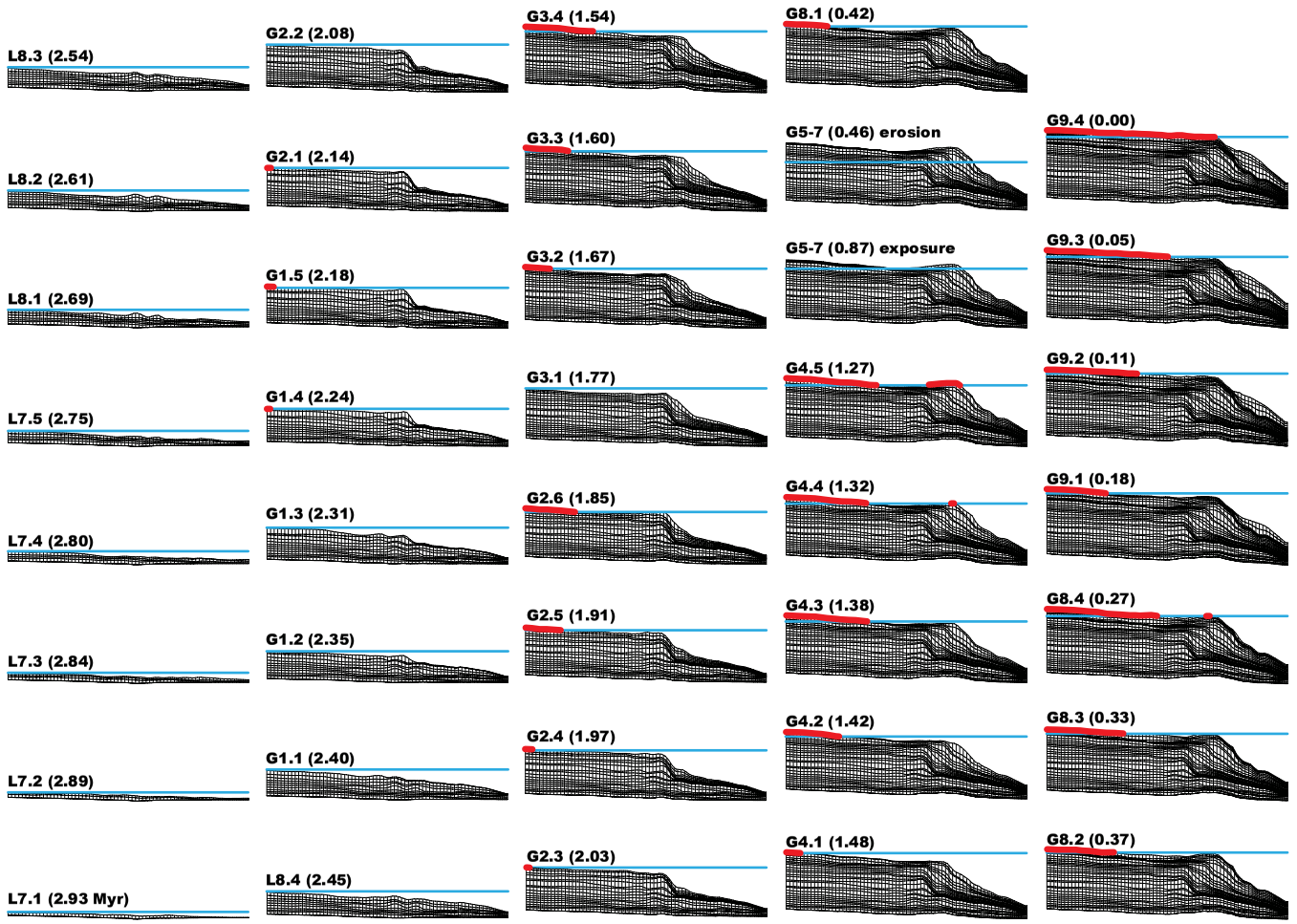

Figure 3.9: Full sequence of sealevel fluctuations and brine source evolution. Relative sealevel (blue line) records three orders of nested cyclicity: a 2nd order rise during Leonardian time and a gradually fall during Guadalupian time; two 3rd order sealevel oscillations L7-G4 and G8-9; and 4th order rises and falls during each high-frequency sequence. A hypersaline environment is prescribed where the platform is exposed, which is the source of refluxing brines (red line); this source expands and contracts in response to sealevel fluctuations and shoreline migration.

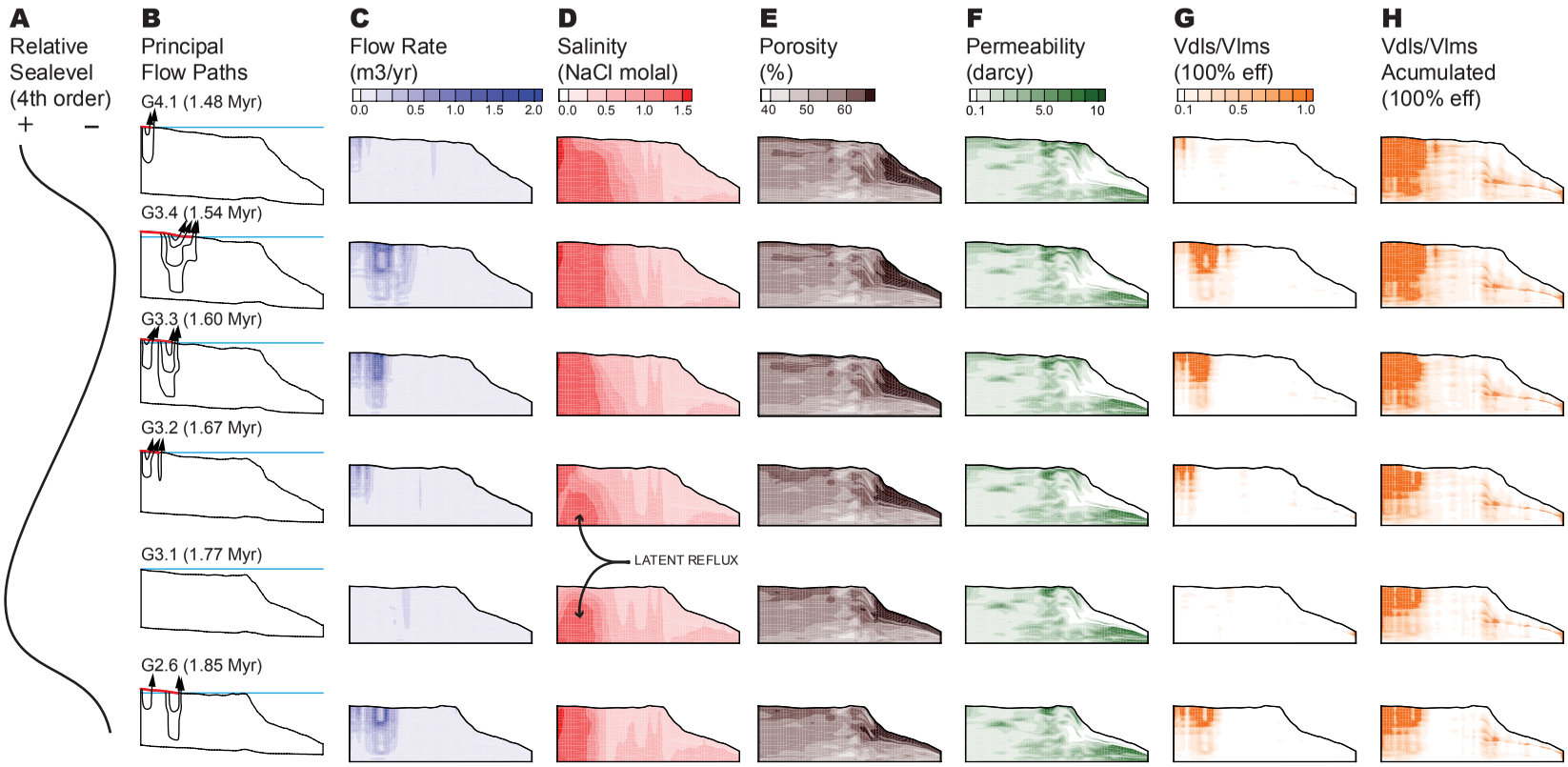

Figure 3.10: Results for one 3rd order sealevel rise and fall cycle and deposition of high-frequency sequence G3. A) Sketch of relative sealevel. B) Fluctuations on relative sealevel, extent of brine source and flow direction during the transgression, regression and subsequent transgression. C) Flow rates associated with brine circulation. D) Salinity distribution associated with brine circulation. E) Evolution of porosity with burial. F) Evolution of permeability as a function of porosity loss. G) Ratio between the potential volume of dolostone that could have formed and the volume of precursor limestone (Vdls/Vlms) for each time step. H) Accumulated dolostone to limestone ratio, so that the dolomite formed during each reflux event is added to that of previous events.

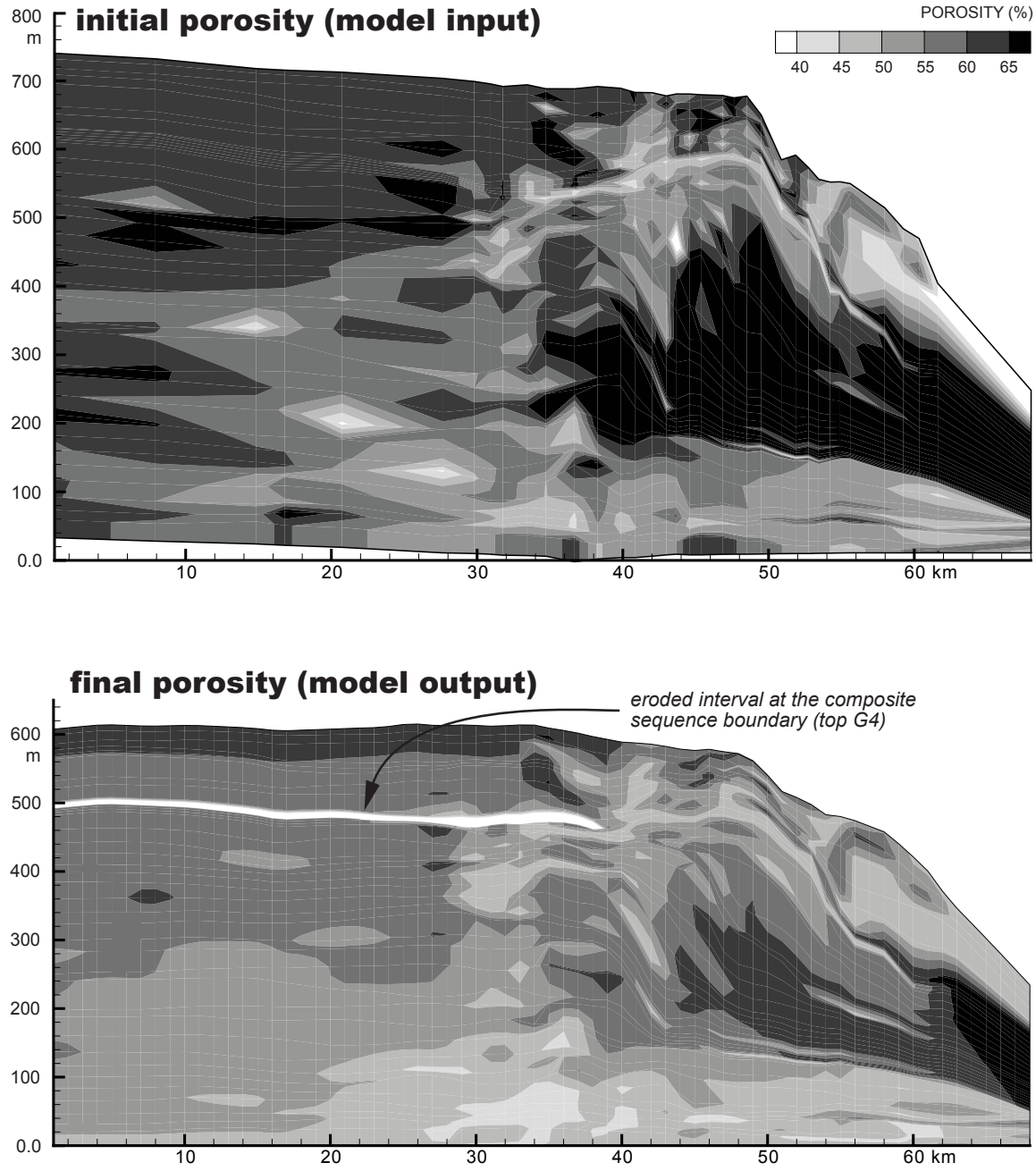

Figure 3.11: A) Model input porosity (Garcia-Fresca et al, in preparation; Chapter 2); decompacted outcrop thickness and porosity based on outcrop facies (after Kerans and Kempter, 2002) and porosity of modern carbonate sediments (after Enos and Sawatsky, 1980). B) Porosity distribution at the end of deposition of the San Andres Formation; loss in porosity is due to differential compaction of the sediments by the overburden following the curves in Figure 3.7B.

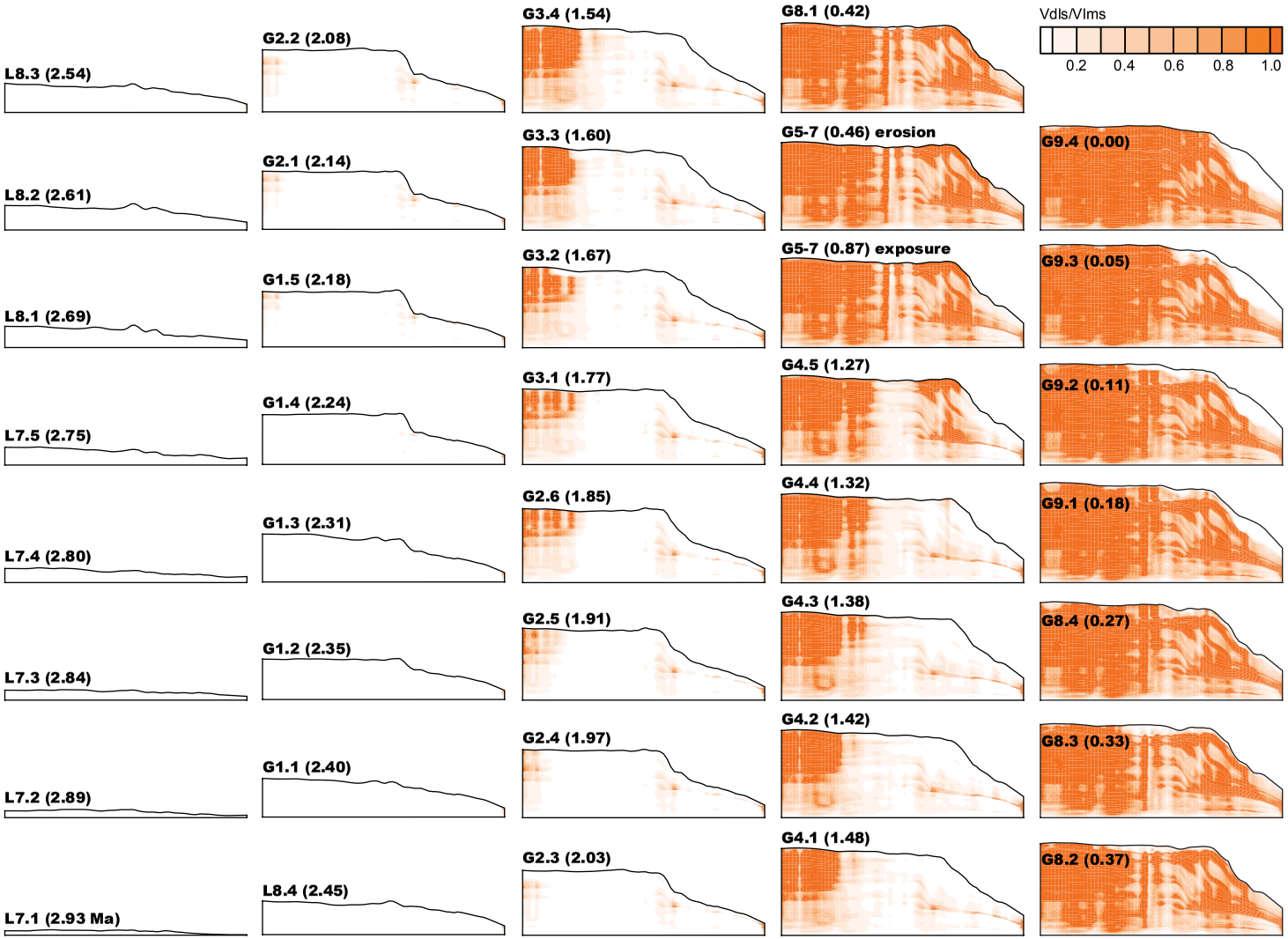

Figure 3.12: Model results showing the accumulated ratio between the potential volume of dolostone that could have formed and the volume of precursor limestone (Vdls/Vlms) for all time steps and a magnesium/calcium replacement efficiency of 50%.

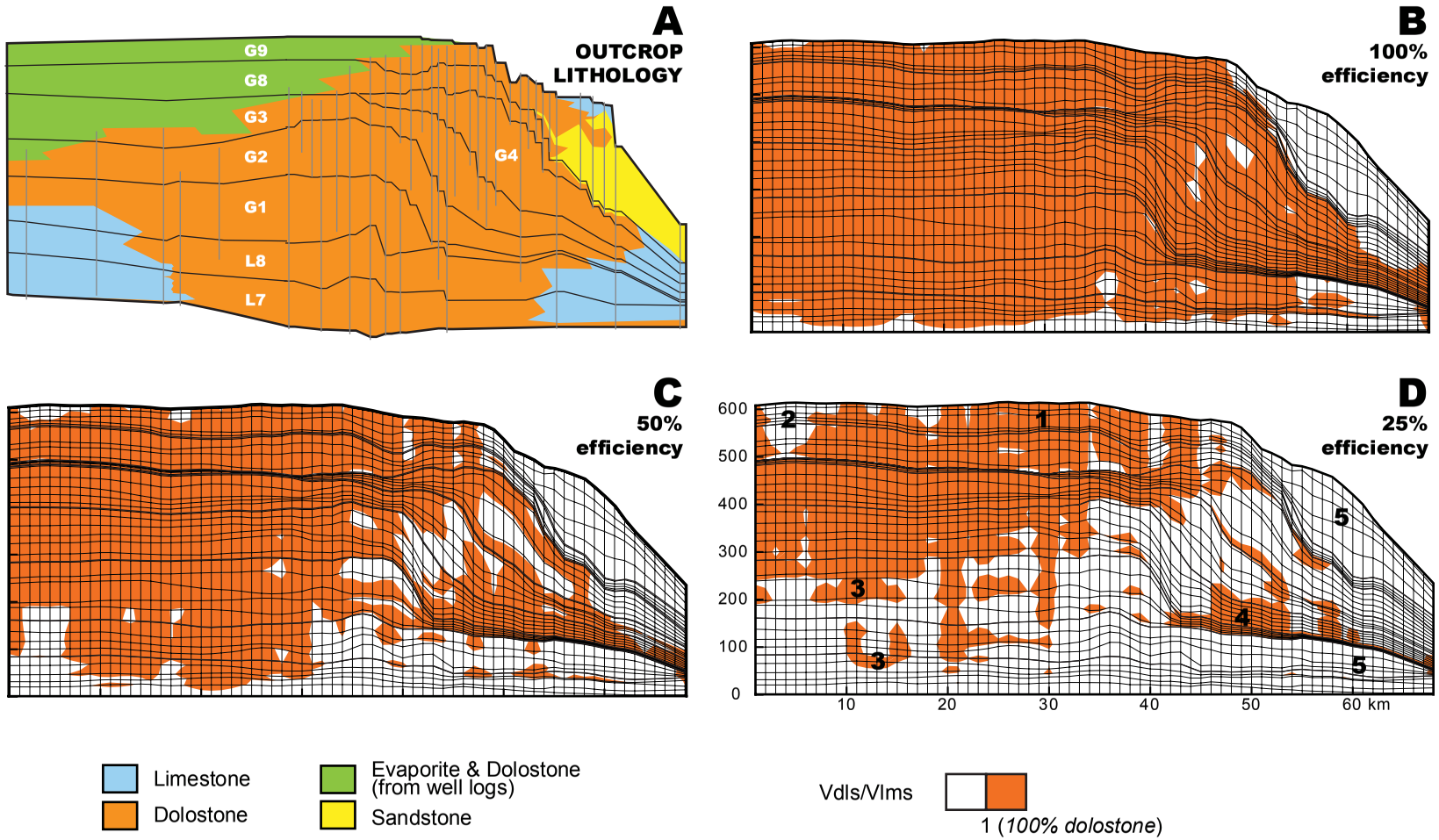

Figure 3.13: Model results for different magnesium/calcium replacement efficiencies, compared to outcrop lithologies. A) Outcrop lithology (after Garcia-Fresca and Lucia, 2007). B) 100% replacement efficiency. C) 50% replacement efficiency. D) 25% replacement efficiency. The variability in results for different efficiencies reflects the sensitivity of reflux dolomitization to the kinetics of the magnesium/calcium replacement reaction. Dolostone bodies across the platform result from different combinations of favorable conditions, such as proximity to the brine source, zones of high permeability, permeability contrasts, and “latent reflux”.

Table 3.1: Hydraulic properties of modeling rock types, used as input in hydrogeological simulations.

Basin2 PARAMETER	RT1	RT2	RT3	RT4	RT5	RT6	
phi0	0.70	0.63	0.61	0.61	0.56	0.49	initial porosity
phi1	0.00	0.00	0.00	0.00	0.00	0.00	irreducible porosity
bpor (km-1)	0.70	0.60	0.50	0.65	0.50	0.40	coefficient of burial compaction
perm_max (darcy)	0.02	0.57	2.02	4.20	7.39	18.07	initial permeability; kH
A_perm	4.30	6.70	7.80	8.30	9.70	11.00	slope of the por-perm curve; A
B_perm (log darcy)	-4.50	-4.50	-4.50	-4.50	-4.50	-4.50	intercept of the por-perm curve; B
p_kxky	1.11	2.97	4.70	9.41	3.21	1.68	permeability anisotropy; kH/kV
alpha_L (cm)	2500	2500	2500	2500	2500	2500	longitudinal dispersivity
alpha_T (cm)	250	250	250	250	250	250	transversal dispersivity
diff_con (cm2/sec)	1.0E-06	1.0E-06	1.0E-06	1.0E-06	1.0E-06	1.0E-06	diffusion coefficiient; D* -Basin2 default
rho_rk (g/cm3)	2.75	2.75	2.75	2.75	2.75	2.75	density of rock grains -Basin2 default

Chapter 4

APPARENT STRATIGRAPHIC CONCORDANCE OF REFLUX DOLOMITE: NEW PREDICTIVE CONCEPTS FROM HIGH-FREQUENCY CYCLE SCALE SYNSEDIMENTARY REACTIVE TRANSPORT MODELS

Abstract

Early-formed stratiform dolomite and coincident high-frequency cycle caps are often interpreted, by association, to have been generated by equivalent time–space events. I investigate this hypothesis using a reactive transport model to (1) evaluate geological, hydrological, and chemical controls on reflux dolomitization of a high-frequency cycle and (2) explore intra- and intercycle episodic brine reflux during consecutive deposition of high-frequency cycles. Simulations are based on partially dolomitized cycles of the Albian Upper Glen Rose Formation. Refluxing brines with a salinity four times that of seawater are capable of dolomitizing a 3-m-thick high-frequency cycle in 0.6 k.y., and to a depth of 100 m in 2.5 k.y. Simulations of episodic brine reflux during deposition of three high-frequency cycles reveal the potential for complex evolution, propagation, and coalescence of multiple dolomite fronts. Unfullfilled dolomitization potential along a flow path and variable dolomitization rate

related to dolomite abundance are primarily responsible for this phenomenon. Results suggest that the observed relationship between dolomite patterns and stratigraphic surfaces may be casual, challenging the existing predictive paradigm that genetically correlates a reflux dolomite body to the immediately overlying stratigraphic surface.

Introduction

Reflux dolomite in partially dolomitized high-frequency cycles (HFC) often underlies the cycle cap and extends downward from it (e.g. Lucia, 1972; Montañez and Read, 1992; Warren, 2000). The cycle cap is interpreted as the source of dolomitizing fluids that generated the dolomite in that particular HFC. Applying sequence stratigraphic principles, different dolomite bodies are correlated to immediately overlying cycle caps and interpreted to be generated at the time represented by the cycle boundary. Understanding the hydrogeological regime is critical to unravel the process of dolomitization (e.g. Land, 1985; Machel, 2004). Flow modeling plays a key role in evaluating proposed dolomitization mechanisms with respect to the magnitude of fluid flow and distribution of solutes (Simms, 1984; Kaufman, 1994; Jones et al., 2002; Whitaker et al., 2004), but do not integrate the reactive nature of the geochemical system. Reactive transport modeling (RTM), which couples hydrodynamics with chemical

reactions, is a technology that is revolutionizing our ability to investigate fluid-rock interactions (e.g. Lichtner et al., 1996; Steefel et al., 2005). Recent investigations of dolomitization using RTMs show significant promise in advancing the understanding and prediction of diagenetic processes and products (Wilson et al., 2001; Jones and Xiao, 2005; Xiao and Jones, 2006, 2007). This RTM study of reflux is unique in that (1) the model design and boundary conditions are constrained with outcrop data from the partially dolomitized Upper Glen Rose Formation (Fm); (2) it is a high-resolution in scale of investigation and heterogeneity of rock properties; and (3) the model simulates episodic reflux during deposition of three high-frequency cycles (HFC) by using a quasi-dynamic grid. Results provide new insights into the dolomitization process and challenge current paradigms relating synsedimentary dolomite patterns to cycle-bounding sequence stratigraphic surfaces.

Geologic setting

Dolomite distribution in the Albian Upper Glen Rose Fm in central Texas increases toward the sequence boundary at the top of the formation and toward progressively more restricted environments updip (Phelps and Kerans, 2009). An idealized Glen Rose HFC is approximately 3 m thick and its upper part is dolomitized (Fullmer, 2005; Figure 4.1A). It consists

of shallow subtidal mud-dominated packstone that shallows upward to a laminated mudstone and is capped by an evaporite-rich wackestone, interpreted as the source of dolomitizing brines. Fullmer (2005) reconstructed the petrophysical properties and thickness of an ideal Glen Rose Fm HFC at the time of deposition (Figure 4.1B). He conducted hydrogeological fluid-flow modeling and magnesium mass-balance calculations and concluded that the upper half of the cycle could be dolomitized in 0.5 k.y. of continued reflux of gypsum-saturated brines. Given the cycle thickness and assuming it was deposited in 20 k.y. (e.g. Goldhammer et al., 1987) at constant sedimentation rate, the evaporite-rich wackestone from which brines originate would have deposited in 2 k.y. It is reasonable to expect that brine was not always present through the duration of evaporite-rich facies deposition. Assuming brine availability to 10-50 % of the wackestone deposition time, reflux durations could range between 0.2-1 k.y. This model adopts Fullmer's (2005) stratigraphic and petrophysical framework but explicitly simulates reflux dolomitization during deposition of several HFCs.

Reactive transport model

I used the reactive transport simulator TOUGHREACT (Xu et al., 2005), which has the ability to simulate fluid flow, heat and solute transport,

chemical reactions including thermodynamics and kinetics, and feedbacks between porosity and permeability. The grid is one-dimensional in order to carry out a high-resolution investigation along a single flow path of brine reflux. The upper 15 m of the model grid consists of five ideal Glen Rose Fm HFCs, beneath which homogenous limestone was specified (Figures 4.1A, 4.2). Domain dimensions are 1 × 1 × 100 m in depth, with a grid spacing ranging from 0.3 to 1 m, designed to capture the petrophysical heterogeneity of the Glen Rose cycle (Figure 4.2). Initial petrophysical properties are based on Fullmer's (2005) reconstructed porosities of 50 to 60% and permeabilities of 0.26 to 2.8 Darcy (1.06×10^{-13} to 2.71×10^{-12} m^2) (Figure 4.1B). The top boundary, which represents the brine-sediment interface, has a specified fluid density and concentration of gypsum-saturated brine of salinity four times that of seawater and calcite, gypsum, and dolomite saturation indices of 0.824, -0.213, and 3.637, respectively. Brines sourced from the cycle cap descend in response to fluid-density gradients and no additional fluid flux is specified. The bottom boundary is open to flow. Simulations are isothermal because early simulations revealed that temperature differences over the depth of the model (3°C) had minimal impact on results. TOUGHREACT does not currently take account of porosity variations due to sediment compaction. Changes in mineral abundance drive changes in porosity, and permeability are

calculated from porosity using the Carmen-Kozeny relationship as described in Xu et al. (2005). Initial mineralogy is uniformly specified as 97% calcite, 2% dolomite, and 1% gypsum (Figure 4.2). The model is initially saturated with seawater in equilibrium with the specified mineralogy. For consistency with previous RTMs of dolomitization, I specified a dolomite precipitation kinetic rate constant at 25°C (k25) extrapolated from the high-temperature experiments of Arvidson and Mackenzie (1999) and a reactive surface area (RSA) of dolomite of 10^3 cm^2/g (representative of a ~50μm-sized crystal; Panda and Lake, 1995; Wilson et al., 2001; Jones and Xiao, 2005). Preliminary simulations failed to produce the amounts of dolomite observed in Glen Rose HFCs, relative to interpreted constraints for timing of cycle deposition and brine residence time. k25 and RSA are a product in the reaction rate equation and manipulating either one should yield identical results. Given the uncertainty inherent in both parameters, I arbitrarily chose to adjust k25 and maintain the value for RSA used by other workers, for consistency. Besides the uncertainty residing on extrapolating k25 from high temperature, a variety of factors can contribute to increase k25 by several orders of magnitude, including temperature and the presence of biological catalysts (Arvidson, personal communication). Increasing k25 by 100, to 4.48×10^{-17} mol/m^2, result in simulated volume and distribution of dolomite

consistent with the geological constraints and with Fullmer's (2005) estimate. Calcite and gypsum kinetics are not simulated as they are assumed to be in thermodynamic equilibrium relative to the significantly slower rate of dolomite precipitation.

The model incorporates the effect of cyclic sedimentation to investigate synsedimentary reflux dolomitization by consecutively inserting complete depositional cycles at the top of the model grid (Figure 4.2), and relocating the brine-source boundary to the top of the newly deposited cycle.

Results

Dolomitization progresses as brine flows down the model (Figure 4.3). After 0.6 k.y. of continuous reflux, the uppermost cycle is completely dolomitized (Figure 4.3A), and sediments are partially dolomitized in a zone that extends to a depth of approximately 13 m. With uninterrupted reflux the sediment column is progressively dolomitized such that after 1 and 2 k.y., dolomite extends to a depth of approximately 18 and 80 m, respectively (Figures 4.3B, C). Complete dolomitization increases porosity by approximately 10% (Figures 4.2 vs. 4.3). Gypsum cements precipitate as a byproduct of calcium enrichment from dolomitization and reduce porosity (Figures 4.3B, C). Although the volume and distribution of

gypsum is variable in space and time, cements initially precipitate ahead of the dolomite front and, as the dolomitization front advances, they are dissolved and reprecipitated down the flow path, a pattern consistent with that described by Jones and Xiao (2005). Gypsum cement occludes up to 30% of porosity after 2 k.y. (Figure 4.3C).

Dolomitization rates vary as a function of location relative to brine source and dolomite front, and additional minor variations in dolomitization rate relate to heterogeneous porosity and permeability (Figure 4.3). The maximum dolomitization rate occurs behind the dolomite front where some calcite is still available. Rates decrease exponentially from this maximum and track dolomite abundance. When all available limestone has been consumed, the dolomitization rate is effectively zero (Figures 4.3B, C) and there was no further dolomite precipitation as cement. The brine continues to be saturated with respect to dolomite throughout the simulation, although saturation decreases behind the dolomitization front. The lack of dolomite cement may be due to high k25 values. This issue requires further investigation.

Synsedimentary dolomitization is simulated by cyclic sedimentation and episodic brine circulation using a quasi-dynamic grid described above.

Simulations commence with a model that has three limestone Glen Rose HFCs at the top of the grid (Cycles 1–3; Figures 4.2, 4.4A). After 0.5 k.y. of brine reflux, the pattern of dolomite and the variation in rate of dolomitization are similar to those derived with a static grid (Figures 4.3A vs. 4.4A). Dolomitization rate increases significantly over time because increased dolomite abundance generates more reactive surface area, which is directly proportional to reactive rate. Cycle 4 is deposited and the next 0.5 k.y. of brine reflux result in progressive development of a second dolomite body in the upper part of the column (Figure 4.4B). Brine refluxing from Cycle 4 also supplies reactants to the deeper dolomite front, initiated during deposition of Cycle 3 (Figure 4.4B). This front advances 13 m, whereas the shallower dolomite front penetrates only 0.5 m (Figure 4.4B). Therefore, after two simulated reflux events, most dolomite in Cycle 3 and nearly all dolomite in Cycles 1 and 2 are generated from brines sourced from the cap of Cycle 4 (Figure 4.4B). This pattern is explained by the unfulfilled dolomitization potential of the refluxing brine during transit through Cycle 4 in conjunction with the increase on dolomitization rate related to increased dolomite abundance. The pattern is repeated for another 0.5 k.y. reflux event sourced from the cap of Cycle 5 (Figure 4.4C). After 1.1. k.y. of reflux, the two deepest dolomite fronts have coalesced (Figure 4.4C). By the end of the simulation a thin dolomite body

of approximately 0.5 m has formed beneath the top of Cycle 5. Cycles 1 through 4 are pervasively dolomitized as the cumulative result of episodic brine reflux associated with the deposition of three HFCs (Figure 4.4C).

Many HFCs in the Glen Rose Fm are partially dolomitized (Figure 4.1). To simulate partially dolomitized cycles, the experiment was repeated reducing the time available for each reflux event from 0.5 to 0.25 k.y. (Figure 4.5). After 0.75 k.y. of combined reflux only Cycle 3 is pervasively dolomitized (Figure 4.5). All other cycles are partially dolomitized, with a respective decrease in abundance of dolomite present in younger cycles (Figure 4.5). Dolomite bodies extend down from cycle caps, although most intracycle dolomite is formed from reflux brines generated from caps of younger cycles, even though these younger cycles may not be dolomitized.

Discussion and conclusions

Model results show that the distribution of dolomite within a HFC may be the net result of intercycle processes, whereby dolomitizing fluids sourced from younger cycles flow across stratigraphically significant boundaries. I also show that modeled dolomitization rates are controlled by variations in dolomite abundance and the unfulfilled dolomitization potential along a

flow path. These factors control the contemporaneous propagation of multiple dolomite fronts and growth and coalescence of discrete dolomite bodies. I expect additional complexity when incorporating the evolution of stratigraphy and associated spatial migration of depositional environments and brine sources in multidimensional space (Moore, 2001; Jones et al., 2002).

Results demonstrate the importance of integrating stratigraphic concepts, hydrogeological processes and geochemistry in understanding early dolomitization and developing predictive concepts. For example, these simulations provide a viable explanation for the spatial dislocation of a brine source and a dolomite body interpreted to be of reflux origin. This may help explain the common conundrum of limestone preservation in otherwise dolomitized reservoirs, especially where limestone occurs in proximity to evaporites (Swart et al., 2005; Ruppel and Jones, 2006). Some of these concepts are directly applicable to other sedimentary and diagenetic systems.

The results presented here imply that (1) observed relationships between dolomite and HFC boundaries may be casual, and intracycle dolomitization may be related to younger brine reflux events; (2) existing

predictive dolomite paradigms are deficient with respect to the concept of spatial dislocation between dolomite and the dolomitizing fluid source; and (3) modification of current interpretations of dolomite distribution and connectivity in the stratigraphic record may be warranted.

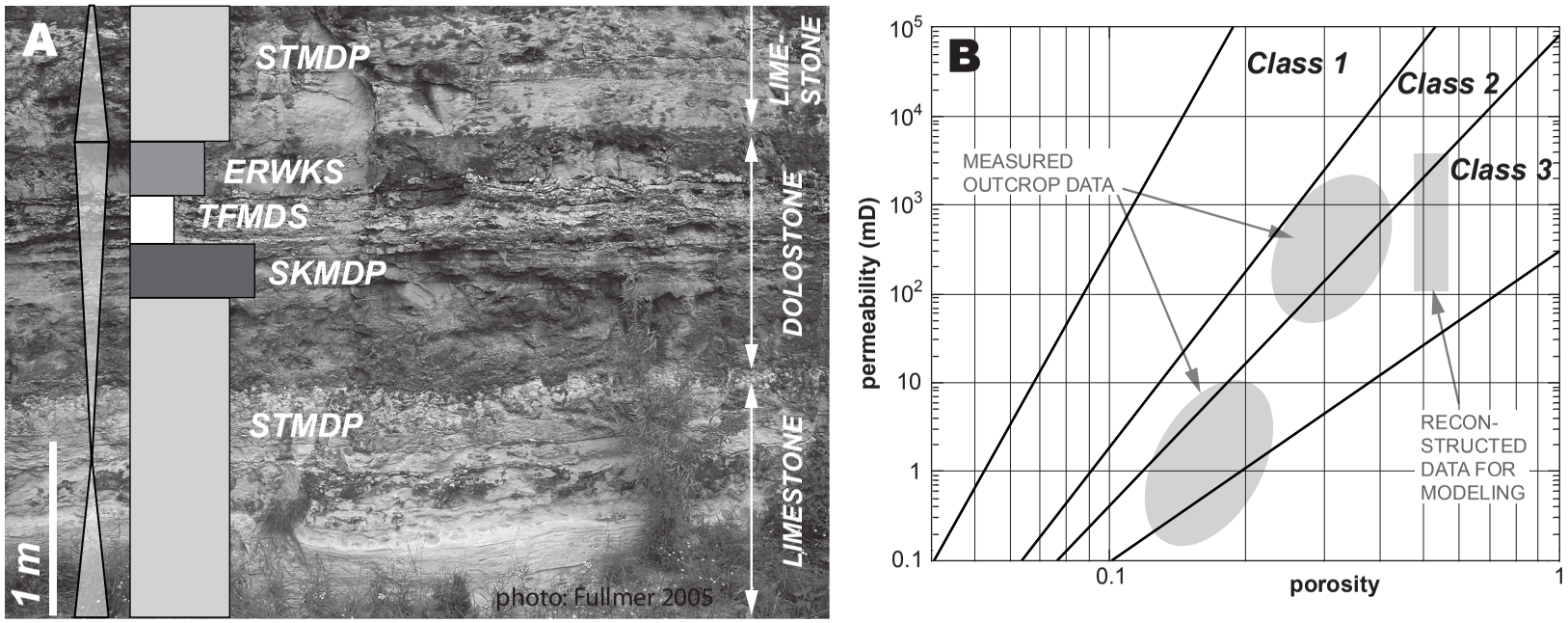

Figure 4.1: Idealized, partially dolomitized HFC of the Albian Upper Glen Rose Fm, central Texas, USA (modified from Fullmer, 2005). (A) Facies and lithology: ERWKS: evaporite-rich supratidal wackestone; TFMDS: laminated tidal-flat mudstone; SKMDP: skeletal mud-dominated packstone; STMDP: miliolid subtidal mud-dominated packstone. (B) Measured outcrop porosity and permeability and reconstructed depositional values prior to compaction and dolomitization, plotted on fields of Lucia's (1995) petrophysical classes.

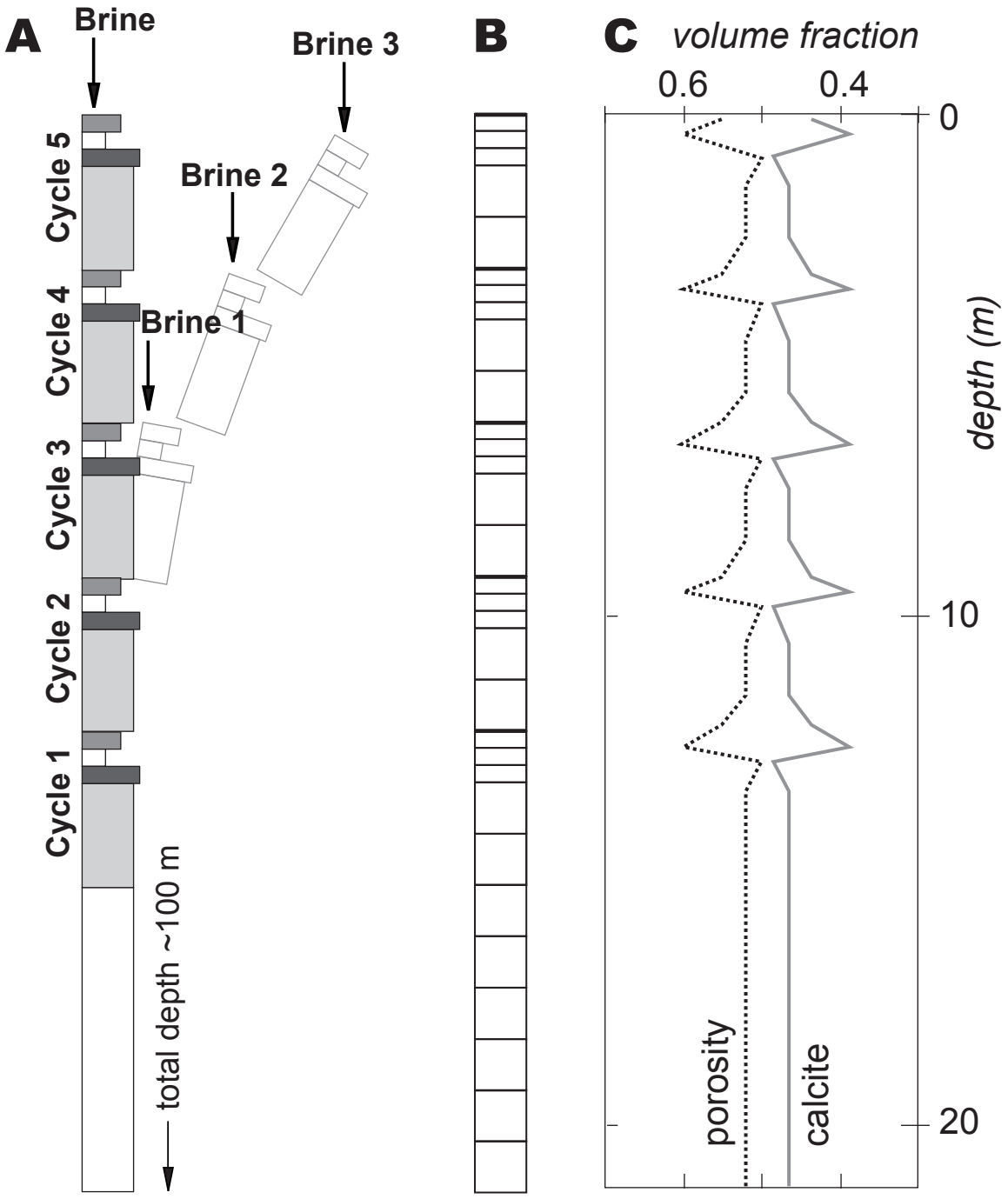

Figure 4.2: Model design, boundary, and initial conditions. (A) Geological model consisting of idealized Glen Rose HFCs (Figure 4.1A) overlying a homogenous limestone; cyclic sedimentation and reflux was simulated by adding cells to the grid. (B) Model grid. Cycle caps are shown in bold. (C) Initial porosity and mineralogy dominated by calcite.

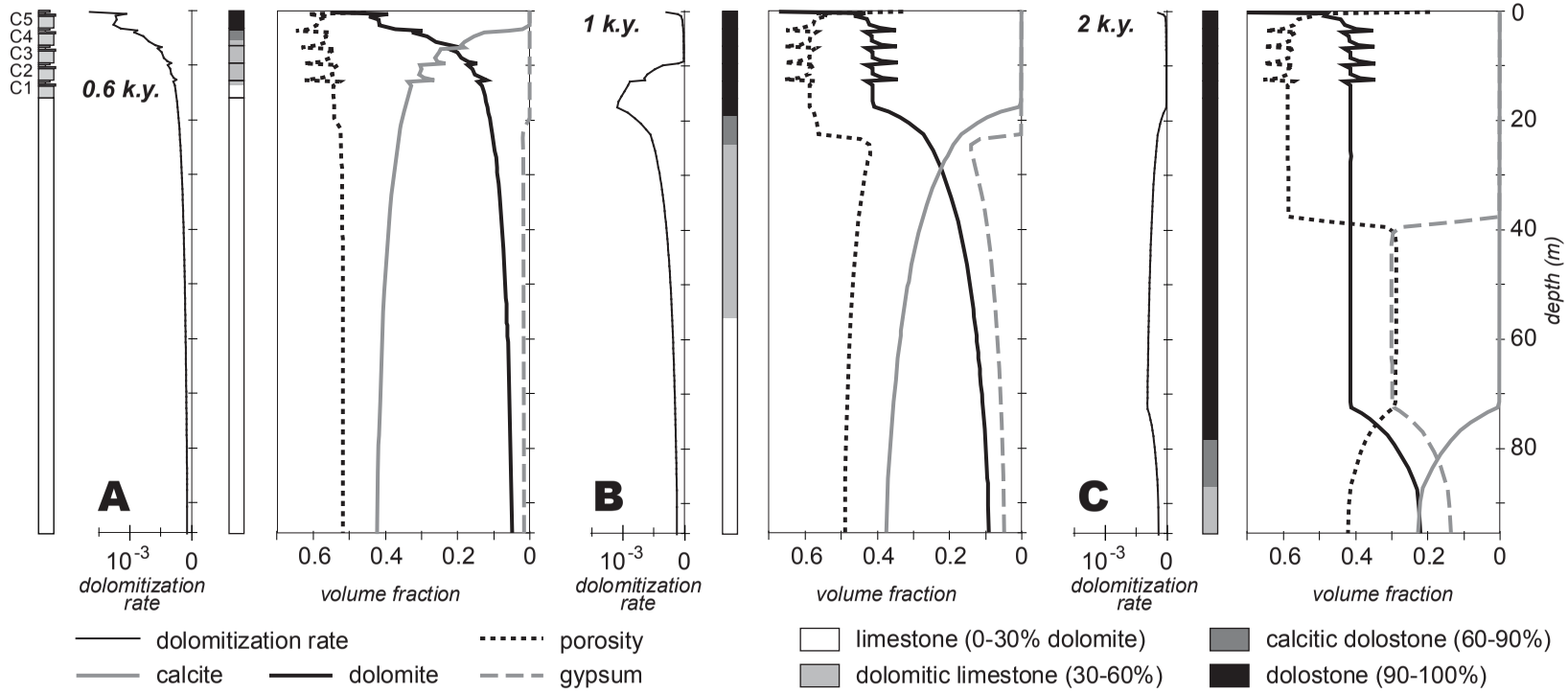

Figure 4.3: Simulated evolution of mineralogy, porosity, and rate of dolomitization after (A) 0.6 k.y.; (B) 1 k.y.; and (C) 2 k.y. of continuous brine reflux.

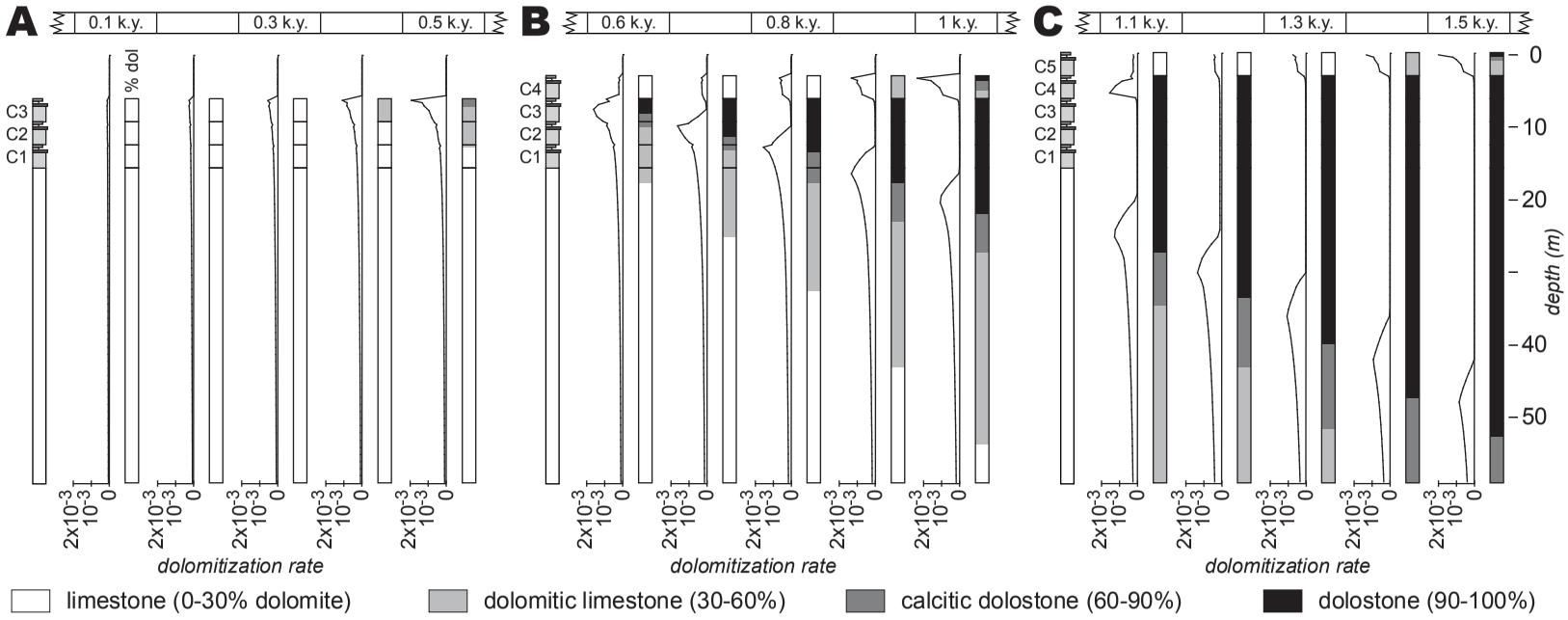

Figure 4.4: Simulated dolomitization by episodic brine reflux associated with deposition of three idealized Glen Rose Fm HFCs (Cycles 3–5); duration of each reflux event is 0.5 k.y. (A) Reflux event associated with Cycle 3. (B) Deposition of Cycle 4 and second reflux event. (C) Deposition of Cycle 5 and third reflux event. For mineralogy key see Figure 4.3.

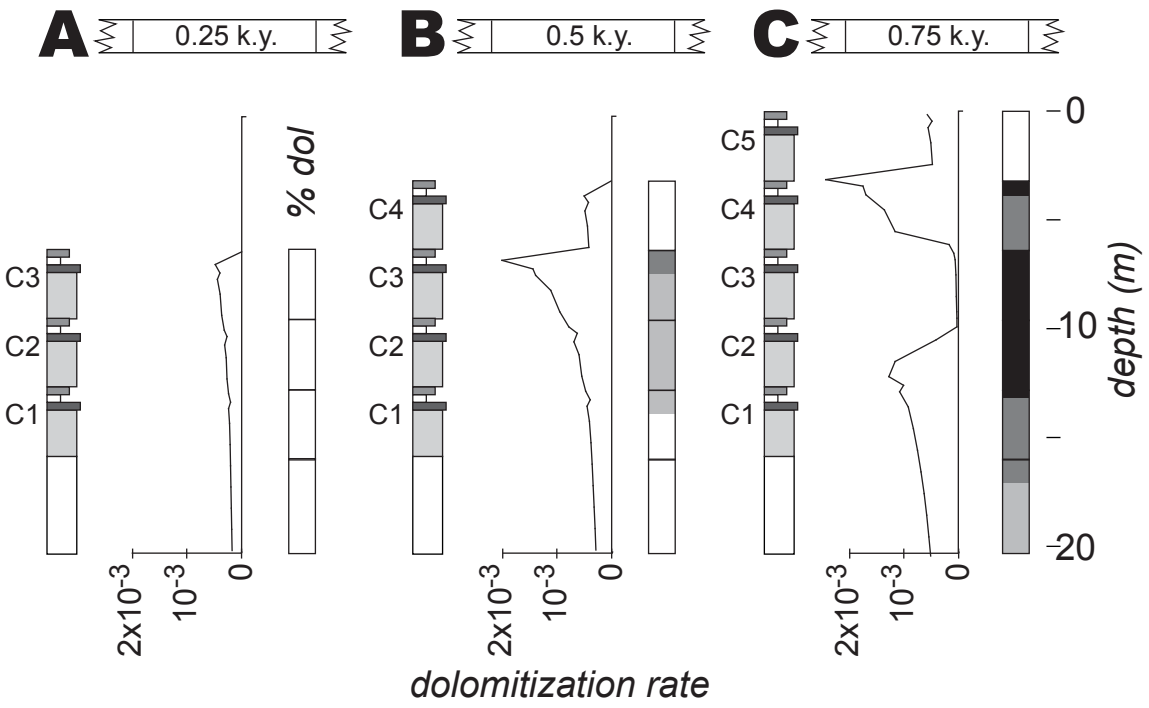

Figure 4.5: Simulated dolomitization by episodic brine reflux associated with deposition of Glen Rose Fm Cycles 4–5. Duration of each brine reflux event is 0.25 k.y. (A) Reflux event associated with Cycle 3. (B) Deposition of Cycle 4 and second reflux event. (C) Deposition of Cycle 5 and third reflux event. For mineralogy key see Figure 4.3.

CONCLUSIONS

This study is unique in that it uses outcrop and subsurface data and observations from modern settings to construct stratigraphically constrained petrophysical models to be used in numerical simulations of reflux. The work presented in the above chapters support the hypotheses presented at the beginning of this dissertation. Reflux is an effective hydraulic mechanism to deliver reactants and dolomitize large carbonate successions. This model contrasts with previous studies that approach reflux dolomitization as a discrete event. It also challenges the paradigm that relates sequence-stratigraphic surfaces and the dolomite bodies immediate to them.

A robust sequence stratigraphic framework and a sophisticated petrophysical model are important to the understanding of spatial and temporal distribution of diagenesis because they can be used to constrain the transient hydrologic, stratigraphic, and geochemical boundary conditions that control the flow of diagenetic fluids during accumulation of the carbonate platform. Relative sealevel fluctuations are a principal control on hydraulic gradients, platform geometry, facies distribution, and location, size and salinity of brine sources. Thus reflux pulses can be

related to sequence stratigraphic surfaces and one can expect it to occur at nested scales, mimicking stratigraphic hierarchy. However, dolomite bodies cut time lines and facies boundaries making this relationship not straightforward. Computer modeling provides stepwise analysis of the process to unravel the intricacies of this relationship.

The San Andres Formation provides a real-scale physical model to identify the sedimentologic and stratigraphic constrains which are indispensable for building a realistic model of reflux dolomitization. A regional-scale outcrop dataset and sequence stratigraphic framework was turned into a petrophysical model following a reservoir characterization method. The model serves as input into hydrogeologic simulations for studying the role of fluid flow and solute transport in early dolomitization by refluxing brine. This model successfully displays the petrophysical heterogeneity of the San Andres Formation at the platform scale, while maintaining the most relevant stratigraphic and depositional features. It provides spatially distributed values of porosity and permeability to input into hydrogeologic simulations described elsewhere. Outcrop and subsurface studies show the spatial distribution of limestone and dolostone across the San Andres Formation and allow the reconstruction of the restricted inner platform. The inner platform is composed mainly of shallow subtidal carbonates to

supratidal carbonates and sulfates and is interpreted as the source of dolomitizing fluids. Hydrogeologic simulations were used to estimate flow rates and salinity distributions over time and potential amount of dolomite generated. I show that relative sealevel-controlled transient boundary conditions result in intricate flow patterns and salinity distributions, and can generate irregular dolomite bodies of complex spatial distribution. Several fluid pulses can coalesce and continue to dolomitize at depth, cutting through time lines and facies boundaries. Dolostone bodies across the platform may be generated by different combinations of favorable conditions, such as proximity to the brine source, zones of relatively higher permeability, and permeability contrasts. This model reveals critical controls on brine reflux and subsequent dolomitization. These include: time, fluid flow rate, brine chemistry, and permeability which are, in turn, a function of sequence stratigraphic factors such as relative sealevel and depositional environments. Kinetics of dolomite precipitation, represented on this study as the efficiency of magnesium/calcium exchange, is also a critical control on this process. Model results confirm the relevance of “latent reflux”, or brines that may continue to dolomitize in the subsurface, after the source has been shut off.

Results from the high-resolution Glen Rose Formation model show that the distribution of dolomite within a HFC may be the net result of intercycle processes, whereby dolomitizing fluids sourced from younger cycles flow across stratigraphically significant boundaries. In addition, dolomitization rates are controlled by variations in dolomite abundance and the unfulfilled dolomitization potential along a flow path that result in contemporaneous propagation of multiple dolomite fronts and growth and coalescence of discrete dolomite bodies. Results show the temporal and spatial dislocation between the dolomitizing fluid source and a dolomite body and imply that observed relationships between dolomite and HFC boundaries may be casual and existing predictive paradigms may need to be reviewed.

These results provide a viable explanation for the spatial dislocation of a brine source and a dolomite body interpreted to be of reflux origin and help explain the common conundrum of limestone preservation in otherwise dolomitized formations, especially where limestone occurs in proximity to evaporites.

The workflow and methodology presented in this dissertation can be applied to other sedimentary and diagenetic systems by modifying model

design, initial and boundary conditions appropriately. Subsurface data could be used instead of outcrop data to develop predictive diagenetic models of reservoirs.

FUTURE WORK

1. Develop 2D and 3D reactive transport models of reflux to address further complexity of dolomitizing front development and amalgamation.
2. Study the sensitivity and interdependence of reactive surface area and reaction rate constant on dolomitization rates.
3. Petrographic and geochemical studies could contribute to unravel the complexity of superimposed brine circulation events and continuous recrystallization of reflux dolomite. Such studies should address the spatial distribution of crystal sizes and habits, crystal zonations and overgrowths, stoichiometry, isotopic and trace element trends and fluid inclusions.
4. Apply similar work approach to predicting reflux dolomite patterns using subsurface datasets and other diagenetic systems.
5. Other stuff.

SUPPLEMENTAL DATA

A: San Andres Formation, far north Algerita Escarpment outcrop files

A1: Measured sections

A2: Thin sections

(A3: Photomosaics)

(A4: Field Photos)

A5: RCRL field trip guidebook, October 2009

B: San Andres Formation petrophysical model files

C: San Andres Formation hydrogeologic model files

D: Glen Rose Formation reactive transport model files

Supplemental data are digital files contained in CDs available through the author or the Walter Geology Library of the University of Texas at Austin.

REFERENCES

Adams JE & Rhodes ML (1960) Dolomitization by seepage reflux. AAPG Bulletin, v 44, p 1912-1920

Altobi YK (2007) Milankovitch Orbital Forcing Control on Shallow-Water Carbonate Cyclicity and Early Dolomitization: Insights from the Lower Cretaceous Cupido Platform, NE Mexico. PhD dissertation, The University of Texas at Austin, 325 p

Amdurer M & Land LS (1982) Geochemistry, hydrology, and mineralogy of the sand bulge area, Laguna Madre flats, south Texas. Journal of Sedimentary Petrology, v 52, no 3, p 703-716

Arvidson RS & Mackenzie FT (1999) The dolomite problem: control of precipitation kinetics by temperature and saturation state. American Journal of Science, v 299, p 257-288

Banner JL (1995) Application of the trace element and isotope geochemistry of strontium to studies of carbonate diagenesis. Sedimentology, v 42, p 805-824

Banner JL (2004) Radiogenic isotopes: systematics and applications to earth surface processes and chemical stratigraphy. Earth-Science Reviews, no 65, p 141-194

Banner JL, Hanson GN & Meyers WJ (1988) Rare Earth Element and Nd isotopic variations in regionally extensive dolomites from the Burlington-Keokuk Formation (Mississippian): Implications for REE mobility during carbonate diagenesis. Journal of Sedimentary Petrology, v 58, no 3, p 415-432

Bear J (1972) Dynamics of fluids in porous media. American Elsevier, New York, 764 p

Beard DC & Weyl PK (1973) Influence of Texture on Porosity and Permeability of Unconsolidated Sand. AAPG Bulletin, v 57, no 2, p 349-369

Bein A, Hovorka SD, Fisher RS & Roedder E (1990) Fluid inclusions in bedded Permian halite, Palo Duro Basin, Texas: Evidence for modification of seawater in evaporite brien-pools and subsequent early diagenesis. Journal of Sedimentary Petrology, v 61, no 1, p 1-14

Bein A & Land LS (1982) San Andres carbonates in the Texas Panhandle: sedimentation and diagenesis associated with Mg-Ca-Cl brines. The University of Texas at Austin, Bureau of Economic Geology, Report of Investigations, no 121, 48 p

Beserra TB & Dorobek SL (1994) Sequence stratigraphy and facies analysis of the Permian San Andres Formation (lower Guadalupian), Northwest Shelf, Permian Basin. In: Garber and Keller (eds) Field Guide to the Paleozoic Section of the San Andres Mountains. PBS-SEPM Publication no 94-35, p 117-132

Bethke CM (1996) Geochemical Reaction Modeling, Concepts and Applications. Oxford University Press, New York, 397 p

Bethke CM, Lee M & Park J (2002) Basin modeling with Basin2 - A Guide to Using the Basin2 Software Package. Release 5.0, http://www.geology.uiuc.edu/~bethke/pdf/Basin2UsersGuide.pdf, 220 p

Box GEP (1979) Robustness in the strategy of scientific model building. In: Launer RL & Wilkinson GN (eds) Robustness in Statistics, Academic Press, New York, p 201-236

Boyd DG (1958) Permian sedimentary facies, central Guadalupe Mountains, New Mexico. New Mexico Bureau of Mines and Mineral Resources Bulletin, no 49, 100 p

Budd DA (2001) Permeability loss with depth in the Cenozoic carbonate platform of westcentral Florida, USA. American Association of Petroleum Geologists Bulletin, v 85, p

1253–1272"Braithwaite CJR, Rizzi G & Darke G (2004) The geometry and petrogenesis of dolomite hydrocarbon reservoirs. Geological Society Special Publication, no 235, 413 p

Carballo JD, Land LS & Miser DL (1987) Holocene dolomitization of supratidal sediments by active tidal pumping, Sugarloaf Key, Florida. Journal of Sedimentary Petrology, v 57, p 153-165

Clement JH (1985) Depositional sequences and characteristics of Ordovician Red River reservoirs, Pennel field, Williston basin, Montana. In Roehl PO & Choquette PW (eds) Carbonate petroleum reservoirs. Springer-Verlag, New York, p 71–84

Colgan RG (1990) Deposition, diagenesis and isotopic stratigraphy of the San Andres Fm (Lower Guadalupian) northern Algerita

Escarpment, New Mexico. MS thesis, Southern Methodist University, 163 p

Cooper GA & Grant RE (1972) Permian brachiopods of West Texas, I. Smithsonian Contributions to Paleobiology, no 14, p 1-232

Cooper GA & Grant RE (1974) Permian brachiopods of West Texas, II. Smithsonian Contributions to Paleobiology, no 15, p 233-794

Cooper GA & Grant RE (1975) Permian brachiopods of West Texas, III. Smithsonian Contributions to Paleobiology, no 19, p 795-1922

Cooper GA & Grant RE (1976) Permian brachiopods of West Texas, IV. Smithsonian Contributions to Paleobiology, no 21, p 1923-2608

Cooper GA & Grant RE (1976) Permian brachiopods of West Texas, V. Smithsonian Contributions to Paleobiology, no 24, p 2609-3160

Cooper GA & Grant RE (1977) Permian brachiopods of West Texas, VI. Smithsonian Contributions to Paleobiology, no 32, p 3161-3370

Cowan PE & Harris PM (1986) Porosity distribution in San Andres Formation (Permian), Cochran and Hockley counties, Texas:. AAPG Bulletin, v 70, p 888–897

Dagan G (1986) Statistical theory of groundwater flow and transport: pore to laboratory, laboratory to formation, and formation to regional scale. Water Resources Research, v 22, no 9, p 120S-135S.

Deffeyes KS, Lucia JF & Weyl PK (1965) Dolomitization of recent and Plio-Pleistocene sediments by marine evaporite waters on Bonaire, Netherlands Antilles. In: Pray LC & Murray RC (eds) Dolomitization and Limestone Diagenesis. SEPM Special Publication, no 13, p 71-88

Eisenberg RA, Conner FJ & Harris PM (1992) Acquisition and analysis of geologic and permeability data in dolomitized cyclic platform carbonates. In: Roberts CA (ed) Proceedings Geotech ’92, Denver, Colorado, August 29-September 1, p 73-85

Eisenberg RA, Harris PM, Grant CW, Goggin DJ & Conner FJ (1994) Modeling reservoir heterogeneity within outer ramp carbonate facies using an outcrop analog, San Andres Formation of the Permian Basin. AAPG Bulletin, v 78, no 9, p 1337-1359

Enos P & Sawatsky LH (1981) Pore networks in Holocene carbonate sediments. Journal of Sedimentary Petrology, v 51, no 3, p 961-985

Fenstemaker T, Halihan T & Sharp JM Jr (2001) Using resistivity to detect movements of variable salinity fluids in the barrier island sediments of Padre Island, Texas. GSA Abstracts with Programs, v 33, no 6, p A-46

Fernandez-Garcia D & Gomez-Hernandez JJ (2007) Impact of upscaling on solute transport: traveltimes, scale of dependence of dispersivity, and propagation of uncertainty. Water Resources Research, v 45, p 1-22

Fogg GE & Lucia FJ (1990) Reservoir Modeling of Restricted Platform Carbonates: Geologic/Geostatistical Characterization of Interwell-Scale Reservoir Heterogeneity Dune Field Crane County Texas. The University of Texas at Austin, Bureau of Economic Geology Report of Investigations no 190, 66 p

Fullmer SM (2005) Modeling Reflux Dolomitization. MS thesis, The University of Texas at Austin, 104 p

Gao G, Hovorka SD & Posey HH (1990) Limpid dolomite in Permian San Andres halite rocks, Palo Duro Basin, Texas Panhandle: Characteristics, possible origin, and implications for brine evolution. Journal of Sedimentary Petrology, v 60, no1, p 118-124

Garcia-Fresca & Jones (in review) Apparent stratigraphic concordance of reflux dolomite: New predictive concepts from high-frequency cycle scale synsedimentary reactive transport models. Geology

Garcia-Fresca B & Lucia FJ (2007) Outcrop and subsurface comparison of lithology distributions in the Permian San Andres Formation – Implications for a dolomitization model. West Texas Geological Society, Fall Symposium 2006, CD-ROM

Garcia-Fresca B, Lucia FJ & Kerans C (2008) Numerical Model of Reflux Circulation during the Deposition of the Permian San Andres Formation, Guadalupe Mountains and Algerita Escarpment. AAPG/SEPM Annual Convention, San Antonio, Texas, April 20-23, 2008, abstract

Gelhar LW, Welty C & Rehfeldt KR (1992) A critical review of data on field-scale dispersion in aquifers. Water Resources Research, v 28, no 7, p 1955-1974

Given RK & Lohmann KC (1985) Derivation of the original isotopic composition of Permian marine cements. Journal of Sedimentary Petrology, v 55, p 430-439

Goldhammer RK (1997) Compaction and decompaction algorithms for sedimentary carbonates. Journal of Sedimentary Research, v 67, no 1, p 26-35

Goldhammer RK, Dunn PA & Hardie LA (1987) High frequency glacio-eustatic sea level oscillations with Milankovitch characteristics recorded in Middle Triassic platform carbonates in northern Italy. American Journal of Science, v 287, no 9, p 853-892

Grant CW, Goggin DJ & Harris PM (1994) Outcrop analog for cyclic-shelf reservoirs, San Andres Formation of Permian Basin: Stratigraphic framework, permeability distribution, geostatistics, and fluid flow modeling. AAPG Bulletin, v 78, no 1, p 23-54

Hardie LA (1967) The gypsum-anhydrite equilibrium at one atmosphere pressure. The American Mineralogist, v 52, p 171-200

Hardie LA (1987) Dolomitization: A critical review of some current views. Journal of Sedimentary Petrology, v 57, n 1, p 166-183

Harland BW, Armstrong RL, Coc AV, Craig LE, Smith AG & Smith DG (1989) A geologic time scale. Cambridge University Press, Cambridge, 263 p

Harris MT (1982) Sedimentology of the Cuttoff Formation (Permian), Western Guadalupe Mountains, West Texas and New Mexico. MS thesis, University of Wisconsin-Madison, 186 p

Hayes PT (1964) Geology of the Guadalupe Mountains, New Mexico. USGS Professional Paper, no 446, 69 p

Hill CA (1996) Geology of the Delaware Basin – Guadalupe, Apache, and Glass Mountains – New Mexico and West Texas. SEPM Permian Basin Section Publication, no 96-39, 480 p

Hinrichs PD, Lucia FJ & Mathis RL (1986) Permeability distribution and reservoir continuity in Permian San Andres shelf carbonates, Guadalupe Mountains, New Mexico, In: Moore GE & Wilde GL (eds) Lower and Middle Guadalupian facies, stratigraphy, and reservoir geometries, San Andres/Grayburg Formations, Guadalupe Mountains, New Mexico and Texas. SEPM Permian Basin Section Publication, no 86-25, p 37-47

Hovorka SD (1987) Depositional environments of marine-dominated bedded halite, Permian San Andres Formation, Texas. Sedimentology, v 34, p 1029-1054

Hovorka SD (1991) Halite pseudomorphs after gypsum in bedded anhydrite – clue to gypsum-anhydrite relationships. Journal of Sedimentary Petrology, v 62, no 6 p 1098-1111

Hunt D & Fitchen WM (1999) Compaction and the dynamics of carbonate-platform development; insights from the Permian Delaware and Midland basins; southeastern New Mexico and West Texas, U.S.A. In: Harris PM, Saller AH, Simo JA (eds) Advances in carbonate sequence stratigraphy; application to reservoirs, outcrops and models. SEPM Special Publication, no v 63, p 75-106

Jennings JW (2000) Spatial statistics of permeability data from carbonate outcrops of west Texas and New Mexico: implications for improved reservoir modeling. The University of Texas at Austin, Bureau of Economic Geology, Report of Investigations, no 258, 50 p

Jennings JW, Ruppel SC & Ward WB (1998) Geostatistical analysis of permeability data and modeling of fluid-flow effects in carbonate outcrops. Reservoir Evaluation and Engineering v 3, no 4, Society of Petroleum Engineers paper, no 65370, p 292-303

Jones GD & Rostron BJ (2000) Analysis of fluid flow constraints in regional-scale reflux dolomitization: constant versus variable-flux hydrogeological models. Bulletin of Canadian Petroleum Geology, v 48, p 230-245

Jones GD & Xiao Y (2005) Dolomitization, anhydrite cementation, and porosity evolution in a reflux system: Insights from reactive transport models. AAPG Bulletin, v 89, p 577-601

Jones GD & Xiao Y (2006) Geothermal convection in the Tengiz carbonate platform, Kazakhstan: Reactive transport models of diagenesis and reservoir quality. AAPG Bulletin, v 90, no 8, p 1251–1272

Jones GD, Smart PL, Whitaker FF, Rostrom BJ & Machel HG (2003) Numerical modeling of reflux dolomitization in the Grosmont platform complex (Upper Devonian), Western Canada sedimentary basin. AAPG Bulletin, v 87, no 8, p 1273-1298

Jones GD, Whitaker FF, Smart PL & Sanford WE (2000) Numerical modeling of geothermal and reflux circulation in Enewetak Atoll: Implications for dolomitization. Journal of Geochemical Exploration, v 69– 70, p 71–75

Jones GD, Whitaker FF, Smart PL & Sanford WE (2002) Fate of reflux brines in carbonate platforms. Geology, v 30, p 371-374

Jones GD, Whitaker FF, Smart PL & Sanford WE (2004) Numerical analysis of seawater circulation in carbonate platforms: II. The dynamic interaction between geothermal and brine reflux circulation. American Journal of Science, v 304, p 250-284

Juster T, Kramer PA, Vacher HL, Swart PK & Stewart M (1997) Groundwater flow beneath a hypersaline pond, Cluett Key, Florida Bay, Florida. Journal of Hydrology, v 197, p 339-369

Katz DA, Buoniconti MR, Montanez IP, Swart PK, Eberli GP & Smith LB (2007) Timing and local perturbations to the carbon pool in the lower Mississippian Madison Limestone, Montana and Wyoming. Palaeo, v 256, p 231-253

Kaufman JK (1994) Numerical models of fluid flow in carbonate platforms: Implications for dolomitization. Journal of Sedimentary Research, v A64, p 128-139

Kelly VC (1971) Geology of the Pecos country, southeastern New Mexico. New Mexico Bureau of Mines Memoir, no 24, 77 p

Kerans C & Fitchen WM (1995) Sequence hierarchy and facies architecture of a carbonate ramp system: San Andres Formation of Algerita Escarpment and western Guadalupe Mountains, West Texas and New Mexico. The University of Texas at Austin, Bureau of Economic Geology Report of Investigations, no 235, 86 p

Kerans C & Kempter (2002) Hierarchical Stratigraphic Analysis of a Carbonate Platform, Permian of the Guadalupe Mountains. AAPG/Datapages Discovery Series, no 5, CD-ROM and color plate

Kerans C & Ruppel SC (1994) San Andres sequence framework, Guadalupe Mountains: implications for San Andres Type Section and subsurface reservoirs. In: Garber RA & Keller DR (eds) Field Guide to the Paleozoic section of the San Andres Mountains. Permian Basin Section-SEPM Publication, no 94-35, p 105-116

Kerans C & Tinker SW (1999) Extrinsic stratigraphic controls on development of the Capitan Reef Complex. In: Saller AH, Harris PM, Kirkland BL & Mazzullo SJ (eds) Geologic framework of the Capitan Reef. SEPM Special Publication, no no 65, p 15-36

Kerans C, Lucia FJ & Senger RK (1994) Integrated characterization of carbonate ramp reservoirs using Permian San Andres Formation outcrop analogs. AAPG Bulletin, v 78, no 2, p 181-216

King PB (1948) Geology of the southern Guadalupe Mountains, USGS Professional Paper, no 215, 183 p

King RH (1947) Sedimentation in Permian Castile Sea. AAPG Bulletin, v 31, p 470-477

Kirkby KC (1982) Deposition, erosion, and diagenesis of the upper Victorio Peak Formation (Leonardian), Southern Guadalupe Mountains, West Texas. MS thesis, University of Wisconsin-Madison, 165 p

Kottlowsky FE, Flower RH, Thompson ML & Foster RW (1956) Stratigraphic studies of the San Andres Mountains, New Mexico. New Mexico State Bureau of Mines and Mineral Resources and New Mexico Institute of Mining and Technology Memoir, no 1, 132 p

Kupecz JA, Montanez IP & Gao G (1993) Recrystallization of dolomite with time. In: Rezak R & Lavoie DL (eds) Carbonate Microfabrics. Frontiers in Sedimentary Geology series, Springer-Verlag, New York, p 187-194

Land LS (1980) The isotopic and trace element geochemistry of dolomite: the state of the art. In: Zenger DH, Dunham JB & Ethington RL (eds) Concepts and Models of Dolomitization. SEPM Special Publication, no no 28, p 87-110

Land LS (1985) The origin of massive dolomite. Journal of Geological Education, v 33, p 112-125

Land LS (1998) Failure to precipitate dolomite at 25 ◦C from dilute solution despite 1000-fold oversaturation after 32 years. Aquatic Geochemistry, v 4, p 361–368

Leary DA & Vogt JN (1990) Diagenesis of the San Andres Formation (Guadalupian), Central Basin Platform, Permian Basin. In: Bebout DG & Harris PM (eds) Geologic and Engineering Approaches in Evaluation of San Andres/Grayburg Hydrocarbon Reservoirs-Permian Basin. The University of Texas, Bureau of Economic Geology Symposia, no SP0005, p 21-48

Lee WT & Girty GH (1909) The Manzano Group of the Rio Grande Valley, New Mexico. USGS Bulletin, no 389, 141 p

Lichtner PC, Steefel CI & Oelkers EH (1996) Reactive transport in porous media. Reviews in Mineralogy, v 34, 438 p

Lindsay RF (1994) San Andres Formation Type and Reference Sections Revisited. In: Garber RA & Keller DR (eds) Field Guide to the Paleozoic section of the San Andres Mountains. SEPM Permian Basin Section Publication, no 94-35, p 133-143

Lloyd ER (1929) Capitan Limestone and associated formations of New Mexico and Texas. AAPG Bulletin, v 6, n 13, p 645-658

Lucia FJ (1968) Recent Sediments and Diagenesis of South Bonaire, Netherlands Antilles. Journal of Sedimentary Petrology, v 38, p 845-858

Lucia FJ (1972) Recognition of evaporite-carbonate shoreline sedimentation. In: Rigby JK & Hamblin WK (eds) Recognition of ancient sedimentary environments. SEPM Special Publication, no no 16, p 160-191

Lucia FJ (1995) Rock fabric/petrophysical classification of carbonate pore space for reservoir characterization. AAPG Bulletin, v 79, p 1275-1300

Lucia FJ (2007) Carbonate Reservoir Characterization: An Integrated Approach (2nd ed). Springer, 336 p

Lucia & Major (1994) Porosity evolution through hypersaline reflux dolomitization. In: Purser BJ, Tucker ME & Zenger DH (eds) Dolomites: A volume in Honour of Dolomieu. IAS Special Publication, no 21, p 325-341

Lucia FJ, Kerans C & Senger RK (1992a) Defining flow units in dolomitized carbonate-ramp reservoirs. Society of Petroleum Engineers paper, no 24702, p 399-406

Lucia FJ, Kerans C & Vander Stoep GW (1992b) Characterization of a Karsted High-Energy Ramp-Margin Carbonate Reservoir: Taylor-Link West San Andres Unit Pecos County Texas The University of Texas at Austin, Bureau of Economic Geology Report of Investigations no 208, 46 p

Machel HG (2004) Concepts and models of dolomitization: a critical reappraisal. In: Braithwaite CJR, Rizzi G & Darke G (eds) The Geometry and Petrogenesis of dolomite hydrocarbon reservoirs. Geological Society Special Publication, no 235, p 7-63

Machel HG & Mountjoy EW (1986) Chemistry and environments of dolomitization—a reappraisal. Earth-Science Reviews, v 23, p 175-222

McKenzie JA, Hsu KJ & Scheneider JF (1980) Movement of subsurface waters under the sabkha, Abu Dhabi, UAE, and its relation to evaporative dolomite genesis. SEPM Special Publication, no 28, p 11-30

Meissner FF (1972) Cyclic sedimentation in middle Permian strata of the Permian Basin, West Texas and New Mexico. In: Elam J & Chaber (eds) Cyclical sedimentation in the Permian Basin (2nd ed). West Texas Geological Society, p 203-232

Melim LA & Scholle PA (2002) Dolomitization of the Capitan Formation forereef Facies (Permian, west Texas and New Mexico): seepage reflux revisited. Sedimentology, v 49, p 1207-1227

Montañez IP & Read JF (1992) Eustatic control on early dolomitization of cyclic peritidal carbonates: evidence from the early Ordovician Upper Knox Group, Appalachians. GSA Bulletin, v 104, p 872-886

Moore CH (2001) Carbonate reservoirs: Porosity evolution and diagenesis in a sequence-stratigraphic framework. Developments in Sedimentology, v 55, Amsterdam, Elsevier, 444 p

Morrow DW (1990a) Diagenesis 1: Dolomite. Part 1: the chemistry of dolomitization and dolomite precipitation. In: McIlreath IA & Morrow DW (eds) Diagenesis, Geosci. Can. Reprint, Series, 4, p 113–124

Morrow DW (1990b) Diagenesis 2: Dolomite. Part 2: dolomitization models and ancient dolostones. In: McIlreath IA & Morrow DW (eds) Diagenesis, Geosci. Can. Reprint, Series, 4, p 125–164

Murray RC (1964) Origin and diagenesis of gypsum and anhydrite. Journal of Sedimentary Petrology, v 34, p 512-523

Needham CE & Bates RL (1943) Permian types sections in central New Mexico. GSA Bulletin, v 54, p 1653-1668

Niemann WL & Rovey CW (2009) A systematic field-based testing program of hydraulic conductivity and dispersivity onver a range in scale. Hydrogeology Journal, v 17, p 307-320

Panda MN & Lake LW (1995) A physical model of cementation and its effects on single-phase permeability. AAPG Bulletin, v 79, no 3, p 431–443

Patterson RJ (1972) Hydrology and carbonate diagenesis of a coastal sabkha in the Persian Gulf. PhD thesis, Princeton University, 469 p

Patterson RJ & Kinsman JJ (1982) Formation of diagenetic dolomite in coastal sabkha along Arabian (Persian) Gulf. AAPG Bulletin, v 66, no 1 p 28-43

Perkins RD, Dwyer GS, Rosoff DB, Fuller J, Baker PA & Lloyd RM (1994) Salina sedimentation and diagenesis: West Caicos Island, British West Indies. In: Purser BH, Tucker ME & Zenger DH (eds) Dolomites: A Volume in Honour of Dolomieu. IAS Special Publication, no 21, p 37-54

Phelps RM, & Kerans C (2009) Allocycles, autocycles and dolomite distribution in the Albian peritidal successions of the Upper Glen Rose, Austin, Texas. AAPG Annual Meeting, Denver, CO, June 7-10, 2009, abstract

Pray LC & Murray RC (1965) Dolomitization and Limestone Diagenesis. SEPM Special Publication, no 13, 180 p

Purser BH, Tucker ME & Zenger DH (1994) Problems, progress and future research concerning dolomites and dolomitization. In: Purser BH, Tucker ME & Zenger DH (eds) Dolomites – A volume in Honour of Dolomieu. IAS Special Publication, no 21, p 3-20

Ross CA & Ross JRP (1987) Biostratigraphic zonation of Late Paleozoic depositional sequences. Cushman Foundation for Foraminiferal Research Special Publication, no 24, p 151-168

Ruppel SC & Cander HS (1988a) Effects of Facies and Diagenesis on Reservoir Heterogeneity: Emma San Andres Field West Texas. The University of Texas at Austin, Bureau of Economic Geology Report of Investigations no 178, 67 p

Ruppel SC & Cander HS (1988b) Dolomitization of shallow-water platform carbonates by sea water and seawater-derived brines: San Andres Formation (Guadalupian), West Texas. In: Shukla V & Baker PA (eds) Sedimentology and Geochemistry of Dolostones. SEPM Special Publication, no 43, p 245-262

Ruppel SC & Jones RH (2006) Key role of outcrops and cores in carbonate reservoir characterization and modeling, Lower Permian Fullerton field, Permian basin, United States, in Harris PM & Weber LJ (eds) Giant Hydrocarbon Reservoirs of the World: From Rocks

to Reservoir Characterization and Modeling. AAPG Memoir, no 88, p 355-394

Saller AH & Henderson N (1998) Distribution of porosity and permeability in platform dolomites: insight from the Permian of West Texas. AAPG Bulletin, no 82, p 1528-1550

Sarg JF & Lehmann PJ (1986) Lower-middle Guadalupian facies and stratigraphy, San Andres-Grayburg Formations, Permian Basin, Guadalupe Mountains, New Mexico. In: Moore GE & Wilde GL (eds) Lower and middle Guadalupian facies, stratigraphy, and reservoir geometries: San Andres/Grayburg Formations, Guadalupe Mountains, New Mexico and Texas. SEPM Permian Basin Section Special Publication, no 86-25, p 1-36

Schincariol RA & Schwartz FW (1990) An experimental investigation of variable density flow and mixing in homogeneous and heterogeneous media. Water Resources Research, v 26, no 10, p 2317-2329

Schlumberger (1989) Log Interpretation Charts. Schlumberger Educational Services, 151 p.

Schmoker JW & Halley RB (1982) Carbonate porosity versus depth; a predictable relation for South Florida. AAPG Bulletin, v 66, no 12, p 2561-2570

Schulze-Makuch D (2005) Longitudinal dispersivity data and implications for scaling behavior. Ground Water, v 43, no 3, p 443–456

Shi (2005) Characterizing Heterogeneity in Low-permeability Strata and Its Control on Fluid Flow and Solute Transport by Thermalhaline Free Convection. PhD Dissertation, The University of Texas at Austin, 229 p

Shields MJ & Brady PV (1995) Mass balance and fluid flow constraints on regional scale dolomitization, late Devonian, Western Canada Sedimentary Basin. Bulletin of Canadian Petroleum Geology, v 43, p 371-392

Shinn EA, Ginsburg RN & Lloyd RM (1965) Recent supratidal dolomite from Andros Island, Bahamas. In: Pray LC & Murray RC (eds) Dolomitization and Limestone Diagenesis. Society of Economic Paleontologists and Mineralogists Special Publication 13, p 112-123

Shukla V & Baker PA (1988) Sedimentology and geochemistry of dolostones. SEPM Special Publication, no 43, 266 p

Sibley DF & Gregg JM (1987) Classification of dolomite rock textures. Journal of Sedimentary Petrology, v 57, no 6, p 967-975

Simmons CT & Narayan KA (1997) Mixed convection below a saline disposal pond. Journal of Hydrology, v 194, p 263-285

Simmons CT, Fenstemaker TR & Sharp JM Jr (2001) Variable-density groundwater flow and solute transport in heterogeneous porous media: approaches, resolutions and future challenges. Journal of Contaminant Hydrology, no 52, p 245-275

Simms M (1984) dolomitization by groundwater-flow systems in carbonate platforms. GCAGS Transactions, no 34, p 411-420

Smith LB, Eberli GP & Sonnenfeld M (2004) Sequence-stratigraphic and paleogeographic distribution of reservoir-quality dolomite, Madison Formation, Wyoming and Montana. In: Grammer GM, Harris PM & Eberli GP (eds) Integration of outcrop and modern analogs in reservoir modeling. AAPG Memoir, v 80, p 67-92

Sonnenfeld MD (1991) High-frequency cyclicity within shelf-margin and slope strata of the upper San Andres sequence, Last Chance Canyon. In: Meader-Roberts S, Candelaria MP & Moore GE (eds) Sequence stratigraphy, facies and reservoir geometries of the San Andres, Grayburg, and Queen Formations, Guadalupe Mountains, New Mexico and Texas. SEPM Permian Basin Section Publication, no 91-32, p 11-51

Sonnenfeld MD (1996) Sequence evolution and hierarchy within the lower Mississippian Madison Limestone of Wyoming. In: Longman MW and Sonnenfeld MD (eds) Paleozoic Systems of the Rocky Mountain Region, RMS-SEPM, p 165-192

Steefel CI, DePaolo D & Lichtner PC (2005) Reactive transport modeling: An essential tool and a new research approach for the Earth sciences. Earth and Planetary Science Letters, no 240, p 539-558

Stevens JD (2007) Variable-Density Groundwater Flow beneath the Wind-Tidal Flats of Padre Island. MS Thesis, The University of Texas at Austin, p 175

Stevens JD, Sharp JM Jr, Simmons CT & Fenstemaker TR (in press) Evidence of fee convection in groundwater: Field-based measurements beneath wind tidal flats. Journal of Hydrology.

Sudicky EA (1986) A natural gradient experiment on solute transport in a sand aquifer: Spatial variability of hydraulic conductivity and its role in the dispersion process. Water Resources Research, v 22, no 13, p 2069-2082

Swart PK, Cantrell DL, Westphal H, Hanford CR, & Kendall CG (2005) Origin of dolomite in the Arab-D reservoir from the Ghawar Field, Saudi Arabia: Evidence from petrographic and geochemical constraints. Journal of Sedimentary Research, v 75, p 476-491

Wang FP, Lucia FJ & Kerans C (1994) Critical scales, upscaling, and modeling of shallow-water carbonate reservoirs. SPE paper, no 27715, p 765-774

Ward RF, Kendall CGSTC & Harris PM (1986) Upper Permian (Guadalupian) facies and their association with hydrocarbons – Permian Basin, west Texas and New Mexico. AAPG Bulletin, v 70, no 3, p 239-262

Wardlaw BR & Grant RW (1990) Conodont biostratigraphy of the Permian Road Canyon Formation, Glass Mountains, TX. USGS Bulletin, no 1895, p 1-18

Warren JK (2000) Dolomite: occurrence, evolution and economically important associations. Earth-Science Reviews, no 52, p 1-81

Warren JK (2006) Evaporites: Sediments, Resources and Hydrocarbons. Springer, 1036 p

Whitaker FF & Smart PL (1993) Circulation of saline groundwaters in carbonate platforms: a review and case study from the Bahamas. In: Horbury AD and Robinson AD (eds) Diagenesis and Basin Development. American Association of Petroleum Geologists, Studies in Geology, no 36, p 113-134

Whitaker FF, Smart PL & Jones GD (2004) Dolomitization: From conceptual to numerical models. In: Braithwaite CJR, Rizzi G & Darke G (eds) The geometry and petrogenesis of dolomite hydrocarbon reservoirs. Geological Society Special Publication, no 235, p 99-139

Wilde GL (1986) An important occurrence of early Guadalupian (Roadian) fusulinids from the Cutoff Formation, western Guadalupe Mountains, Texas In: Moore GE &Wilde GL (eds) Lower and Middle Guadalupian Facies, Stratigraphy, and Reservoir Geometries, San Andres/Grayburg Formations, Guadalupe Mountains, New Mexico

and Texas. SEPM Permian Basin Section Publication, no 86-25, p 65-68

Wilson AM, Sanford WE, Whitaker FF & Smart PL (2001) Spatial patterns of diagenesis during geothermal circulation in carbonate platforms. American Journal of Science, v 301, p 727-752

Wilson EW, Hardie LA & Phillips OM (1990) Dolomitization front geometry, fluid flow patterns, and the origin of massive dolomite: the Triassic Latemar buildup, Northern Italy. American Journal of Science, v 290, p 741-796

Wood WW, Sanford WE & Al Habashi ARS (2002) The source of solutes to the coastal-sabkha aquifer of Abu Dhabi. GSA Bulletin, v 114, p 259-268

Xiao Y & Jones GD (2006) Reactive transport modeling of carbonate and siliciclastic diagenesis and reservoir quality prediction. SPE paper, no 101669, p 1-10

Xiao Y & Jones GD (2007) Reactive transport models of limestone-dolomite transitions: Implications for reservoir connectivity. International Petroleum Technology Conference, Dubai, U.A.E. paper, no 11199, p 1-11

Xu T, Sonnenthal EL, Spycher N & Pruess K (2005) TOUGHREACT User's Guide: A simulation program for nonisothermal multiphase reactive geochemical transport in variably saturated geologic media. Lawrence Berkeley National Laboratory Report, no LBNL-55460, 192 p

Zenger DH & Dunham JB (1980) Concepts and models of dolomitization – An introduction. In: Zenger DH, Dunham JB & Ethington RL (eds) Concepts and Models of Dolomitization. SEPM Special Publication, no 28, p 1-9

Zenger DH & Mazzullo SJ (1982) Dolomitization. Benchmark Papers in Geology, v 65. Hutchinson Ross Publishing Company, 426 p

Zenger DH, Dunham JB & Ethington RL (1980) Concepts and Models of Dolomitization. SEPM Special Publication, no 28, 320 p

Zoback ML (1981) Cainozoic evolution of the state of stress and the style of techtonism of the Basin and Range province of the western United States. Royal Society of London Philosophical Transactions, v 300, p 407-434

Vita

Beatriz Garcia-Fresca Grocin was born in Pamplona, Basque Country, on October 7, 1973, the daughter of Damian Garcia-Fresca and Garbiñe Grocin. She completed high school in Pamplona, entered The University of the Basque Country in Bilbao, where she participated in a exchange program with The University of Texas for a year, and received a Bachelor of Science degree in geology in 1997. From 1998 to 2001 she was employed as a hydrogeologist at the Basque Energy Board and the Texas Water Development Board. She entered the graduate program at The University of Texas at Austin in 2001 and received a master's degree in Geological Sciences in May of 2004. After a brief parenthesis exploring the exhilarating world of cheese, she reentered the Graduate School at the University of Texas at Austin in August of 2005. After obtaining her Ph.D, she accepted a job with the carbonate research group at Chevron ETC in sunny California.

Permanent address:
Belateko Monastegia kalea, 1, 1B
31011 Iruñea
Basque Country (Spain)
tritxe@gmail.com

This thesis was typed by the author.